NASA/TM—2008-214702

Effects of Palladium Content, Quaternary Alloying, and Thermomechanical Processing on the Behavior of Ni-Ti-Pd Shape Memory Alloys for Actuator Applications

Glen Bigelow
Glenn Research Center, Cleveland, Ohio

July 2008

NASA STI Program . . . in Profile

Since its founding, NASA has been dedicated to the advancement of aeronautics and space science. The NASA Scientific and Technical Information (STI) program plays a key part in helping NASA maintain this important role.

The NASA STI Program operates under the auspices of the Agency Chief Information Officer. It collects, organizes, provides for archiving, and disseminates NASA's STI. The NASA STI program provides access to the NASA Aeronautics and Space Database and its public interface, the NASA Technical Reports Server, thus providing one of the largest collections of aeronautical and space science STI in the world. Results are published in both non-NASA channels and by NASA in the NASA STI Report Series, which includes the following report types:

- TECHNICAL PUBLICATION. Reports of completed research or a major significant phase of research that present the results of NASA programs and include extensive data or theoretical analysis. Includes compilations of significant scientific and technical data and information deemed to be of continuing reference value. NASA counterpart of peer-reviewed formal professional papers but has less stringent limitations on manuscript length and extent of graphic presentations.

- TECHNICAL MEMORANDUM. Scientific and technical findings that are preliminary or of specialized interest, e.g., quick release reports, working papers, and bibliographies that contain minimal annotation. Does not contain extensive analysis.

- CONTRACTOR REPORT. Scientific and technical findings by NASA-sponsored contractors and grantees.

- CONFERENCE PUBLICATION. Collected papers from scientific and technical conferences, symposia, seminars, or other meetings sponsored or cosponsored by NASA.

- SPECIAL PUBLICATION. Scientific, technical, or historical information from NASA programs, projects, and missions, often concerned with subjects having substantial public interest.

- TECHNICAL TRANSLATION. English-language translations of foreign scientific and technical material pertinent to NASA's mission.

Specialized services also include creating custom thesauri, building customized databases, organizing and publishing research results.

For more information about the NASA STI program, see the following:

- Access the NASA STI program home page at *http://www.sti.nasa.gov*

- E-mail your question via the Internet to *help@ sti.nasa.gov*

- Fax your question to the NASA STI Help Desk at 301–621–0134

- Telephone the NASA STI Help Desk at 301–621–0390

- Write to:
  NASA Center for AeroSpace Information (CASI)
  7115 Standard Drive
  Hanover, MD 21076–1320

Effects of Palladium Content, Quaternary Alloying, and Thermomechanical Processing on the Behavior of Ni-Ti-Pd Shape Memory Alloys for Actuator Applications

Glen Bigelow
Glenn Research Center, Cleveland, Ohio

Level of Review: This material has been technically reviewed by technical management.

Contents

Figures

Tables

Effects of Palladium Content, Quaternary Alloying, and Thermomechanical Processing on the Behavior of Ni-Ti-Pd Shape Memory Alloys for Actuator Applications

Glen Bigelow
National Aeronautics and Space Administration
Glenn Research Center
Cleveland, Ohio 44135

Abstract

The need for compact, solid-state actuation systems for use in the aerospace, automotive, and other transportation industries is currently driving research in high-temperature shape memory alloys (HTSMA) having transformation temperatures above 100 °C. One of the basic high temperature systems under investigation to fill this need is NiTiPd. Prior work on this alloy system has focused on phase transformations and respective temperatures, no-load shape memory behavior (strain recovery), and tensile behavior for selected alloys. In addition, a few tests have been done to determine the effect of boron additions and thermomechanical treatment on the aforementioned properties. The main properties that affect the performance of a solid state actuator, namely work output, transformation strain, and permanent deformation during thermal cycling under load have mainly been neglected. There is also no consistent data representing the mechanical behavior of this alloy system over a broad range of compositions. For this thesis, ternary NiTiPd alloys containing 15 to 46 at.% palladium were processed and the transformation temperatures, basic tensile properties, and work characteristics determined. However, testing reveals that at higher levels of alloying addition, the benefit of increased transformation temperature begins to be offset by lowered work output and permanent deformation or "walking" of the alloy during thermal cycling under load. In response to this dilemma, NiTiPd alloys have been further alloyed with gold, platinum, and hafnium additions to solid solution strengthen the martensite and parent austenite phases in order to improve the thermomechanical behavior of these materials. The tensile properties, work behavior, and dimensional stability during repeated thermal cycling under load for the ternary and quaternary alloys were compared and discussed. In addition, the benefits of more advanced thermomechanical processing or training on the dimensional stability of these alloys during repeated actuation were investigated. Finally, the effect of quaternary alloying on the thermal stability of NiTiPdX alloys is determined via thermal cycling of the materials to increasing temperatures under load. It was found that solid solution additions of platinum and gold resulted in about a 30 °C increase in upper use temperature compared to the baseline NiTiPd alloy, providing an added measure of over-temperature protection.

Chapter 1—Introduction and Background

1.1 Discovery of Shape-Memory Alloys

Shape-memory alloys (SMAs) are a unique family of metals exhibiting an ability to recover macroscopic deformation introduced at low temperature simply by heating the material through a transformation temperature. Shape-memory effect (SME) is therefore the ability of a material to return to a preset shape upon finishing the transformation. It was first discovered in Au-47.5 at.% Cd by Chang and Read in 1951 (ref. 1) and later found in 1961 by Buehler et al. in the Ni-Ti system (ref. 2) while trying to develop lightweight high-temperature aerospace alloys (ref. 3). Between these times and since, several other alloy systems exhibiting SME were discovered, including CuAlNi (ref. 4), NiAl (ref. 5), NbRu (ref. 6), CuZn (ref. 7), InTl (refs. 8 and 9), TaRu (ref. 6), NiMnGa (ref. 10), FePt (ref. 11), FeNiCoTi (ref. 12), and FeMnSi (ref. 13). The same alloys exhibiting SME also to some extent exhibit superelasticity. This is the ability to recover large elastic strains immediately upon the removal of the causative stress, while the material is in a certain temperature range.

1.2 Phase Structure

In the majority of SMAs, the high-temperature parent or "austenite" phase is a strongly ordered phase, often cubic in nature. In binary NiTi, the high-temperature austenite is a strongly ordered B2 phase (CsCl structure), where titanium atoms form a simple cubic structure, with one nickel atom residing at the body center location of each unit cell (Figure 1.1) (refs. 14 to 16). Depending upon the thermomechanical processing, thermal history, and alloying additions to the NiTi, the austenite can form a number of different martensite structures (refs. 17 and 18). Upon cooling, the B2 structure can transform to B19 or B19' directly, or to B19' via a two step transformation of B2 ↔ B19 ↔ B19' or B2 → R → B19'. Orthorhombic B19 martensite is a shear transformation of the B2 {110} along the <1-10>, and B19' is a shear of the B19 martensite along the {001}<110> of the parent B2 structure. Rhombohedral R phase is formed by an elongation of the parent B2 austenite along <111>. The rhombohedral transformation is martensitic in nature, and nucleation and growth of the phase initiates at dislocations or other defects in the material (ref. 19). In addition, except for the R phase transformation, all the transformations of the B2 to B19 or B19' are reversible in nature, as the habit planes of the austenite and martensite phases are coherent, and the same ordering is maintained in the austenite phase when the material is heated through the transformation to reform the parent phase. The twins formed by the B19 and B19' martensites upon cooling through the transformation are a self-accommodating thermoelastic martensite, that is, while individual twins produce a localized shear deformation, the sum of the shear deformations from all the twins formed is approximately zero in each of the three principle directions, leading to zero net shape change in the bulk material (ref. 20). However, when the material is in the low temperature martensite state, and a stress greater than the detwinning stress for the martensitic twins is applied, macroscopic deformation occurs. This deformation is accommodated by shearing of twins whose (110) or (001) planes contain the shear elements. Upon heating through the transformation, the martensite reverts back to the parent austenite state, recovering both the strain due to martensite twin formation and strain due to deformation by detwinning. This behavior is the shape-memory effect (Figure 1.2).

Superelasticity, on the other hand, arises when stress applied to the high temperature B2 phase causes stress induced martensite to form. When the stress is removed, the austenite again becomes energetically favorable, and the martensite reverts back to the parent phase, recovering the deformation. This transformation can only occur in a temperature range where the critical stress for slip is greater than the critical stress for martensitic shear. The highest temperature at which stress induced martensite can be formed before plastically deforming the material by slip is called the martensite deformation temperature (M_d).
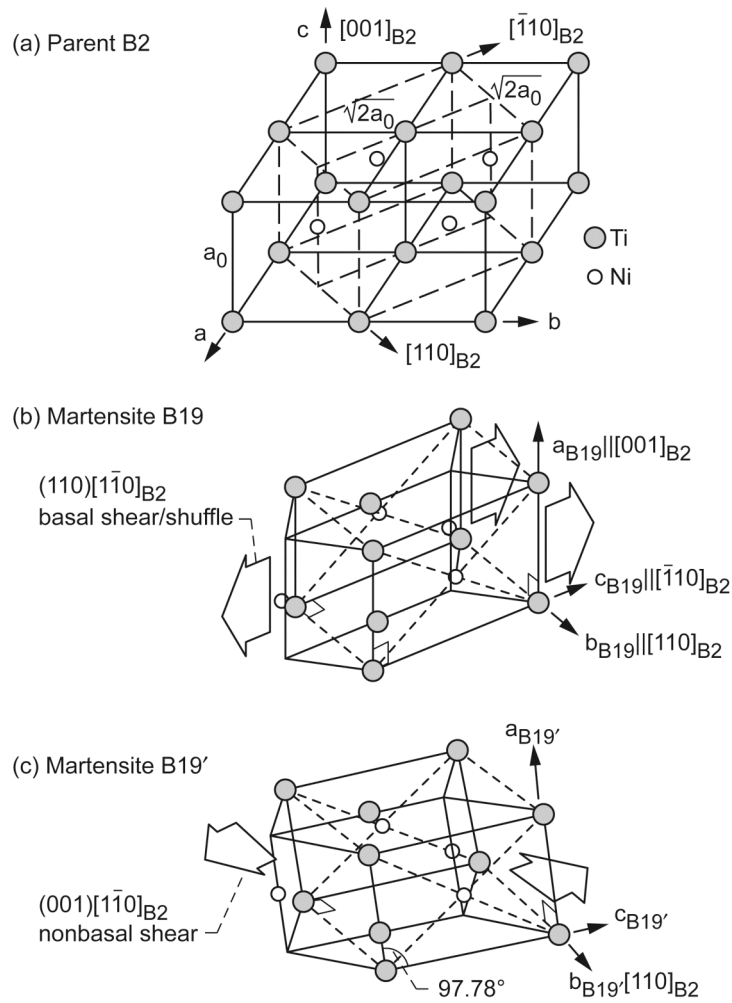
Figure 1.1.—Phase structure of ordered B2 parent "austenite" and the transformational relationship to the B19 and B19´ martensites. (a) A set of four B2 cells with a face-centered tetragonal cell outlined by dashed lines. (b) orthorhombic B19 martensite formed by shear/shuffle of the habit plane $(110)_{B2}$ along $[1\text{-}10]_{B2}$ direction, close packed (habit) planes are indicated by thin dotted lines. (c) monoclinic B19´ martensite formed by a non basal shear $(001)[1\text{-}10]_{B2}$ to the B19 structure to produce a monoclinic β angle, close packed (habit) planes are indicated by thin dotted lines (ref. 21).
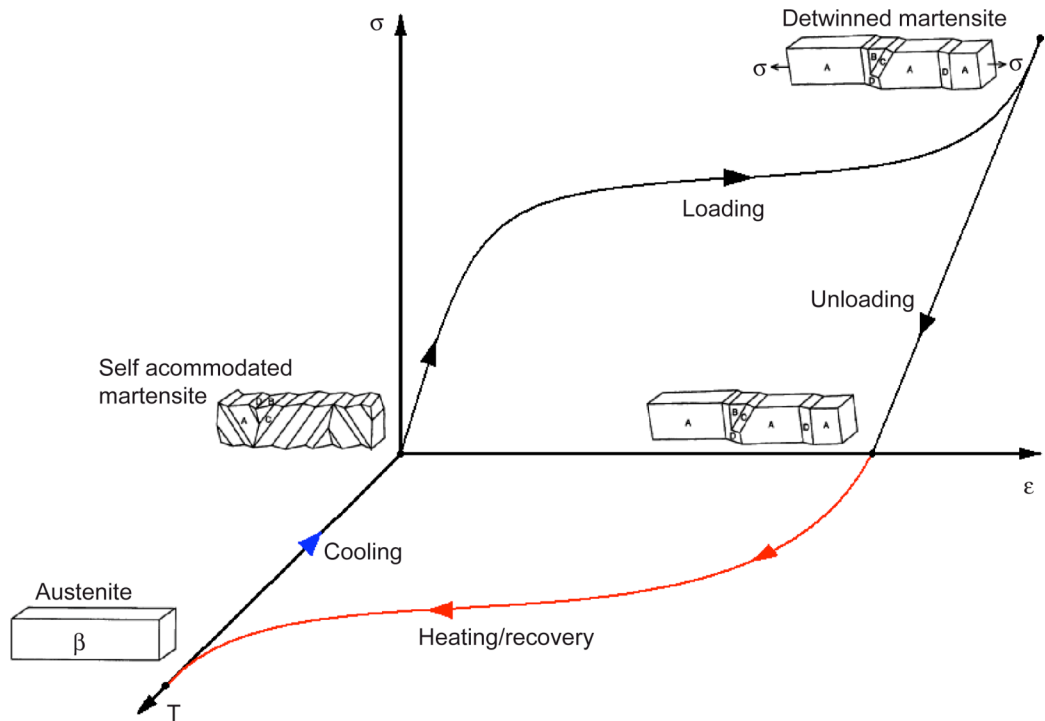
Figure 1.2.—Shape-memory effect wherein high temperature austenite is cooled to form a self accommodated martensite structure. Martensite twins are sheared through the application of stress, and "detwinned" martensite is formed. Heating through transformation to the original high temperature recovers the residual strain by the transformation to austenite.

1.3 Methods for Determining Transformation Temperatures

When cooling the material from the high temperature austenite phase, there is a specific temperature, based on the materials thermomechanical history and present stress state, at which the austenite begins to transform into martensite and also a specific temperature at which this martensite transformation is complete. Likewise, on heating the material from the low temperature martensite state, there are specific temperatures at which the transformation from martensite to austenite, referred to as the reverse transformation (RT) begins and ends. These temperatures are commonly referred to as the martensite start (M_S), martensite finish (M_F), austenite start (A_S), and austenite finish (A_F), respectively (ref. 22). It is important to know these temperatures so that the alloy can be effectively used for a specific application. The thermal hysteresis (H), or difference in temperature between the A_F and M_S temperatures is also important, as it gives an indication of how much time at a certain heating/cooling rate it would take for the material to be cycled between the parent and martensite phases, and also, how precise strain can be controlled with an adjustment in temperature.

In order to determine these transformation temperatures, a variety of standardized methods can be used. Differential scanning calorimetry (DSC) measures the heat transfer between a sample of the material and its surroundings as a function of temperature as it is heated and cooled through the transformation (ref. 23). This information is plotted, and the transformation temperatures measured as the intersection of the base line and the maximum gradient line of a lambda type curve (Figure 1.3(a)). Sometimes it is more useful to measure the temperatures at which the magnitude of the heat flux between the material and its surroundings reaches a maximum during the transformation. In these instances, the martensite peak (M_P) and austenite peak (A_P) are measured as the points in the transformation for which the slope of the curve is equal to zero.

An alternate method, known as a bend free recovery test (BFR), is often used to measure transformation temperatures, but is limited to measurement of only the reverse transformation. In this method, a rectangular bar of the material is bent around a cylindrical mandrel to a specified angle (ref. 24). The sample is then heated through the reverse transformation (RT) and the amount of recovery measured as the instantaneous angle as a function of temperature (Figure 1.3(b)).

Both of the methods described are only used to determine transformation temperatures in a stress free state. Measurements of essentially any other property, such as resistivity, thermal expansion, modulus, etc. can also be used to determine the characteristic transformation temperatures. However, load-bias testing, also known as constant load dilatometry (CLD) can be used to measure transformation temperatures in a more realistic setting. For this test, a sample is held under constant load while it is heated and cooled through the transformation, and the length or strain change in the sample as a function of temperature is recorded. The transformation temperatures are then calculated from the intersections of best fit lines along the linear portions of the curve, corresponding to coefficient of thermal expansion (CTE) strain and the maximum gradient lines of the portions of the data corresponding to the transformations (Figure 1.3(c)).
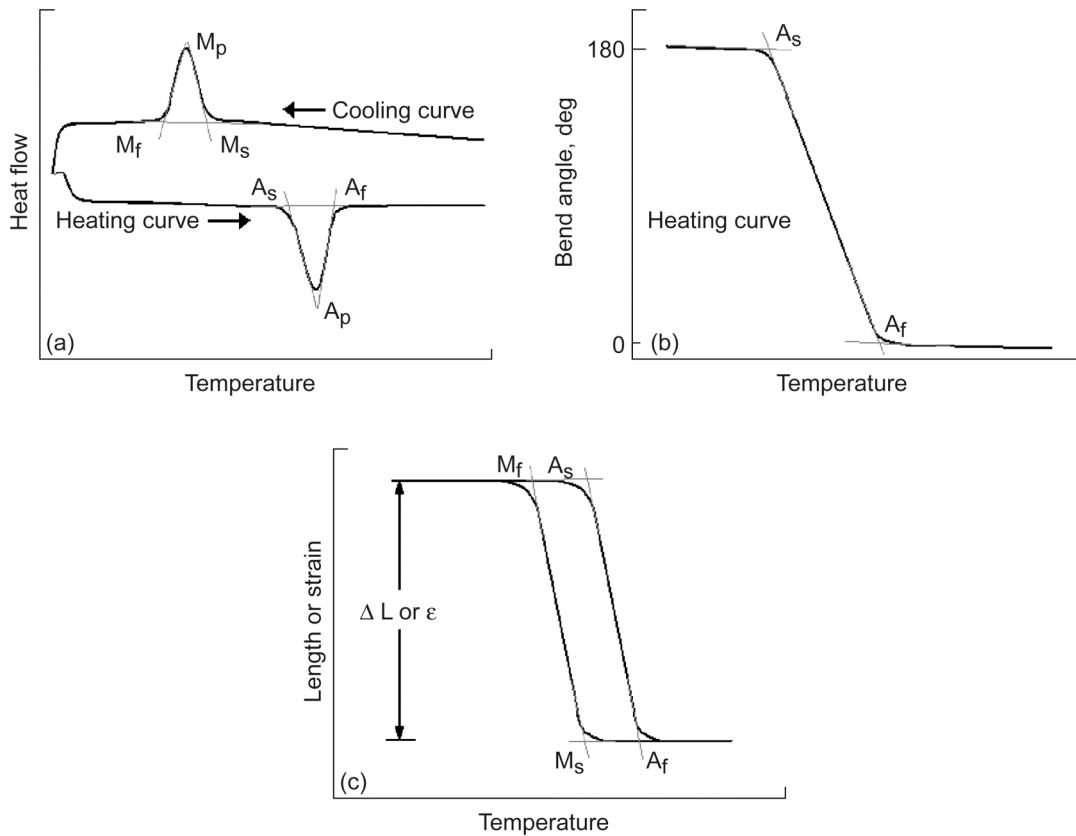
Figure 1.3.—Methods for determination of transformation temperatures: (a) differential scanning calorimetry, (b) bend, free recovery, (c) load-bias/constant-load dilatometry.

1.4 Applications for Shape-Memory Alloys

The discovery of the shape-memory effect has prompted a flurry of investigation into the use of these alloys as actuator materials. In a power to weight comparison, shape-memory alloys can output from 200 to 10,000 W/kg of actuator, comparable to hydraulic actuators and more than either pneumatic actuators or DC motors while occupying much less space (ref. 25). In addition to lower weight and higher energy density than other actuators, shape-memory alloy actuators require minimal volume for placement, have no moving parts that could wear out or produce friction, can be operated on minimal power, and are easier to inspect, all contributing to decreased operational costs. The list of prospective applications for shape-memory and superelastic materials is great, and yet, a lag in the development of appropriate materials has prevented many applications from reaching fruition.

Currently, commercial shape memory alloys are integrated into switches, robotics, controllers, temperature sensitive valves, pipe couplings, and medical implants. Shape-memory alloys tailored to exhibit superelasticity are used to form springs, eyeglass frames, orthodontic arch wires, surgical catheter lead wires, stents, and brassiere underwires. However, there are many more applications which require the development of stable, work-producing high-temperature shape-memory alloys (HTSMAs), such as passive and active control of aerodynamic surfaces, high temperature valves and springs, and automotive applications.

In many cases (aerospace, automotive, and power generation, to name a few), the integration of HTSMA actuators could be used to improve performance and efficiency. For instance, current aircraft engines basically operate in a single configuration meant to be most efficient during a certain portion of the flight envelope. Additional adaptive structures could make these systems more versatile and therefore maximize the performance/efficiency during every part of the operation (Figure 1.4). However, because space is extremely limited and weight is a valuable commodity, hydraulic and pneumatic actuators cannot be used. Shape memory actuators such as NiTi would be ideal due to their low weight, small volume, low power input and high work output. However, because these systems operate at high temperature, and binary NiTi has a transformation temperature range below about 100 °C (ref. 26), systems with higher transformation temperatures have to be developed in order to provide actuation in these applications.
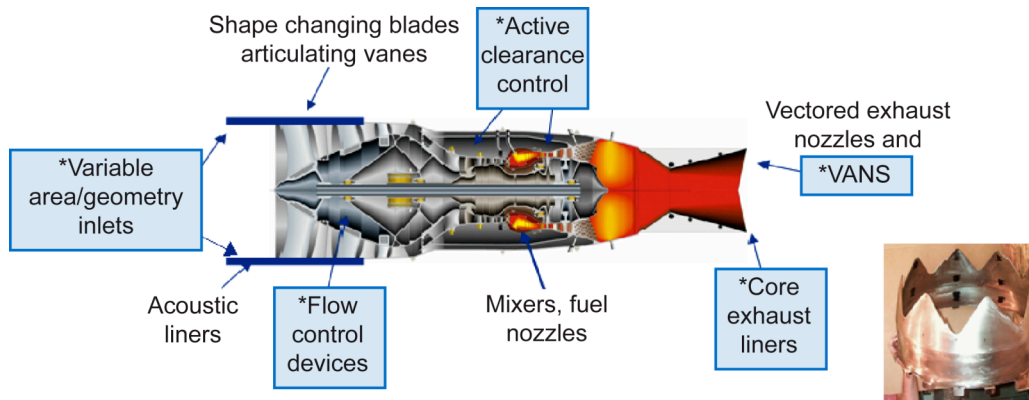
Figure 1.4.—Schematic aircraft engine illustrating areas where high-temperature shape-memory alloy (HTSMA) actuators could be used in adaptive structures to improve versatility and therefore improve performance of the engine throughout the various portions of the flight. Those areas that are currently in development are starred and shown with a box around them.

1.5 Binary NiTi

Of all of the SMA systems discovered, NiTi, dubbed Nitinol after its composition and place of discovery (**Ni Ti N**aval **O**rdnance **L**ab), has been shown to be the most commercially viable and practical alloy for actuator applications. In fully annealed near-stoichiometric NiTi, the high temperature B2 austenite phase transforms directly to monoclinic B19' upon cooling through the transformation, which reverts directly to B2 austenite upon heating. A one directional B2 → R → B19' phase change occurs upon cooling in alloys which have been cycled or thermomechanically treated (refs. 18, 27, 28, and 29). This unidirectionality is logical considering that R phase is an dilatational transformation of B2 which occurs by nucleation and growth at dislocations and other defects in the parent austenite, and so cannot be formed from the B19' martensite (ref. 19).

Transformation temperatures in binary NiTi are highly dependant on composition (refs. 30 to 32). For near equiatomic (Ni~50 at.% Ti) compositions, temperatures drop drastically on the nickel rich side of stoichiometry, ranging from ~70 °C for Ni-50 at.% Ti to approximately –120 °C at only 51 at.% nickel. However, the titanium rich side of stoichiometry is slightly less sensitive to compositional changes, with excess titanium precipitating out as Ti_2Ni, leaving a near stoichiometric matrix composition (Figure 1.5). Small deviations in composition on either side of stoichiometry can give rise to large amounts of precipitation, depending on the aging process (refs. 33 and 34). Hysteresis temperature is small for binary NiTi, ranging from 20 to 40 °C (ref. 35), giving it high bandwidth capability as an actuator. Overall, binary NiTi has a useable transformation temperature (M_S) range from subzero to approximately 70 °C (ref. 26).

Superelasticity in NiTi was first reported in 1981 (refs. 36 and 37), and stable superelasticity (repeatable superelastic behavior during cyclic loading/unloading) accomplished in 1982 (ref. 38). Completely recoverable superelastic strains up to 5 to 8% can be achieved for most compositions, and up to 10% in very specific cases (refs. 39 and 40).
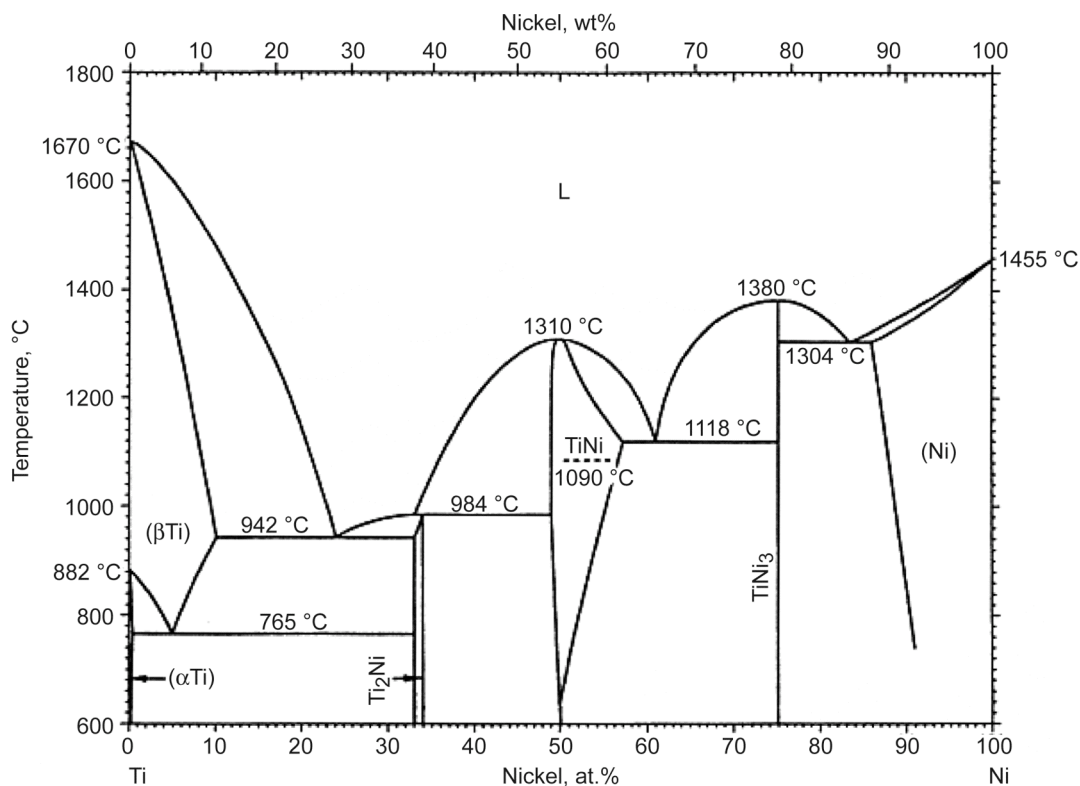
Figure 1.5.—Equilibrium Ti-Ni phase diagram (ref. 50).

Nitinol has many properties desirable for actuators, including small hysteresis temperature, high work output, stable microstructure, and excellent corrosion resistance (refs. 32 and 41). In the shape-memory state, NiTi can produce a peak work output of nearly 21 J/cm^3 (ref. 42) and routine work outputs of 10 J/cm^3 (ref. 43). At low stresses, thermal cycling results in minimal to zero permanent plastic deformation, as low temperature deformation of the martensite is fully recovered by the shear transformations rather than by slip. Corrosion resistance in Nitinol is provided by a strong, stable layer of titanium dioxide which forms on the surface of the material, acting as an inhibitor to corrosion of the bulk (refs. 44 and 45). Though well suited to fulfilling the need for low temperature actuators and superelastic components, NiTi cannot fulfill the need for actuators having ever increasing transformation temperatures. The restriction imposed by its maximum working transformation temperature of ~70 °C is further strengthened by the fact that at elevated temperatures, the mechanical performance of the alloy swiftly degrades as yield strength decreases and superelasticity decreases and disappears (refs. 46 and 47). While its corrosion resistance is sufficient within its operating temperature range, this property also begins to degrade at higher temperatures (refs. 48 and 49).

1.6 NiTiX High-Temperature Shape-Memory Alloys

Applications building on the properties and popularity of the binary NiTi alloys have fueled the ever increasing need for shape-memory alloys having increased transformation temperatures (refs. 21 and 51). To meet the need, several ternary alloy systems such as NiTiAu, NiTiHf, NiTiPd, NiTiPt, and NiTiZr, have been evaluated. For the majority of these alloys, the research performed to this point was very basic, consisting mainly of a determination of transformation temperatures as a function of alloy content, and no-load recovery tests to determine shape-memory behavior (refs. 52 to 55). In each of these systems, transformation temperatures decrease or remain relatively unchanged up to approximately 10 at.% ternary addition. At contents >10 at.%, transformation temperatures increase linearly in relation to ternary addition (Figure 1.6). For those alloy additions which substitute for nickel, this increase in temperature continues until 50 at.% addition at which point the system becomes TiX. For those which substitute for titanium, transformation temperatures can only be improved by additions up to approximately 20 at.%, above which the microstructure is no longer single phase.
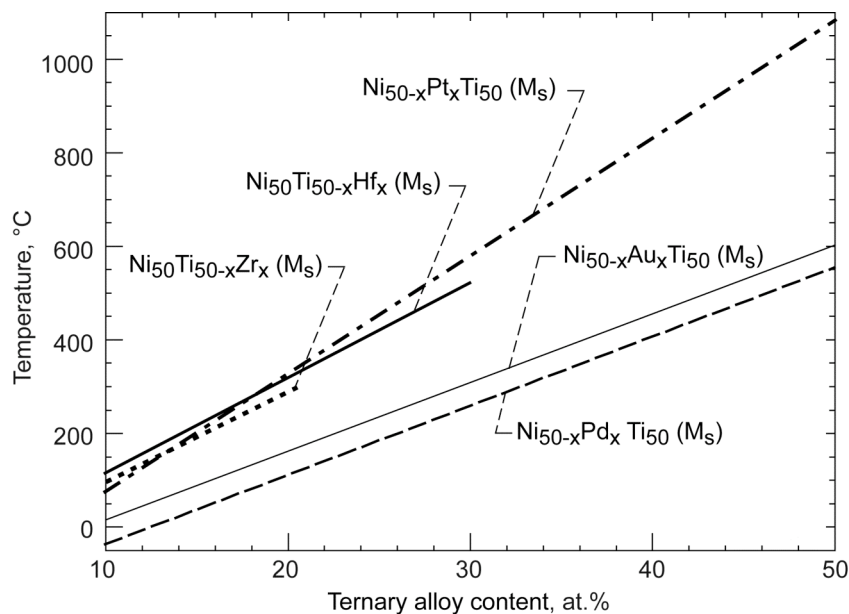
Figure 1.6.—Increase in transformation temperature (M$_s$ or M$_p$) with increasing ternary alloy content for NiTiX alloys (ref. 56).

1.6.1 NiTiPt High-Temperature Shape-Memory Alloys

Presented here is a summary of the NiTiPt system, compositions of which are now being developed in wire form for actuator demonstrations. The purpose is to illustrate the extent of research needed to understand and develop HTSMAs for use as actuators, as well as the properties needed for a good actuator material in general. Of the transformation temperature augmenting alloying additions to NiTi mentioned previously, platinum produces the greatest increase in transformation temperatures per quantity of alloy addition, with Ti – 50 at.% Pt yielding transformation temperatures near 1050 °C (M_S) (refs. 52, 57, 58, and 59). However, though most promising in terms of high temperature ability, the NiTiPt system was one of the least studied systems until recently, when a study focusing on two compositions, $Ni_{30}Ti_{50}Pt_{20}$ and $Ni_{20}Ti_{50}Pt_{30}$ was conducted to determine the microstructure, transformation temperatures, and mechanical and work properties (ref. 60). The $Ni_{30}Ti_{50}Pt_{20}$ and $Ni_{20}Ti_{50}Pt_{30}$ alloys studied had transformation temperatures as shown in Table 1.1.

TABLE 1.1.—TRANSFORMATION TEMPERATURES FOR $NiTiPt_{20}$ AND $NiTiPt_{30}$ ALLOYS STUDIED IN (ref. 60)

Alloy ID	M_F (°C)	M_S (°C)	A_S (°C)	A_F (°C)	Hysteresis ($A_F - M_S$) (°C)	Technique
20Pt (Ext 8)	232	266	271	297	31	DTA
30Pt (Ext 7)	534	560	594	615	55	DTA
30Pt (Ext 19)	529	562	568	597	35	DTA

While both alloys were capable of 100% no-load strain recovery, their actual performances under load varied greatly. In isothermal monotonic yield tests on the 20 at.% platinum alloy, the yield strength at temperature decreased slightly as temperature was increased from room temperature to below the A_S. At temperatures above the A_F, the yield strength increased dramatically. For the 30 at.% platinum alloys, yield strengths decreased continuously from room temperature, through the transformation, and at temperatures above the A_F. Correspondingly, the 20 at.% platinum alloy exhibited good work output, achieving a maximum of 8.7 J/cm^3, while the 30 at.% platinum alloy exhibited poor to no work output, with a maximum of 0.1 J/cm^3. This agrees well with the determination that for a material to exhibit good work output and therefore be useful as a HTSMA actuator, the critical stress for slip must be lower than the critical stress for martensite twin formation or deformation, or at a minimum, the austenite phase must be stronger than the martensite phase (ref. 56).

1.6.2 NiTiPd High-Temperature Shape-Memory Alloys

While not as effective as platinum additions in increasing the transformation temperatures, the increase in transformation temperatures due to palladium additions still make NiTiPd a good candidate as a high temperature shape-memory alloy. For an application requiring a transformation temperature attainable from either of the NiTiPt and NiTiPd systems, NiTiPd could even present itself as being more desirable due to the large difference in material price between expensive platinum and the more economical palladium. In addition to being more cost effective than NiTiPt, NiTiPd alloys are more stable than Hf, Zr, and HfZr alloyed NiTi alloys with regard to microstructure and transformation temperature when thermally cycled, as shown by a comparison of the research from Zhu et al. (ref. 61), Pu et al. (ref. 55), and Hsieh and Wu (refs. 62 and 63).

Nickel and palladium form a continuous solid solution (Figure 1.7) and NiTi and PdTi form a continuous pseudobinary solid solution (ref. 64) from 0 at.% PdTi (100 at.% NiTi) to 100 at.% PdTi (Figure 1.8) with palladium atoms preferentially substituting in nickel lattice sites (ref. 65). Palladium substitutions for nickel in stoichiometric NiTi decrease the M_S transformation-temperature at contents up to 10 at.% palladium ($M_F = -39$ °C, $M_S = -26$ °C, $A_F = -7$ °C) (ref. 52). Above 10 at.%, transformation temperatures increase linearly with palladium content producing alloys with $M_F = 215$ °C and $A_F = 269$ °C for $Ni_{20}Ti_{50}Pd_{30}$ (ref. 68) and up to M_S temperatures as high as 510 to 563 °C for $Ti_{50}Pd_{50}$ (refs. 57, 69, and 70). As in binary NiTi, variations in composition from stoichiometry, $(Ni+Pd)_{50}Ti_{50}$, in a $Ni_{20+x}Pd_{30}Ti_{50-x}$ alloy produced a sharp decrease in transformation temperature with compositions on the nickel rich side, while titanium rich compositions produced a more gradual decrease in transformation temperature as the excess titanium is removed from the matrix by the formation of $Ti_2(Ni,Pd)$ (ref. 71). Hysteresis temperatures for NiTiPd alloys range between 15 and 30 °C (ref. 52), and can possibly be decreased by further thermal cycling (refs. 72 and 73).
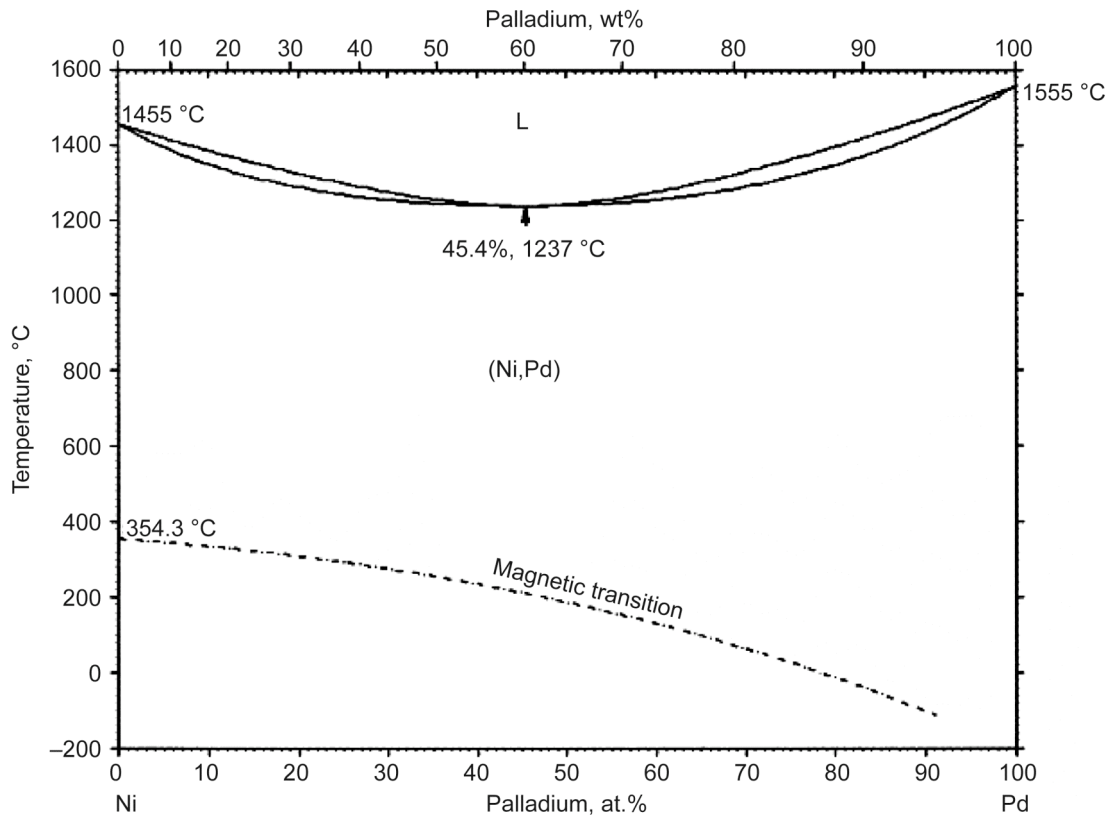
Figure 1.7.—Nickel-palladium equilibrium phase diagram showing complete miscibility between the two elements (ref. 66).
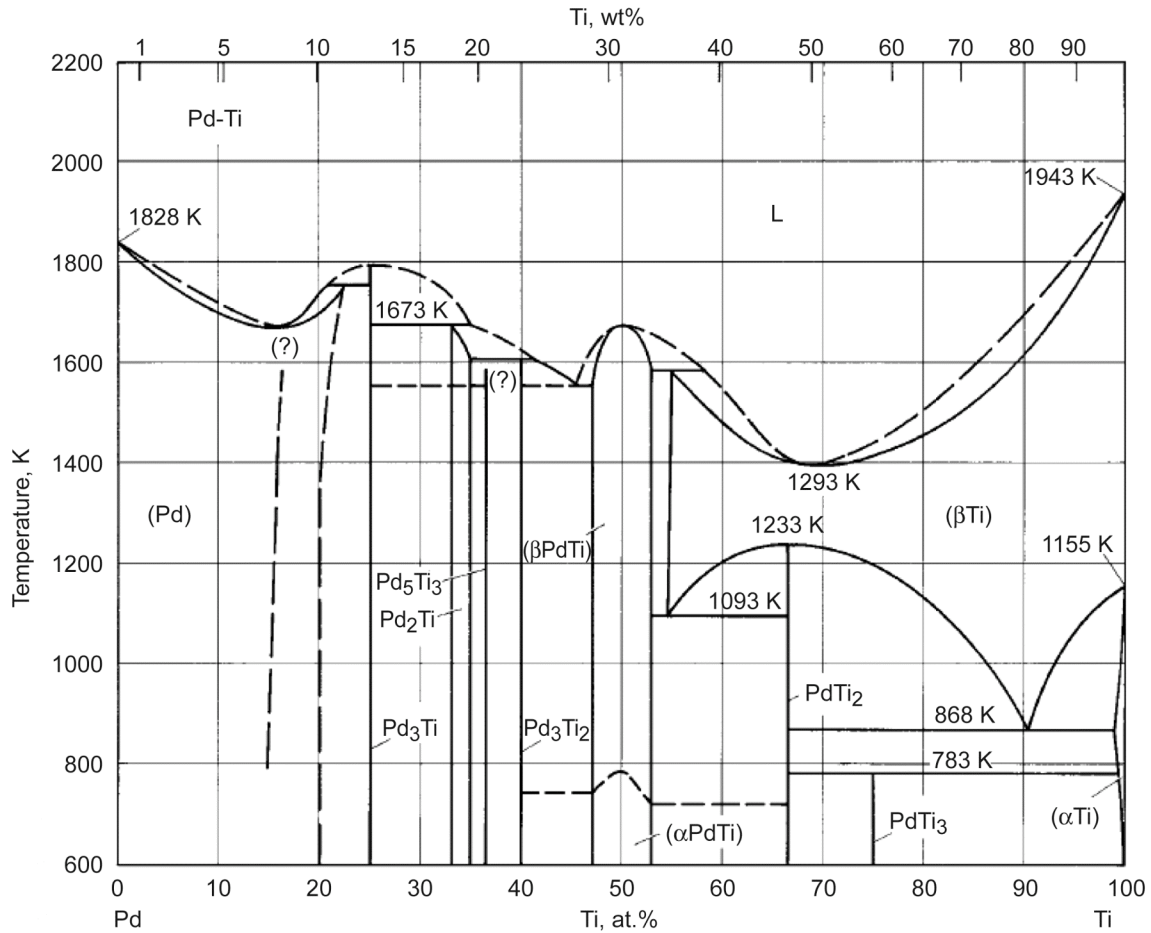
Figure 1.8.—Palladium-titanium equilibrium phase diagram showing the high temperature B2 and low temperature martensite phases near Ti - 50 at.% Pd (ref. 67).

Palladium additions to NiTi also cause changes in the transformation behavior. In annealed NiTi, the B2 phase converts directly to monoclinic B19' upon cooling through the transformation. Along with causing a decrease in transformation temperature, palladium additions of approximately 2 to 10 at.% cause a two step B2 → R → B19' transformation to occur on cooling. Above approximately 10 at.% palladium, a B2 ↔ B19 transformation occurs (refs. 52 and 64), unless the alloy is cooled below 0 °C, in which case, B19 can further transform to B19' for palladium contents up to approximately 17 at.% (ref. 74). Tian and Wu have reported that the B2 ↔ B19 ↔ B19' transformation can also occur in titanium rich samples which have been solution annealed and quenched to prevent precipitation of the excess titanium as Ti_2Ni (ref. 75).

The ability of NiTiPd to achieve unconstrained shape recovery is a function of palladium content, ductility, and test temperature. As the amount of palladium in the alloy increases, the transformation temperatures are increased, but this improvement is offset by a decrease in the maximum recoverable strain. Alloys with palladium compositions near 30 at.% can fully recover strains of up to 6% imposed at room temperature, with the maximum strain being limited by the ductility of the alloy (ref. 52). In $Ni_{13}Pd_{37}Ti_{50}$ strained in torsion, Khachin et al. (ref. 76) achieved complete recovery of 4% strain. Alloys with >40 at.% palladium and TiPd were able to recover at most, 0.5% tensile strain, exhibiting poor shape-memory properties (ref. 77). For a given composition, increases in test temperature decrease the shape-memory recovery ability of the material, as the critical stress for slip decreases with temperature, allowing more of the deformation of the material to be accommodated by slip rather than by martensite twin shear (ref. 78). While the temperatures for recovery and recrystallization increase with palladium

content (ref. 79), with higher palladium content alloys, another problem presents itself; in a Ti-50 at.% Pd alloy, recrystallization was shown to occur in the martensitic phase (refs. 80 and 81), softening the alloy.

Several methods have been proposed to improve the shape-memory characteristics of NiTiPd: solid solution strengthening with a fourth element, precipitate strengthening, and thermomechanical processing. Attempts to solid solution strengthen NiTiPd have been made by alloying with boron. Alloys having compositions of $Ni_{22.3}Pd_{27}Ti_{50.7}$ (ref. 82) and $Ni_{20}Pd_{30}Ti_{50}$ (ref. 83) were doped with boron additions. Neither case resulted in an improvement in shape-memory properties or transformation temperatures. However, Yang and Mikkola (ref. 82) reported an increase in room temperature ductility attributed to the grain refinement effect of the boron, and Suzuki et al. (ref. 83) reported that tensile strength and ductility were nearly doubled at 170 °C by 0.2 at.% boron additions, also probably due to refined grain sizes. An increase in shape-memory behavior was achieved by Shimizu et al. (ref. 71) in a nonstoichiometric $Ti_{50.6}Pd_{30}Ni_{19.4}$ alloy by precipitation of a homogeneous distribution of fine Ti_2Ni type precipitates. The realized recovery rate of ~90% for a sample deformed to 6% tensile strain at 100 °C was an improvement compared to a recovery rate of 76% for a stoichiometric $Ti_{50}Pd_{30}Ni_{20}$ alloy. Goldberg et al. (ref. 78) reported an improvement in recoverable strain in a $Ti_{50}Pd_{30}Ni_{20}$ alloy after cold rolling and annealing at 400 °C, resulting in complete recoverability of >5% tensile strains in samples tested at temperatures up to 247 °C, and superelastic behavior at a temperature of 262 °C. Cai et al. reported increased M_S temperatures and transformation strains in a $Ti_{50.6}Pd_{30}Ni_{19.4}$ alloy through thermal cycling of the sample under load (ref. 84). In both cases where thermomechanical processing was used to improve properties, improvements were attributed to an increased critical stress for slip in the martensite phase through grain refinement or dislocation processes, ensuring that the critical stress for slip was higher than the critical stress for martensite twin deformation. Thus, when stress was applied to the material, any deformation strain was realized as martensite twin shear, which is recoverable, rather than non-recoverable slip. Therefore the recoverable strain (superelastic or transformation) is improved. While there have been a number of other studies on the NiTiPd system, much of it has involved studies on thin films rather than bulk materials (ref. 85), and as with the bulk studies described above, none of this work involved the transformation characteristics of the alloy under load.

1.7 Proposed Research

The need for HTSMAs with transformation temperatures in the range of 100 to 1000 °C is great. Since only a few alloys, such as $Ni_{30}Ti_{50}Pt_{20}$, with transformation temperatures nearing 300 °C have even been identified for possible commercial use as viable actuator materials (stable and work-producing) more effort is needed to develop comparable systems. Thus, development of alloys with similar and greater transformation temperatures, such as those alloys based on NiTiPd, warrant further investigation and development. Consequently, this thesis was conducted in order to further the knowledge and development on the NiTiPd HTSMA system.

Currently, the $Ni_{19.5}Ti_{50.5}Pd_{30}$ alloy is the only one that has been characterized in the literature in any detail in terms of its strength, shape-memory effect, and microstructural stability, but the key properties for actuator applications – work output or shape-memory response under load, as well as dimensional stability are lacking. Evaluations of the strength, work output, and viability of NiTiPd alloys with increasing palladium content have never been published, and therefore are needed. Also needed is a determination of the maximum "practical" palladium alloying content that could be used in a ternary alloy, and therefore the maximum transformation temperatures available for various applications, while still allowing functionality as an actuator. In addition, tests are needed to determine the effect of quaternary alloying on the strengths of the martensite (critical stress for twinning) and austenite (critical stress for slip) phases. Also, the effects of both training and quaternary alloying on dimensional stability need to be evaluated. Finally, the effect of quaternary alloying on the thermal stability needs to be evaluated to determine if the maximum operating temperature of the materials could be increased without detrimentally affecting the strength and performance of the alloy, as a solid state actuator material. All of these research "needs" are addressed in detail in the balance of this thesis.

Chapter 2—Materials and Procedures

2.1 Sample Preparation

Samples were produced and prepared for testing following standard procedures which have been successfully used to produce various other high temperature shape-memory alloys for testing. All steps were completed at the NASA Glenn Research Center in Cleveland, Ohio, except for extrusion, which was performed by Haynes, Inc. in Kokomo, Indiana.

2.1.1 Material Processing

All of the alloys tested were produced by vacuum induction melting of high purity elemental constituents (99.98 wt% Ni, 99.95 Ti, 99.995 Pd, 99.995 Pt, 99.995 Au, 99.5 Hf) in a graphite crucible. Although densities of the constituent materials vary greatly (4.54 g/cm^3 for titanium to 21.45 g/cm^3 for palladium), the circulation of the melt due to the oscillating magnetic field produced by the induction coils ensured complete mixing of the constituents. Melting and casting of the ingots were performed inside a vacuum induction furnace which was evacuated to 10^{-3} torr and subsequently backfilled with argon to a final pressure of 20 torr. This evacuation and backfilling procedure was repeated a total of three times before melting. The induction furnace was equipped with tilt-pour capability, and the melts were cast into a 25.4 mm diameter by 102 mm long copper mold with a funneled pouring basin. The hot top resulting from additional alloy material remaining in the pouring basin was utilized to compensate for shrinkage in the ingot during solidification. Each ingot was homogenized in a vacuum furnace at 1050 °C for 72 hr and allowed to furnace cool. Following homogenization, the ingots were placed into mild steel extrusions cans with a mild steel end cap and then vacuum sealed. Extrusion of all compositions was performed at 900 °C and an area reduction ratio of 7:1.

2.1.2 Sample Machining

The extruded rods for each alloy were cut by electrical discharge machining (EDM) into 50.8 mm long sections, which were then center drilled on each end to allow turning on a lathe. Using a computer numerically controlled lathe (CNC), cylindrical blanks were rough turned to an outside diameter of 9.525 mm to remove the steel can. Both ends were threaded with standard 3/8 inch-24 UNF-2A threads. Samples were then rough and then finish machined to produce a 16.4 mm long by 3.81 mm diameter gage section. The final machining pass utilized a feed rate of 0.0254 mm/revolution and a cutting tool with tip radius of 0.397 mm, resulting in a surface roughness of 0.0002 mm. Final sample dimensions are as shown (Figure 2.1).
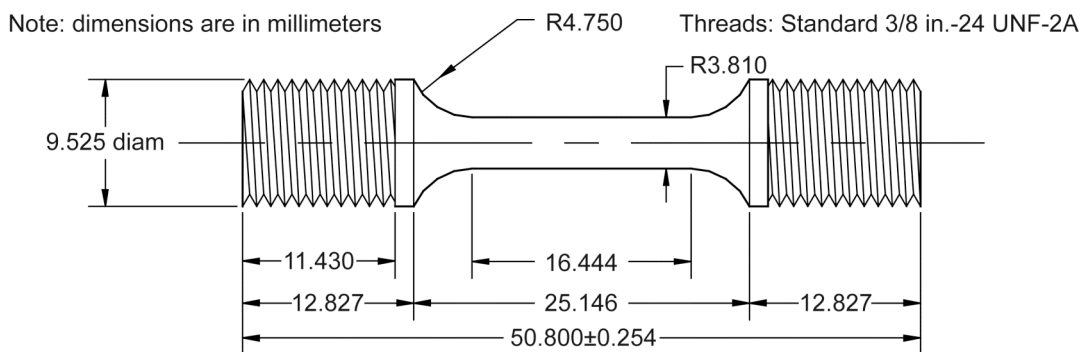
Figure 2.1.—Configuration of the standard cylindrical dog-bone tensile sample.

2.1.3 Pre-test Sample Preparation

Individual tensile samples were double wrapped in tantalum foil, heat treated at 400 °C for 1 hr, and furnace cooled to relieve residual stresses in the material from the extrusion and machining processes. Tantalum foil acts to getter oxygen and reduce oxidation of the sample during heat treatment. One type K thermocouple was spot welded to the gage section of each sample using a Unitek Equipment 250 Dual Pulse Stored Energy Power Supply with maximum output of 250 W at 6700 A. Initially a gentle 5%/8% medium-width dual pulse was used to tack the thermocouple wires axially along the gage section of the sample beginning approximately four millimeters from the middle and ending evenly at the middle. Once intimate contact was achieved between thermocouple wire and sample, a heavier 10%/12% short width pulse was used to strengthen the weld. While ensuring a strong weld, this method reduces the possibility of arcing and limits the likelihood of thermally shocking the sample, either of which could produce a crack initiation site. Also, by welding the wires along the axial direction of the sample rather than circumferentially, the gage section was less susceptible to the detrimental effects of the welding process since no one cross sectional area of the gage contained all of the damage incurred by the attachment process. This technique also provided the added benefit of strengthening the thermocouple wire against premature failure.

2.2 Mechanical Testing

The experimental setup allowed testing of samples in tension at high temperatures up to and including 700 °C. This enabled mechanical characterization of the sample in the martensite and austenite states (monotonic tension) as well as testing over a range of temperatures during thermal cycling at load (load-bias).

2.2.1 Equipment Description

Cylindrical dog-bone samples were tested in an MTS 810 servo-hydraulic load frame utilizing an MTS FlexTest SE 493.02 digital controller and MTS FlexTest Station Manager version 3.5C control software. The digital controller updated at a rate of 1024 samples/second per channel and allowed for multiple control channels to be operated and triggered simultaneously. For example, if required, control could be switched from a strain rate mode to a constant load mode while temperature was independently ramped. The load frame was outfitted with an MTS 609 alignment fixture, 551.21A-03 load cell with a 100 kN/22 kip load capacity, 646 water cooled hydraulic collet grips, and 680 hot grip extension bars with adapter collets (Figure 2.2). Threaded inserts with internal 3/8 inch-24 threads were used to grip the threaded ends of the samples. Strain was measured using an MTS Model 632.51B-04 high temperature extensometer with a 12.7 mm gage length and $-10/20\%$ strain range with a 6 V excitation source. The extensometer used alumina v-chisel extension rods having a 5 mm diameter and 85 mm length, which were held in contact with the sample by a frictionless knife edge holding fixture exerting a 780 gram hold down force (Figures 2.3, 2.4).

Heating was achieved using an Ameritherm NovaStar 7.5 kW induction heater in line with a GC Controls temperature controller, which monitored temperature from the sample thermocouple and took remote setpoint input from the FlexTest system. Power output of the Ameritherm was 7.5 kW at a nominal frequency ranging from 50 to 485 kHz. A three section coil was used to provide inductive coupling to the specimen and hot grip inserts. The middle of the specimen gage section was heated by a single loop coil, while two sets of three loop coils were used to heat the hot-grip inserts to provide temperature uniformity throughout the gage and to counteract heat flow away from the sample to the water cooled grips. Two Acromag 450T-V2-V0-1-DIN-NCR signal isolators running on a 1-10VDC

input and a 1-10VDC, 10 kΩ min output signal were used to prevent signal feedback between the FlexTest SE controller, the GC Controller, and the Ameritherm induction heater. Two Doric 600 Series converters monitored thermocouples spot welded to each hot grip insert and sent 0 to 1370 °C signals to the FlexTest system using a 0 to 10 V range. Cooling of the sample was aided by a muffin fan, which was operated only once the temperature was well below the transformation range (Figure 2.3).
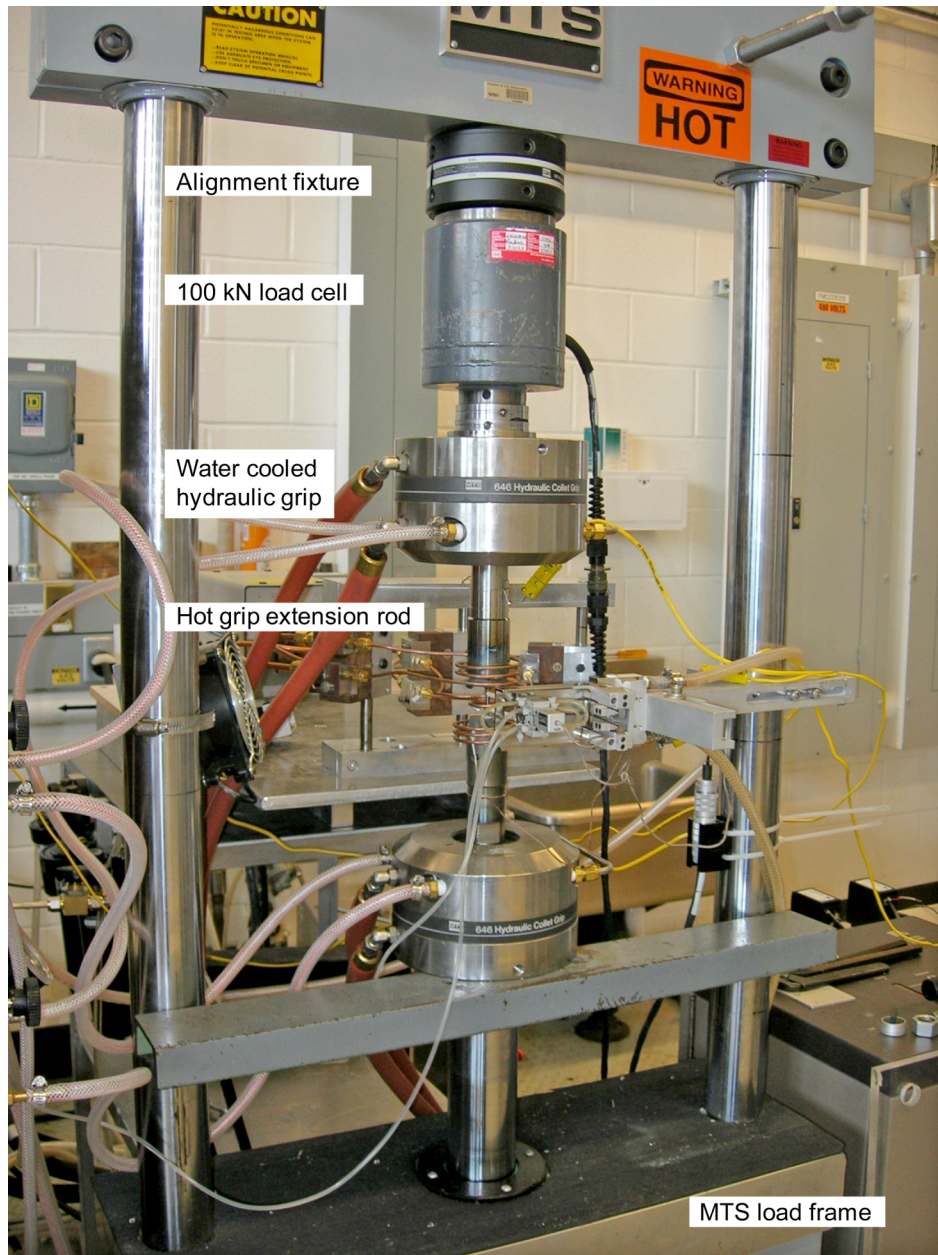
Figure 2.2.—Load frame setup equipped with 100 kN load cell, water cooled hydraulic grips and hot grip extension bars.

MTS 646 hydraulic collet grip

646 Hydraulic Collet Grip

Max.

Muffin fan

Hot grip extension rods

MTS

Knife edge holding fixture

MTS -10/+20% Extensometer
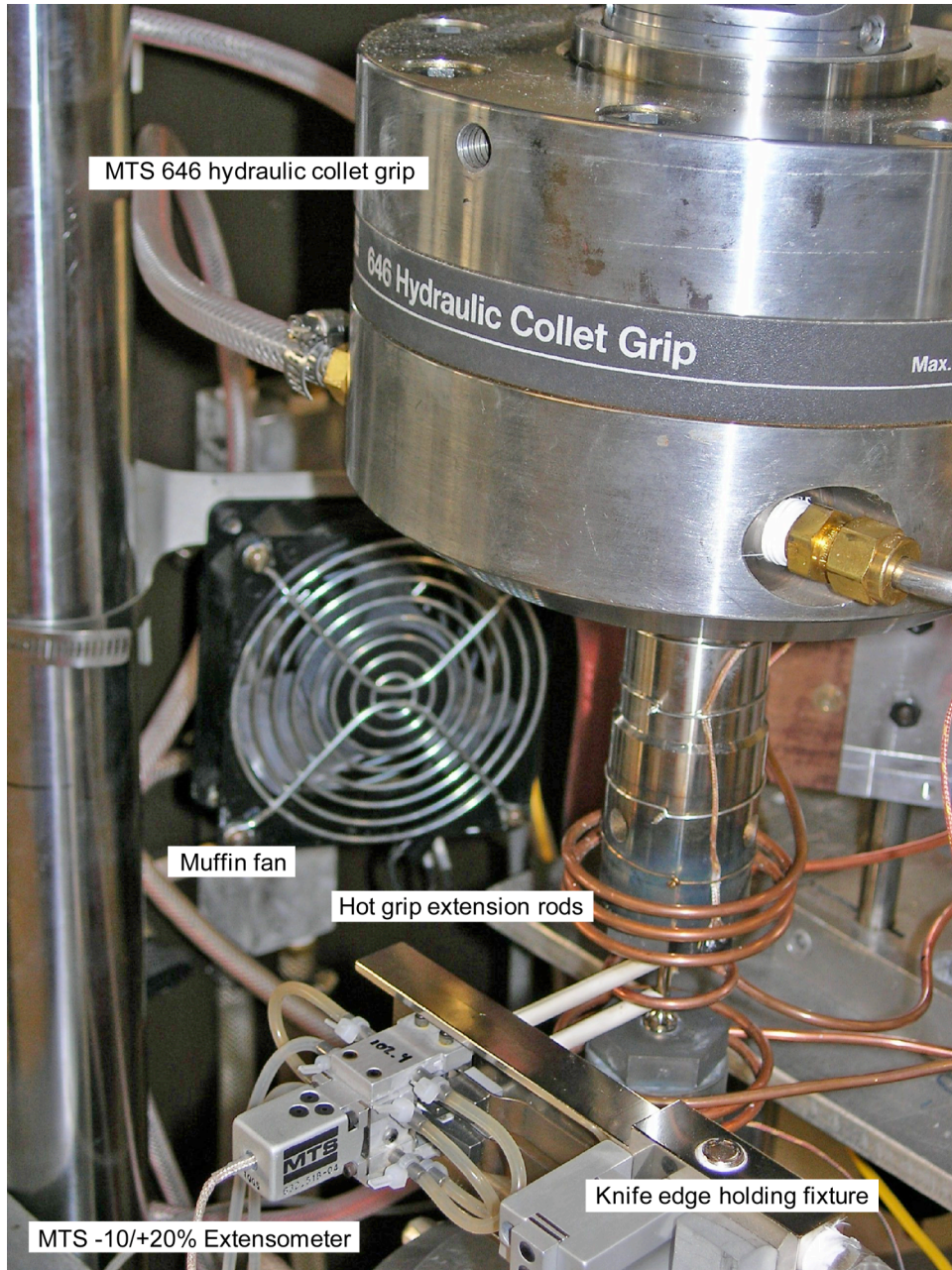
Figure 2.3.—Setup for mechanical testing illustrating placement of collet grips, hot grip extension rods, extensometer, and cooling fan.
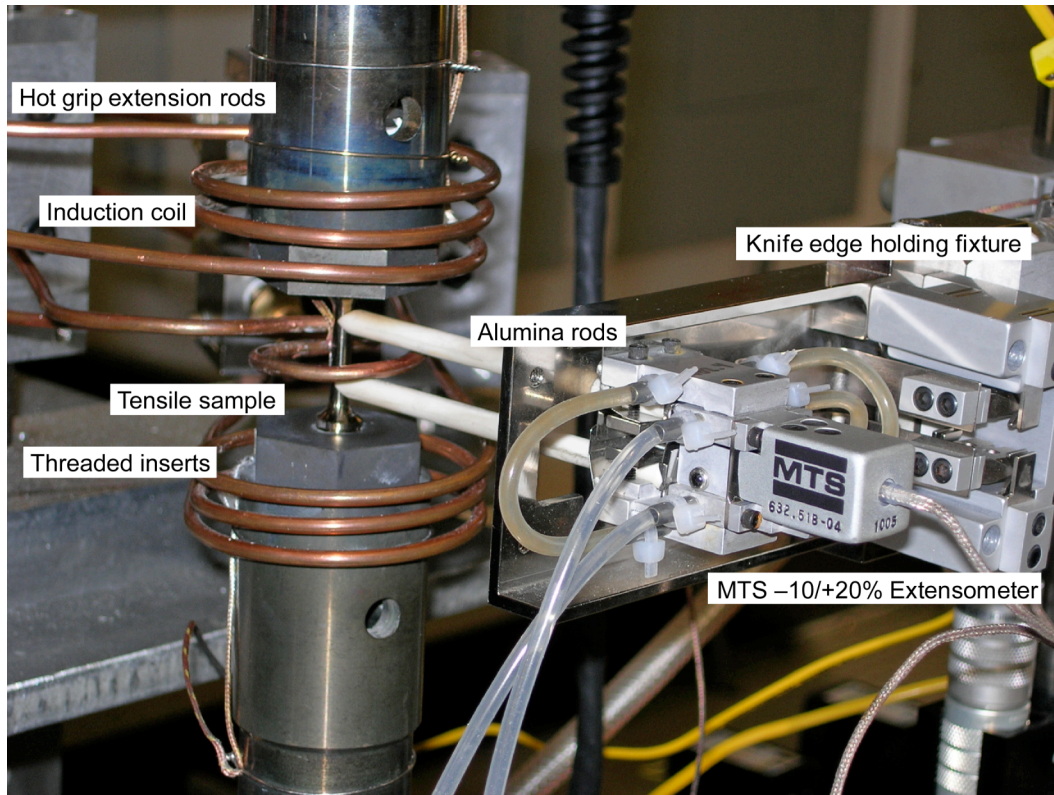
Figure 2.4.—Setup for sample fixturing and heating illustrating placement of hot grip extension rod, threaded insert, extensometer, and tensile sample.

2.2.2 Monotonic Isothermal Tension Tests

Monotonic tension tests were performed on virgin samples by inductively heating them while controlling load at 0 kg, holding at the isothermal test temperature for approximately 5 min to allow any thermal fluctuations to stabilize, and subsequently straining them in strain control at a strain rate of 1×10^{-4} sec^{-1}. For the majority of the alloy compositions, only two monotonic isothermal tension tests were performed: one at 50 °C below M_f, and one at 50 °C above A_f. Using this scheme, the normalized temperatures with respect to absolute zero (T_{Mf-50}/T_{Mf}) and (T_{Af+50}/T_{Af}) vary only between 0.87 and 0.93 for the M_f–50, and 1.06 and 1.14 for the A_f+50 (Appendix A Tables A.1, A.2). In this way, the strength of the material in its fully martensitic or austenitic state could be determined.

2.2.3 Load-Bias Tests

Load-bias tests were performed in tension by straining the sample at a rate of 1×10^{-4} sec^{-1} until the target load was reached, at which point the load was held constant. The sample was then thermally cycled from the low temperature martensitic state through the transformation to a high temperature at which the sample was fully austenitic. Finally, the sample was allowed to cool back through the transformation under load until the initial starting temperature was reached. For the purpose of this thesis, standardized load-bias tests were run whereby the sample was loaded to produce successive equivalent stresses of 0, 99, 197, 295, 393, 517, and 689 MPa, or until failure occurred. For each load applied to the sample, the sample was thermally cycled two times, the first cycle allowing the sample to "reset" at load, and the subsequent cycle used to measure transformation temperatures, "open loop strain", and transformation strain (Figure 2.5) as described below. Transformation temperatures (austenite start (A_S), austenite finish (A_F), martensite start (M_S), and martensite finish (M_F)) were calculated from the intersection of best fit
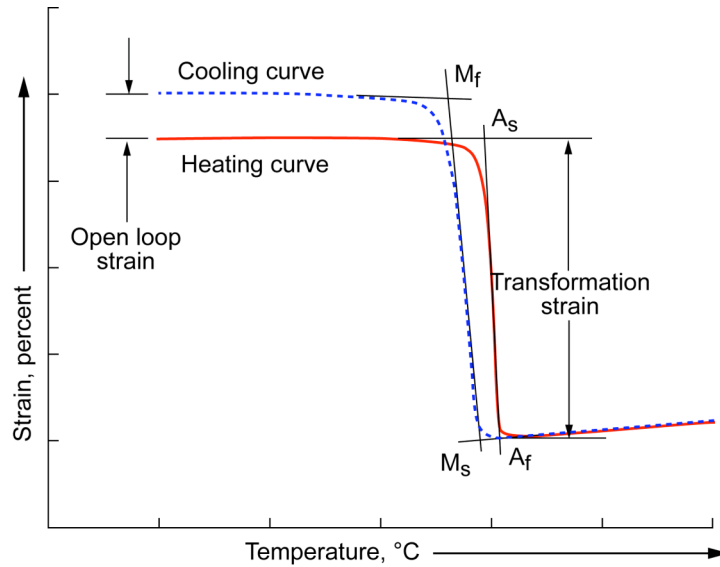
Figure 2.5.—Calculation of the amount of plastic deformation per cycle, referred to as the open loop strain (ε_{OL}), the amount of strain recovered through heating, referred to as the transformation strain (ε_{Tf}), and the transformation temperatures, A_s, A_f, M_s, and M_f from a constant load strain-temperature cycle.

lines along the linear portions of the strain-temperature curves and a best fit line passing through the maximum inflection point of the data within the transformation.

Transformation temperatures indicate the microstructure of a sample at a specific temperature, and can be used to show the effect of stress on the thermodynamics of the transformation. Open loop strain (ε_{OL}) was measured by subtracting the strain at the end of the second cooling cycle from the strain at the beginning of the second heating cycle. This strain is a measurement of the plastic deformation in the sample after a cycle due to dislocation processes. As such, this parameter can be utilized to gain information about the mechanical stability of an alloy. Ideally, an actuator alloy would have an open loop strain of zero, meaning that it would return to the same position cycle after cycle, but most alloys exhibit some amount of plastic deformation or ε_{OL}. Regardless of the contribution of ε_{OL} to the stability of the materials studied, the relative work output (work per volume) (J/cm^3) of the alloy was determined through the use of equation (2.1), where the transformation strain (ε_{Tf}) is calculated as the difference of the respective strains at the A_S and A_F temperatures while the sample is held at a constant applied stress (σ_{app}) (in MPa).

$$Work = \varepsilon_{Tf} * \sigma_{app} \tag{2.1}$$

2.2.4 Training

To determine the effect of thermomechanical processing on alloy properties, training, or thermomechanical cycling, was performed. A cycle is a thermal path whereby the sample is heated from a temperature at which it is in the martensitic state, through the transformation to the austenitic state, and then cooled back through the transformation to the initial start temperature. Samples were "processed" by thermally cycling twice at zero load to relieve any residual stresses from loading, cycling twice at 172 MPa to determine the baseline open loop stress, and cycling ten times at 345 MPa to train the sample.

The samples were then cycled ten times at 172 MPa to determine the effect of the training on the open loop strain. (Stresses were chosen for reasons described in Chapter 5.) The samples were then cycled ten

more times at 345 MPa followed by ten cycles at 172 MPa to determine the effect of further training on the open loop strain and the long term stability of the material.

Standard trained load-bias tests (described in Section 2.2.3) were also performed on trained samples to determine the effect of training on the open loop strain at various stresses as well as the effect of training on transformation strain and work output of the alloy.

2.2.5 Thermal Stability

Samples were also evaluated for dimensional stability at elevated temperatures by running thermal stability tests. For this set of tests, trained samples were cycled thermally between 50 °C and some upper temperature under a constant load equivalent to 172 MPa. The sample was cycled originally ten times, with the upper temperature reaching 350 °C, and both the transformation strains and open loop strains were measured. Once completed, the upper temperature of the cycle was increased by 10 °C and ten additional thermal cycles under load were performed. This process was repeated until ten cycles with an upper temperature of 450 °C were completed. The data was then used to assess the stability of the alloy with respect to the upper cycling temperature.

2.3 Material Characterization

Material characterization was performed on specimens of each alloy composition after final heat treatment. This consisted of chemical analysis and density measurements to measure the composition and density of each alloy, and microscopy to determine the types and amounts of phases present. These data were used to determine the effect, if any, of alloy additions on the microstructure, as well as to confirm the stoichiometry of each alloy.

2.3.1 Chemical Analysis and Density

Chemical analysis was performed to quantitatively determine bulk compositions and impurity content. Specimen preparation consisted of removal of any surface contamination using abrasive paper or a rotary dremmel tool and rinsing with petroleum ether to remove surface oils. Compositions of metallic elements and impurities were determined using the Varian Vista Pro Inductively Coupled Plasma (ICP) Emission Spectrometer, with a maximum process error of plus/minus 1 to 3% of the measured value. Nitrogen and oxygen contents were determined using the Leco TC-436 Nitrogen/Oxygen Determinator. Carbon and sulfur contents were measured using the Leco CS-444LS Carbon/Sulfur Determinator. Archimedes' Principle was used to calculate the density of samples weighed in a Mettler XS205 Analytical Balance with an attached density apparatus. Samples were weighed while in air and while submersed in a known-density liquid. For a more detailed description of the methods used for chemical analysis and density measurements, see Appendix B.

2.3.2 Scanning Electron Microscopy

Samples for scanning electron microscopy were analyzed in the as-polished condition. They were prepared for microstructural analysis using a Streuers Prepamatic 7 automatic polishing machine. Samples were initially ground using a 220 grit piano wheel. Following rough grinding, the samples were polished using three intermediate steps: 6 μm diamond slurry, 3 μm diamond slurry, and 1 μm diamond slurry. The final step involved an attack polish using colloidal silica, water, hydrogen peroxide, and ammonium hydroxide to help remove any scratches left over from the previous steps.

Samples were imaged using JEOL 840 SEM and Hitachi 4700 FE-SEM along with a Phillips CM-200 TEM. Energy dispersive x-ray spectroscopy (EDS) was used to qualitatively discern the relative fractions of constituent elements in each phase or type of particle imaged. The results of the EDS were used along with data from previous SEM and TEM studies to identify the phases and particles present. Particle sizes and volume fractions were measured using digital image processing of SEM photos.

Dynamic Young's modulus, shear modulus, and Poisson's ratio were determined by impulse excitation of vibration (ref. 86). During this test, the sample was heated at a rate of 200 °C/hr and temperature measured via a thermocouple located near the sample. Note that actual sample temperature could not be measured because thermocouple attachment would have interfered with the modulus measurements. Also, the martensite to austenite phase transformation is very endothermic, and so during transformation, sample temperatures were actually lower than the measured furnace temperature. However, during the zero-load load-bias tests used to determine transformation temperatures, the thermocouple was attached to the specimen, giving accurate transformation temperatures with behavior. Therefore, the data from the dynamic modulus measurements was adjusted to reflect the transformational behavior at the correct temperatures.

Chapter 3—Properties of Ternary Ni-Ti-Pd Alloys

3.1 Material Characterization

Five different ternary $Ni_{49.5-X}Ti_{50.5}Pd_X$ alloys (x = 15, 20, 25, 30, 46) were melted, cast, homogenized, and extruded as described previously. Hereafter the alloys are differentiated by palladium content and/or in-house extrusion number such that the $Ni_{34.5}Ti_{50.5}Pd_{15}$ alloy would be referred to as Ext 36 or 15Pd, for example. See Table 3.1 for a cross reference between extrusion number and alloy composition. Density was measured as a basic material characteristic. Unlike many other alloy systems where compositions can vary by a percent or two without largely affecting properties, those of NiTi based shape-memory alloys such as NiTiPd can vary widely with only a fraction of a percent variation in composition from stoichiometry ($Ni_{50-x}Ti_{50}Pd_x$). To ensure that the final matrix composition was near stoichiometric but not nickel rich, which would have caused decreased transformation temperatures, a slightly titanium rich aim composition ($Ni_{49.5-x}Ti_{50.5}Pd_x$) was chosen for all alloys. Measurements of the actual compositions were made after extrusion and heat treatment for comparison to the target compositions and to determine the amount of carbon, nitrogen, and oxygen present. Microstructural analysis of each alloy was performed to determine the phases present and their relative amounts to corroborate data from the chemical analysis as to the stoichiometry of each alloy. Also, measurements were taken of the size and volume fraction of any minor phases present.

TABLE 3.1.—COMPOSITION AND DENSITY FOR THE FIVE TERNARY NiTiPd
ALLOYS PROCESSED

Sample ID	Density g/cm^3 Ti:Ni eq	Ti	Ni	Pd	Au	C	N	O	
Ext. 36		39.41	33.55	26.84	0.03	0.09	0.00	0.04	wt%
15Pd	**6.974**								
at.%	*49.7:49.7*	*49.7*	*34.5*	*15.2*	*0.0*	*0.4*	*0.011*	*0.2*	*at.%*
Ext. 37		38.11	27.61	34.11	0.03	0.065	0.002	0.039	wt%
20Pd	**7.231**								
at.%	*49.9:49.6*	*49.9*	*29.5*	*20.1*	*0.0*	*0.3*	*0.009*	*0.2*	*at.%*
Ext. 38		36.29	21.89	40.97	0.73	0.055	0.002	0.039	wt%
25Pd	**7.406**								
at.%	*49.6:49.8*	*49.6*	*24.4*	*25.2*	*0.2*	*0.06*	*0.011*	*0.16*	*at.%*
Ext. 24		35.20	16.98	47.65	0.01	0.078	0.004	0.061	wt%
30Pd	**7.504**								
at.%	*49.6:49.7*	*49.6*	*19.5*	*30.2*	*0.0*	*0.4*	*0.017*	*0.3*	*at.%*
Ext. 50		31.51	2.76	65.53	0.01	0.075	0.004	0.078	wt%
46Pd	**8.087**								
at.%	*49.4:49.7*	*49.4*	*3.5*	*46.2*	*0.0*	*0.5*	*0.023*	*0.4*	*at.%*

3.1.1 Composition and Density

Density of the five prepared ternary alloys increased linearly with palladium content, from 6.97 g-cm^{-3} for the 15 at.% palladium alloy to 8.09 g-cm^{-3} for the 46 at.% palladium alloy (Table 3.1). Quantitative chemical analysis (Table 3.1) conducted on the alloys revealed that the nickel compositions were on target, with a maximum measured deviation of 0.08 at.% The average titanium composition was 49.6 at.%, which with process error, still overlaps the specified composition of 50.5 at.% titanium. Nitrogen ranged from 0.009 to 0.023 at.% Carbon and oxygen contents for all five alloys were from 0.3 to

0.5 at.% and 0.2 to 0.5 at.% respectively, with the exception of the $Ni_{24.5}Ti_{50.5}Pd_{25}$ alloy, which contained 0.06 at.% carbon and 0.16 at.% oxygen. Even though the ratios of Ti:Ni-equivalents (Ni + Pd) from the quantitative analysis indicate that some of the alloys may be slightly nickel-equivalent rich (e.g., 49.4:49.7 for the 46Pd alloy), the ultimate determination of the composition of each alloy relative to stoichiometry, given the uncertainty in the compositional analysis (±2% of the measured value), comes from an analysis of the microstructure.

3.1.2 Microstructure

Scanning electron microscopy of the five ternary NiTiPd alloys after extrusion and heat treatment revealed a room temperature martensitic microstructure with a low density distribution of two types of particles (Figure 3.1). Experience has shown that in titanium rich alloys, titanium loss occurs during melting and casting due to the formation of TiC which lowers the titanium composition of the final matrix. If, perchance, there is still titanium in excess of 50 at.% in the melt after the formation of the carbides, this will also be drawn out by the formation of Ti_2Ni type particles or Ti_4Ni_2O, leaving a near stoichiometric matrix. The first of the two types of particles, indicated on the SEM micrographs as the black phase, was previously determined via TEM to be Ti(C,O) with an fcc NaCl type crystal structure with Fm3m symmetry (ref. 87).

Energy dispersive x-ray spectroscopy (EDS) of the gray particles showed that they were titanium rich TiNiPd particles. Previous TEM analysis on similar particles in $Ni_{19.5}Ti_{50.5}Pd_{30}$ determined that they were $Ti_2(Ni,Pd)$ (ref. 87), an intermetallic phase which formed interdendritically during the solidification of a titanium rich melt and had the same crystalline structure as Ti_2Ni, which similarly occurs in titanium rich binary NiTi. When studied in the SEM using EDS, the relative fractions of the elements in the $Ti_2(Ni,Pd)$ phase, the particle morphology, and phase volume fractions were similar to those originally studied and identified in a previous TEM study (ref. 87). Given these similarities, the fact that there is almost no solubility for excess titanium in these materials and, therefore, no chance for precipitation by aging, the fact that the EDS showed this phase to be titanium rich, and that there is only one second phase likely on the titanium rich side of stoichiometry, it was determined that the intermetallic phase in all the ternary alloys was $Ti_2(Ni,Pd)$.

Oxygen can be found in either the Ti(O,C) or as part of an oxygen stabilized Ti_4Ni_2O phase. The only way to differentiate between TiO, TiN, and TiC is by a measurement of the lattice parameters: TiO = 4.177 Å, TiN = 4.256 Å, and TiC = 4.3285 Å (ref. 66). In the Ni19.5Ti50.5Pd30 alloy, for example, the Ti(O,C) particle has a lattice parameter of 4.4 Å. However, the Ti_4Ni_2O and Ti_2Ni have the same crystal structure and lattice parameters, and so are virtually indistinguishable. Both types of particles, the Ti(O,C,N) and the $Ti_2(Ni,Pd)$ were present in all five alloys and ranged in size from approximately 0.5 to 3 μm and 0.5 to 8 μm in diameter, respectively. The volume fraction of Ti(O,C) ranged from 0.5 to 0.7% and that of $Ti_2(Ni,Pd)$ from 1.5 to 3.3%, with no alloy having more than a total of 4 vol% of particles (Table 3.2).

TABLE 3.2.—SIZE AND VOLUME FRACTION OF SECOND PHASE PARTICLES IN NiTiPd ALLOYS

Aim Composition (at.%)			Extrusion (#)	Particle Size (μm) (min, max, avg)						Volume Fraction (%)	
Ni	Ti	Pd		Ti(C, N)			Ti₂(Ni,Pd)			Ti(C, N)	Ti₂(Ni,Pd)
34.5	50.5	15	36	0.5	2.65	1.09	0.69	2.99	1.41	0.52	2.12
29.5	50.5	20	37	0.5	2.00	1.14	0.69	7.71	1.89	0.59	1.83
24.5	50.5	25	38	0.5	2.99	1.11	0.69	4.48	1.3	0.49	1.48
19.5	50.5	30	24	0.5	1.78	0.97	0.36	3.55	1.49	0.72	3.26
3.5	50.5	46	50	0.5	2.17	1.03	0.55	4.54	1.59	0.70	2.26
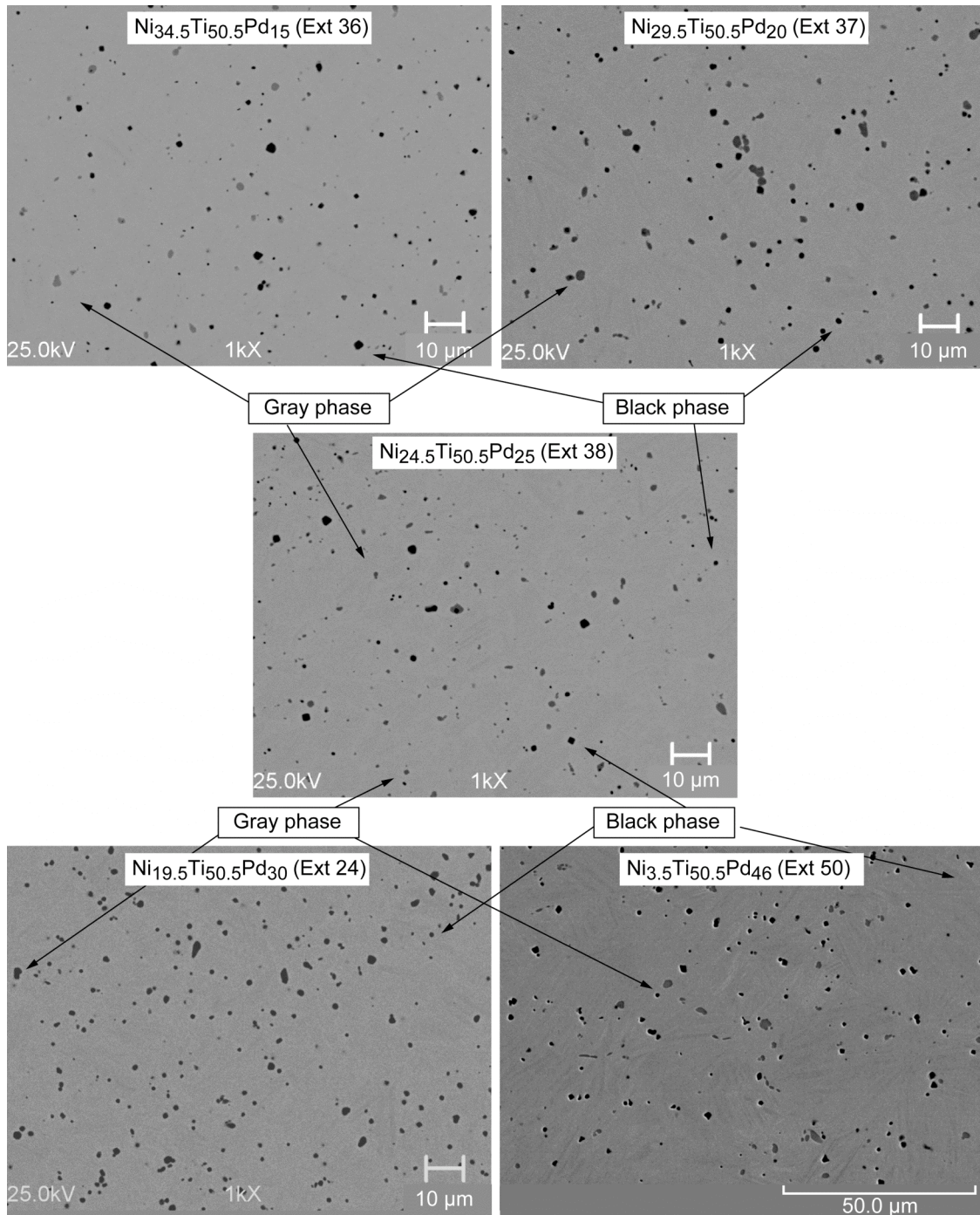
Figure 3.1.—SEM photomicrographs of the five ternary alloys showing a low density distribution of $Ti_2(Ni,Pd)$ type particles (gray phase) and $Ti(O,C)$ particles (black phase).

3.2 Transformation Temperatures

The transformation temperatures of each alloy were determined from zero-load load-bias curves in which samples were held at essentially 0 kg and cycled at a rate of 20 °C/min from 50 °C to at least 100 °C above the temperature at which the transformation was seen to finish (Figure 3.2). These curves indicate a single phase transformation between martensite and austenite in all alloys, except for that of $Ni_{34.5}Ti_{50.5}Pd_{15}$. Behavior in the $Ni_{34.5}Ti_{50.5}Pd_{15}$ alloy could have resulted from several different factors. First, because the alloy was a low palladium content alloy with a thermomechanical history from extrusion and heat treatment, the observed behavior could be an indication of a two phase transformation involving the R-phase or transformation from orthorhombic to monoclinic martensite. A second plausible explanation is that in these alloys, the dynamic modulus is fairly linear with temperature above and below the transformation, but drops drastically from the A_S to the A_F temperatures (Figure 3.3). Since tuning on the digital controller for the frame was performed using a sample at room temperature, where the modulus is higher, when the modulus drops as the sample transforms, load control can become somewhat erratic, and although load variation was only a few kilograms, the softening of the alloy could have lead to instantaneous over-straining of the sample. The last possible cause is that this behavior was a result of differential heating, since one grip was a few degrees warmer than the other. Further testing is underway to determine the exact cause.
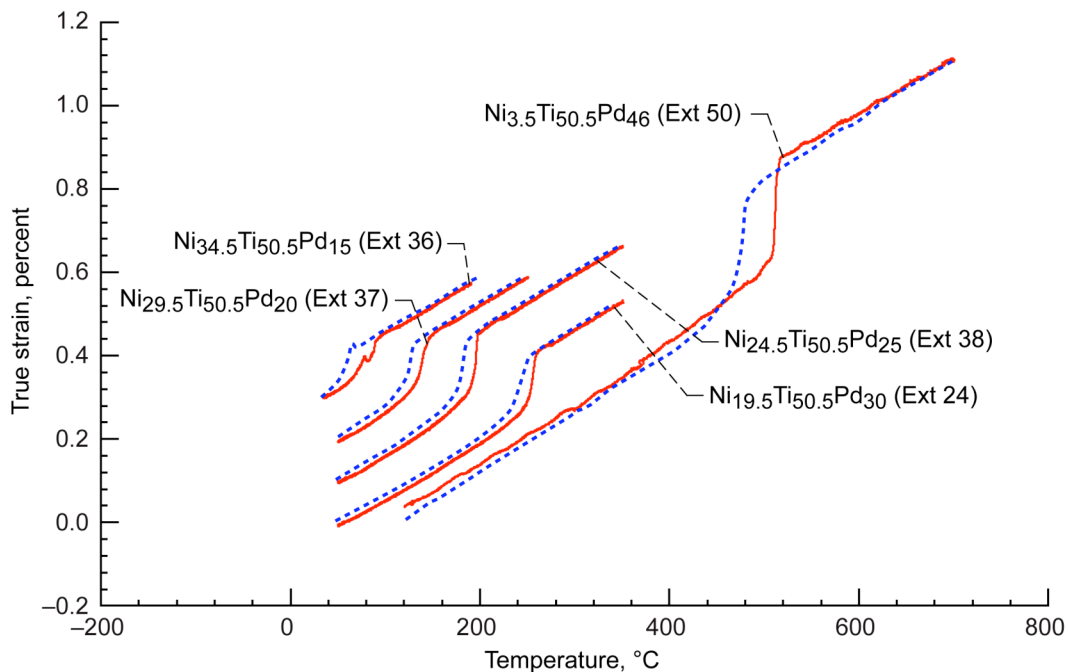
Figure 3.2.—No-load load-bias curves for each of the five ternary NiTiPd alloys showing transformations of each during heating from the low temperature martensite phase to the high temperature austenite phase, and cooling back to the initial state.
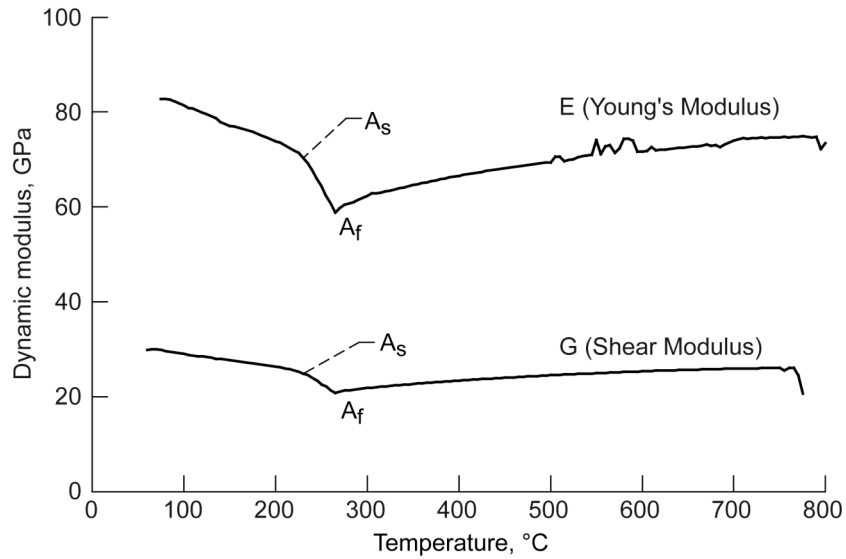
Figure 3.3.—Dynamic modulus measurements with respect to temperature for $Ni_{19.5}Ti_{50.5}Pd_{30}$ showing decreases in the Young's and shear moduli that occur during heating through the transformation.
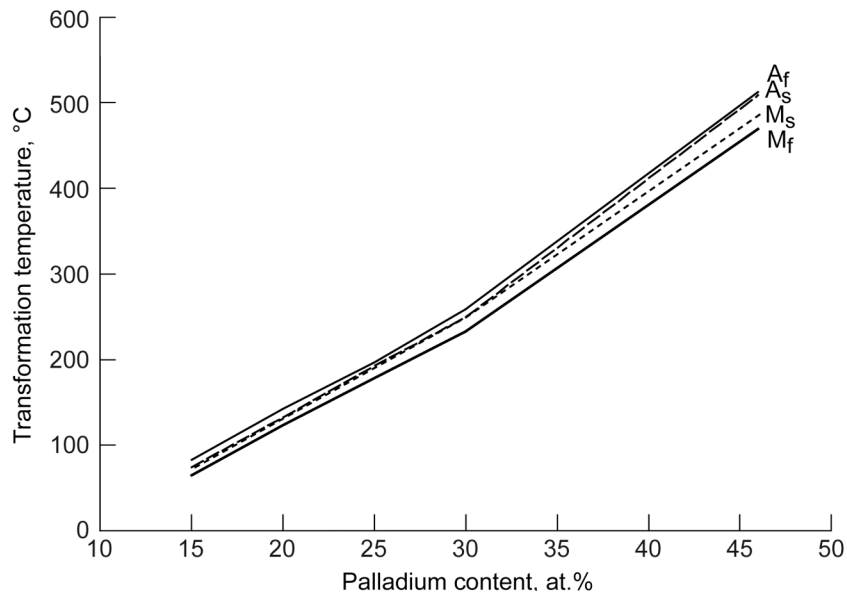
Figure 3.4.—Variation in transformation temperatures with change in palladium content for the NiTiPd alloys studied.

Transformation temperatures varied linearly with palladium content, ranging from 65 °C (M_S) in the $Ni_{34.5}Ti_{50.5}Pd_{15}$ alloy to 469 °C (M_S) in $Ni_{3.5}Ti_{50.5}Pd_{46}$ (Table 3.3, Figure 3.4). The hysteresis measurement A_F-M_S is essentially the same at approximately 10 °C for all alloy contents up to $Ni_{19.5}Ti_{50.5}Pd_{30}$, and only rises to 28 °C for the $Ni_{3.5}Ti_{50.5}Pd_{46}$ alloy. Assuming parallel transformation curves between the A_S/A_F and M_F/M_S, this value is a measurement of how much temperature change is needed to change the direction of transformation, once the material has already partially transformed. The full transformation range between the A_F and M_F, a measurement of the width of the entire transformation, rises from ~19 °C for

the 15, 20, and 25 at.% palladium alloys to 26 and 44 °C for the 30 and 46 at.% alloys, respectively. Hysteresis measurements give an indication of the actuator bandwidth—how quickly the material can be cycled between the fully austenitic and fully martensitic states. Transformation temperatures tell a user what upper temperature the material can be held at and still retain the ability to transform or actuate (A_S), and how far the sample needs to be cooled from the austenite state to fully reset the alloy (M_F).

TABLE 3.3.—TRANSFORMATION TEMPERATURES AND HYSTERESIS

Composition (at.%)			Extrusion	Transformation Temperature (°C)				Hysteresis (°C)	
Ni	Ti	Pd		M_F	M_S	A_S	A_F	A_F-M_S	A_F-M_F
34.5	50.5	15	36	65	73	75	83	10	18
29.5	50.5	20	37	123	132	133	143	11	20
24.5	50.5	25	38	178	190	193	197	7	19
19.5	50.5	30	20	214	241	238	265	24	51
19.5	50.5	30	24	233	249	250	259	10	26
3.5	50.5	46	50	469	485	509	513	28	44

3.3 Isothermal Monotonic Tension Testing

From previous experience, it is known that one condition for a viable SMA actuator material is that the material must be stronger when fully austenitic than when fully martensitic. For a viable actuator, the critical stress for slip, indicated by the yield stress in the austenite state must be greater than the critical stress for martensite twin formation or deformation (boundary migration). In this way, stress induced deformation of a sample will be reflected as deformation of the martensite twins (which is reversible), rather than deformation via dislocation processes (which is permanent). Also, when a load is applied in order to strain the martensite and held constant through transformation to gain work from the shape change, the higher critical stress for slip in the austenite will prevent permanent deformation caused by the applied load such that any deformation of the austenite is purely elastic (and therefore also reversible). Thus, using this knowledge and the yield data from the monotonic tension tests, alloys can be screened using monotonic tension tests to determine compositions that would be sub-optimal as actuator materials.

Each alloy produced was tested in monotonic tension at a minimum of two isothermal temperatures (M_F–50 °C and A_F+50 °C) to determine the relative strengths of the austenite and martensite phases (Figures 3.5, 3.6). With increasing palladium content from 15 to 46 at.%, the yield strength of the martensitic phase (M_F–50 °C), which is a measurement of the critical stress for shear, or detwinning, gradually increased from 97 to 365 MPa (Table 3.4). In the same alloys with palladium content ranging from 15 to 20 at.%, the yield strength of the austenite phase decreased steadily from 437 MPa for 15 at.% palladium to a minimum of 98 MPa for the 46 at.% palladium alloy. Therefore, as each alloy goes through the transformation from martensite to austenite, there is a change in yield stress corresponding to the change in crystalline structure. This is referred to here as the relative yield strength, or the difference between the yield stress of the material in the austenite and martensite conditions, σ_y^A-σ_y^M.

TABLE 3.4.—YIELD STRESS FOR MARTENSITE AND AUSTENITE PHASES WITH RELATIVE VALUES CALCULATED FROM THE EXPERIMENTAL DATA

Pd Content (at %)	Extrusion	Martensite 0.2% Yield Stress (MPa)	Austenite 0.2% Yield Stress (MPa)	ΔYield (A_Y-M_Y) (MPa)
15	36	97	437	340
20	37	131	443	312
25	38	164	423	259
30	24	196	355	159
46	46	365	98	−267
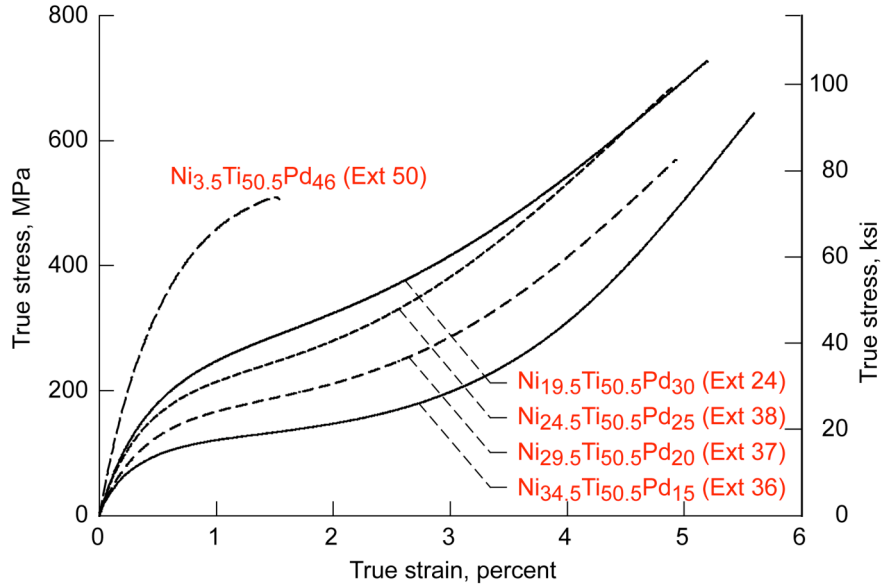
Figure 3.5.—Results for monotonic tension tests for the five ternary alloys at temperatures equal to M_F–50 °C.
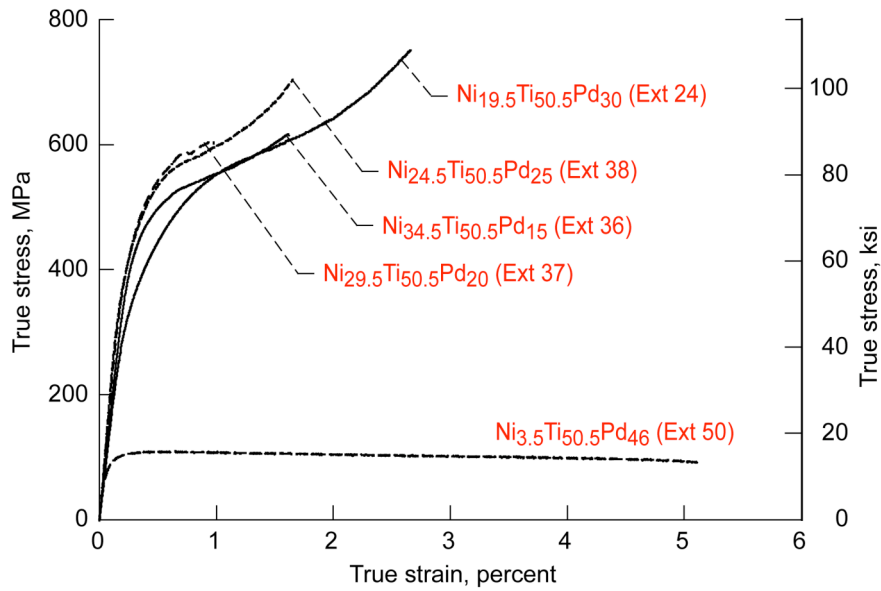
Figure 3.6.—Results for monotonic tension tests for the five ternary alloys at temperatures equal to A_F+50 °C.
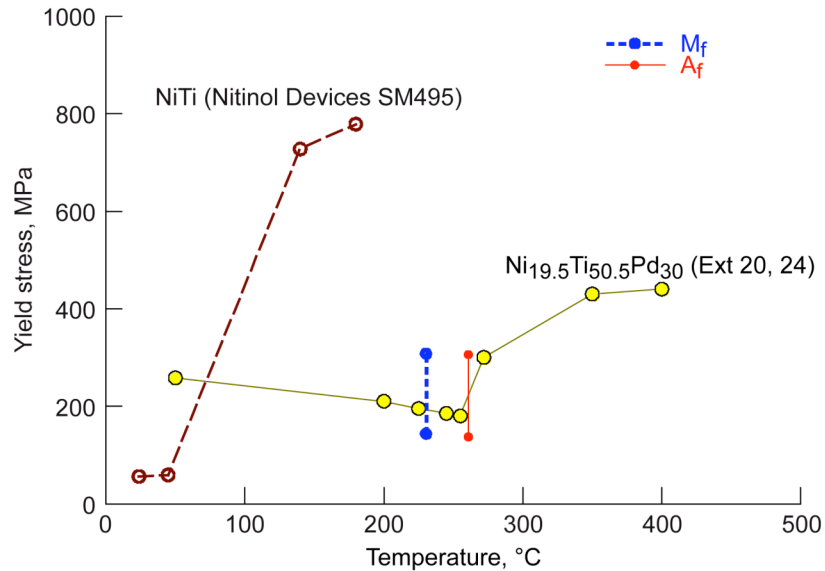
Figure 3.7.—Summary of 0.2 percent offset yield stresses as a function of temperature for binary NiTi and a $Ni_{19.5}Ti_{50.5}Pd_{30}$ alloy (Extrusion 20) illustrating tensile yield behavior throughout the full temperature range and the relative strengths of the martensite and austenite phases.

In binary NiTi, which in effect has 0 at.% palladium, the difference in yield strength between the martensite and austenite phases is large, >669 MPa (Figure 3.7), and therefore NiTi has excellent actuation capability and work output. For the low palladium content alloys, the relative yield strength ($\sigma_y^A - \sigma_y^M$) is somewhat smaller than that for binary NiTi, but is still strongly positive (Table 3.4). If a full range of tests at various temperatures over the transformation range were performed on these alloys, the yield stress as a function of temperature would resemble that of the $Ni_{19.5}Ti_{50.5}Pd_{30}$ alloy of extrusions 20 and 24, which shows a slight decrease in yield stress with increasing temperature in the martensite with a yield minimum (and also ductility minimum) minimum around the A_S, and then an increase in yield stress with increasing temperature above the A_S. Such behavior is representative of the response typically seen for alloys that turn out to be good actuator materials. However, in the higher palladium alloys such as the 46 at.% palladium alloy, the austenite phase is weaker than the martensite phase, which would be detrimental for a shape memory alloy actuator.

Overall, there is a general decrease in the difference between the austenite and martensite phase strengths (or critical stress for slip—critical stress for shear) with increasing palladium content, until approximately 37 at.% palladium where the strengths of the two phases are expected to be equal, and above which there is a reversal in strength level, where the critical stress for slip is less than the critical stress for shear (Figure 3.8). In total, over the range of alloys tested, this difference in yield strength decreases from +341 MPa for 15 at.% palladium to –267 MPa for 46 at.% palladium. It can be seen that while palladium additions to NiTi produce the desired benefit of increased transformation temperatures, it also results in a decrease in the relative yield stresses until there is a reversal of the relative yield stresses of austenite and martensite phases at high palladium content. Consequently, alloys such as the $Ni_{3.5}Ti_{50.5}Pd_{46}$ would not be expected to behave well as actuators.

3.4 Load-Bias Testing

The best way to screen a material for performance as an actuator is by running load-bias tests on the materials as described in Chapter 2: Materials and Procedures. Load-bias tests were performed on all five alloys (Figures 3.9-13), with the 15 and 20 at.% palladium alloys showing good work capability up to 295 MPa, and the 25 and 30 at.% alloys showing good work capability up to 393 MPa. The 46 at.% alloy

failed to perform any work, and instead elongated to failure, thus confirming the results of the monotonic tension tests, which qualitatively indicated that the $Ni_{3.5}Ti_{50.5}Pd_{46}$ alloy did not possess the appropriate mechanical properties to be a viable actuator material.
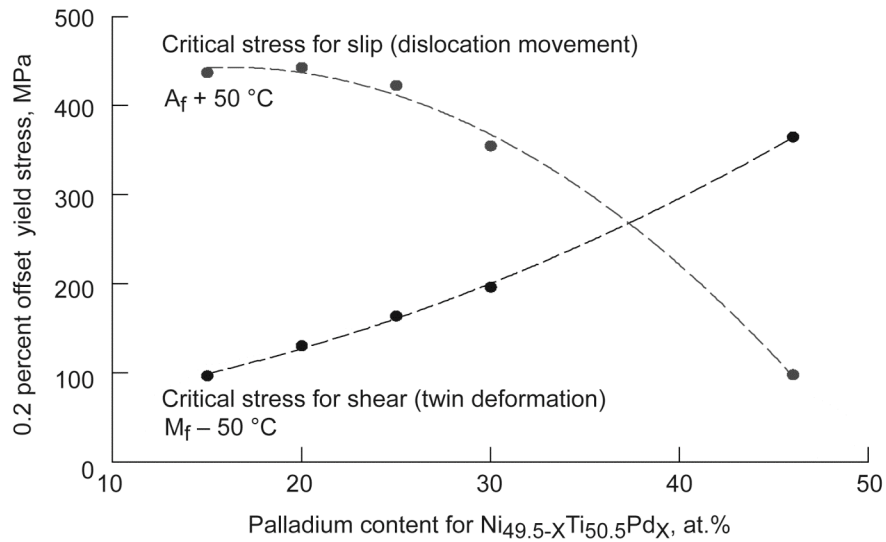
Figure 3.8.—Summary of 0.2 percent offset yield stresses for the martensite and austenite phases as a function of palladium content for ternary NiTiPd alloys. The figure shows that at palladium contents above 37 at.%, relative strengths of the martensite and austenite phases are no longer capable of supporting meaningful work output.
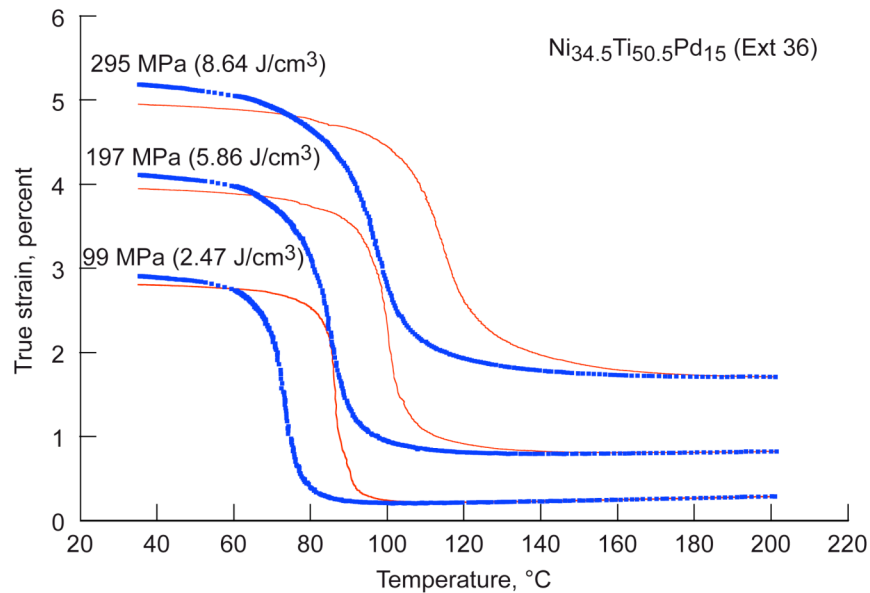
Figure 3.9.—Load-bias curves for the $Ni_{34.5}Ti_{50.5}Pd_{15}$ alloy at incrementing stress levels. Work output at each stress level is shown.
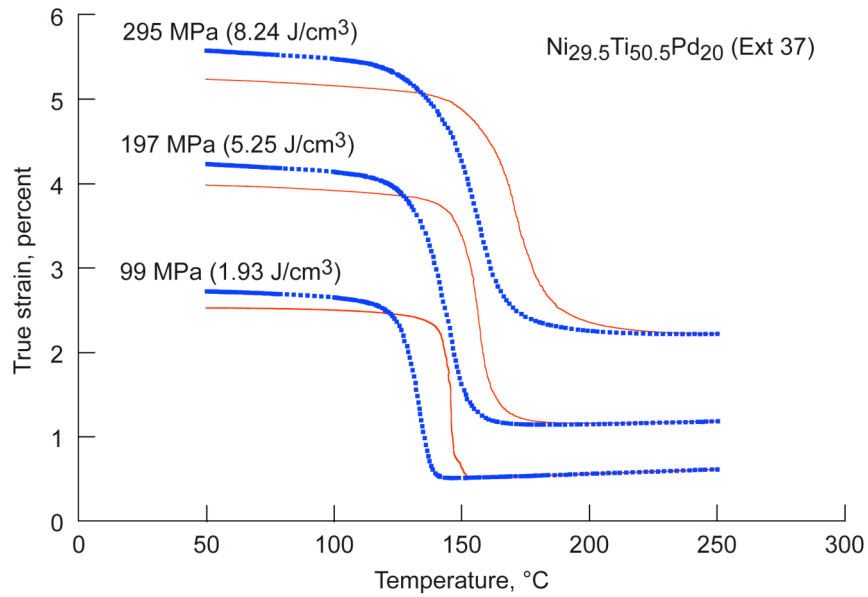
Figure 3.10.—Load-bias curves for the Ni$_{29.5}$Ti$_{50.5}$Pd$_{20}$ alloy at incrementing stress levels.
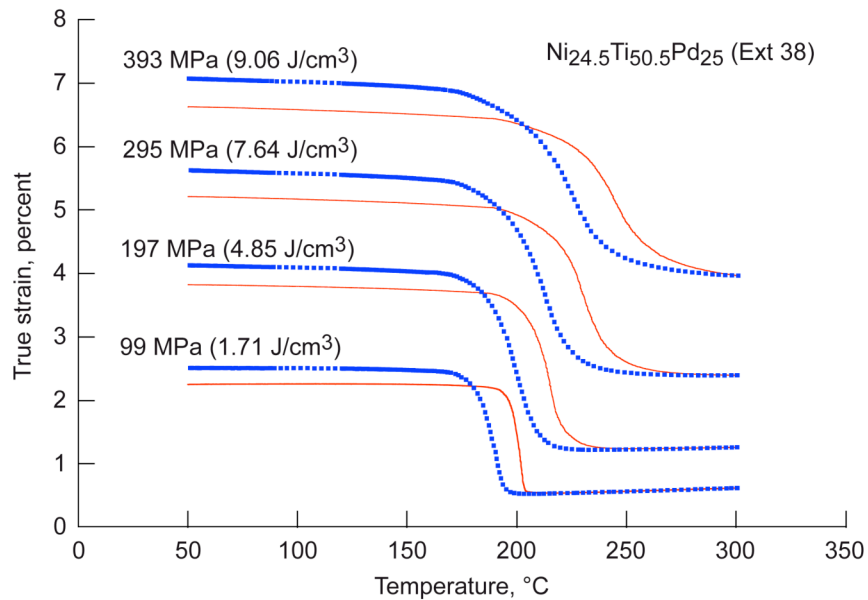
Figure 3.11.—Load-bias curves for the Ni$_{24.5}$Ti$_{50.5}$Pd$_{25}$ alloy showing strain as a function of temperature behavior at incrementing stress levels.
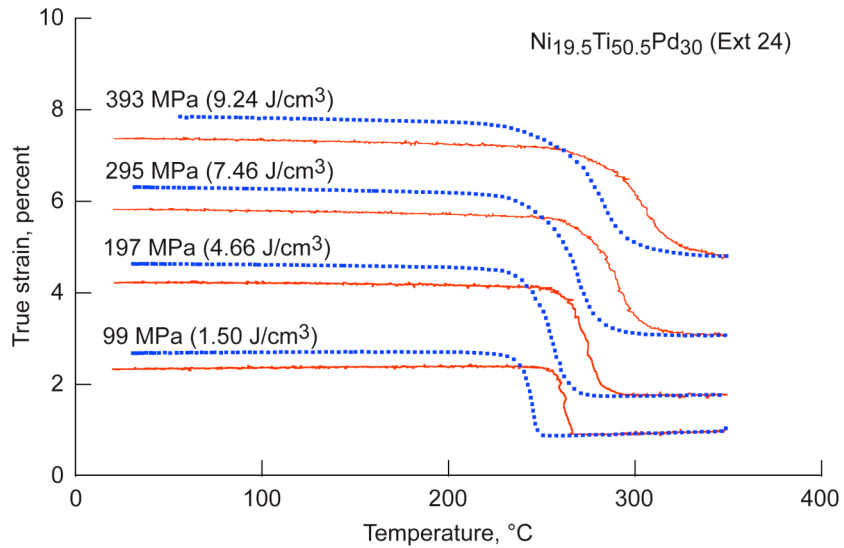
Figure 3.12.—Load-bias curves for the $Ni_{19.5}Ti_{50.5}Pd_{30}$ alloy at incrementing stress levels.
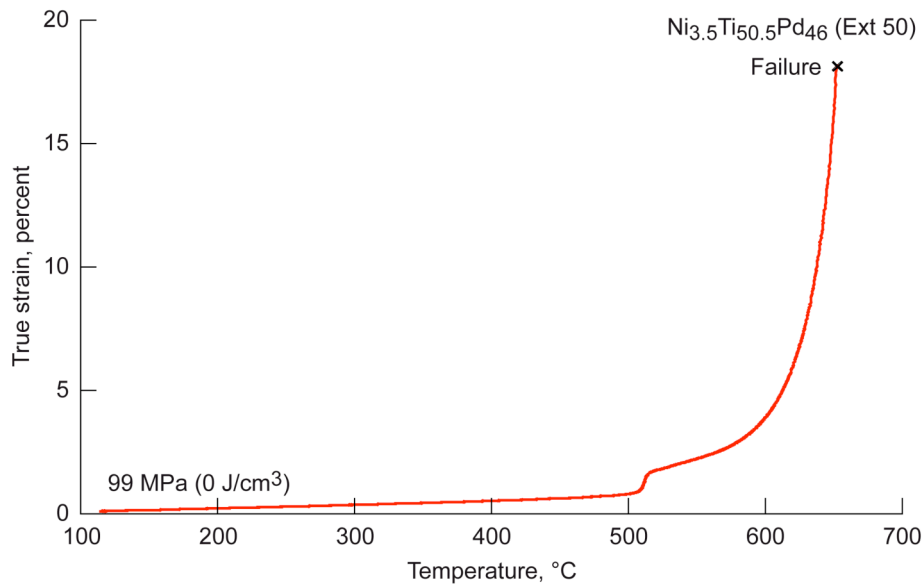
Figure 3.13.—Load-bias behavior for the $Ni_{3.5}Ti_{50.5}Pd_{46}$ alloy at 99 MPa showing the lack of strength in the austenite phase, causing elongation to failure at temperatures above A_F.

3.4.1 Open Loop Strain, Transformation Strain, and Work Output

Standard load-bias tests (0, 99, 197, 295, 393 MPa) on each of the alloys revealed that for each alloy composition, the per-cycle open-loop strain (ε_{OL}) increased as the applied stress increased (Table 3.5, Figure 3.14). Cross-linking the data for all compositions, it can be seen that at each stress level applied to the samples, the open loop strain increased linearly as a function of palladium content (Figure 3.15). For example, at 295 MPa, the open loop strain increases from 0.23% for 15 at.% palladium to 0.48% for 30 at.% platinum. This increase in open-loop strain with increasing palladium content is because as the relative strengths of the martensite and austenite phases approach each other at higher palladium contents, it becomes easier to generate dislocations upon the application of load. Therefore, more of the deformation produced by the application of load goes toward permanent deformation strain (ε_{OL}) in the form of dislocation generation and movement rather than recoverable deformation strain (ε_{TF}) in the form of twin shear.

TABLE 3.5.—OPEN-LOOP STRAIN FOR TERNARY NiTiPd ALLOYS AS A FUNCTION OF STRESS

Applied Stress (MPa)	Open-Loop Strain ε_{OL} (%)				
	$Ni_{34.5}Ti_{50.5}Pd_{15}$	$Ni_{29.5}Ti_{50.5}Pd_{20}$	$Ni_{24.5}Ti_{50.5}Pd_{25}$	$Ni_{19.5}Ti_{50.5}Pd_{30}$	$Ni_{3.5}Ti_{50.5}Pd_{46}$
0	0.000	0.000	0.000	0.000	0.000
99	0.101	0.194	0.261	0.336	>18
197	0.163	0.245	0.307	0.392	——
295	0.234	0.339	0.413	0.479	——
393	——	——	0.450	0.455	——
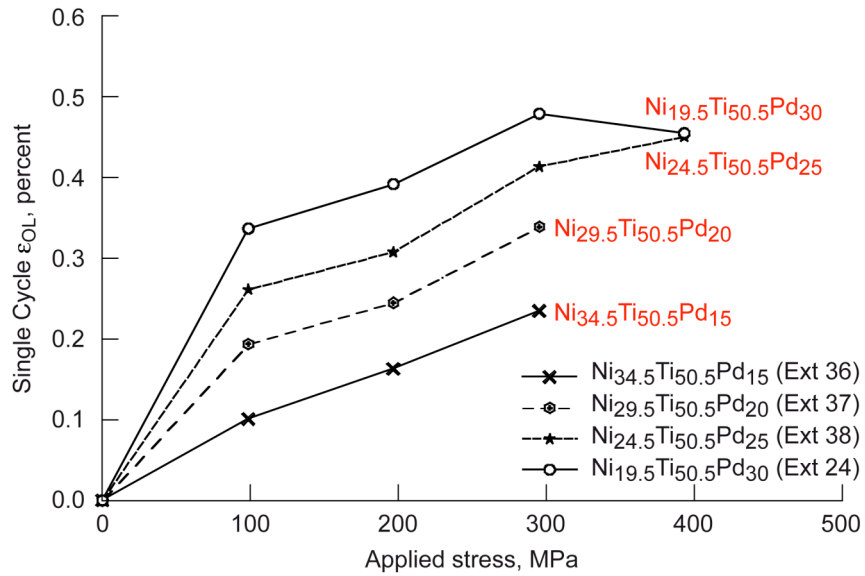
Figure 3.14.—Permanent deformation (open loop strain) as a function of applied stress for thermally cycled NiTiPd alloys.
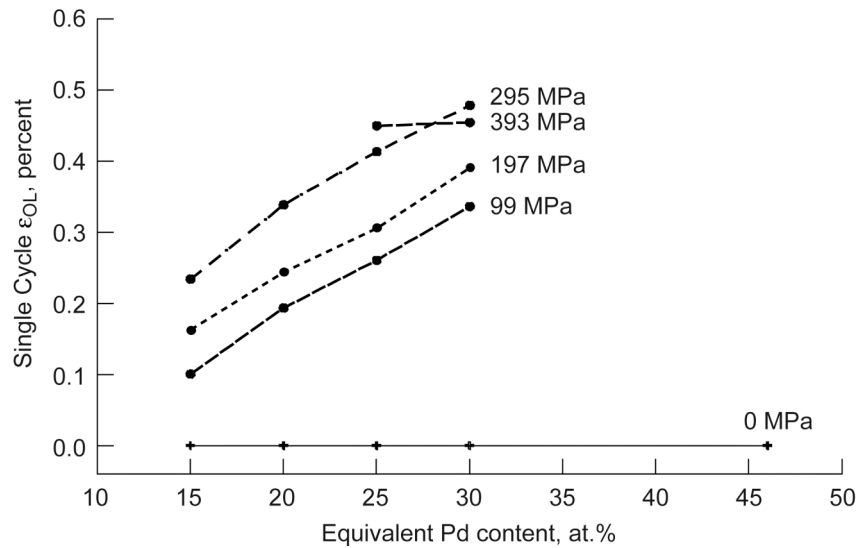
Figure 3.15.—Permanent deformation per cycle as a function of palladium content for NiTiPd samples thermally cycled at constant load.
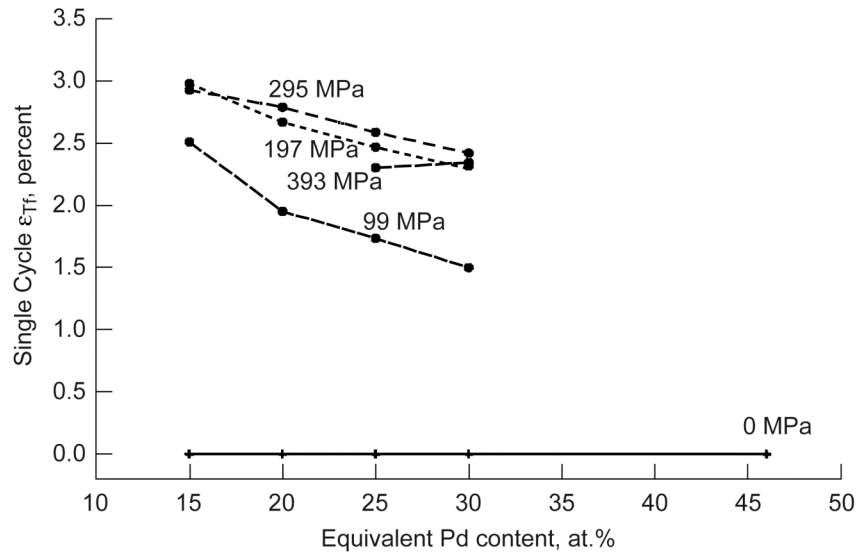
Figure 3.16.—Transformation strain as a function of palladium content for NiTiPd samples thermally cycled at constant load.
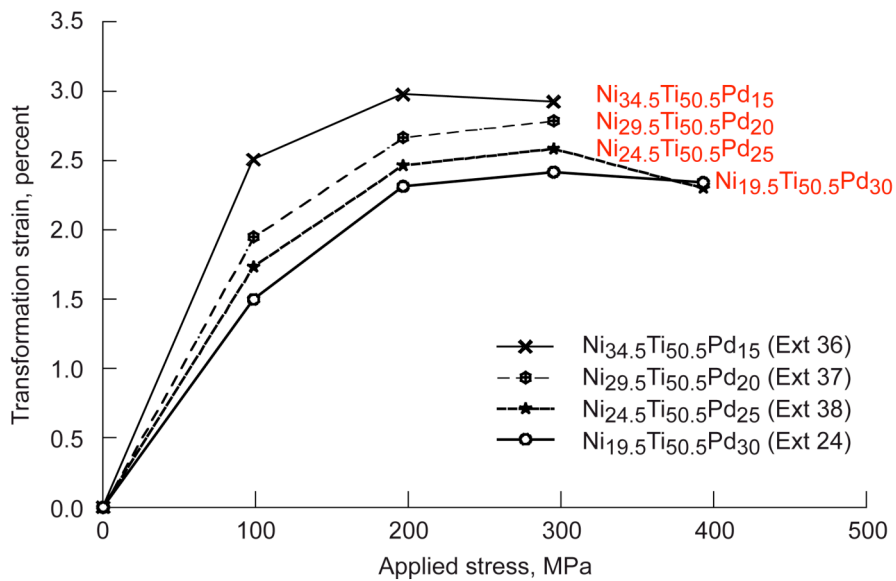
Figure 3.17.—Transformation strain as a function of applied stress for NiTiPd alloys thermally cycled at constant load.

Due to the decrease in relative yield stress at higher palladium contents, transformation strain (in essence a measurement of the number of twins re-oriented by the applied stress and the magnitude of shear on all of them) decreased with increasing palladium content (Figure 3.16). For a given alloy composition, though, transformation strain increased with the magnitude of the applied stress, as more twin variants were re-oriented by the higher stress (Table 3.6, Figure 3.17). This increase in transformation strain with applied stress occurs up to some peak strain value, which was 2.98% at 197 MPa for the 15 at.% palladium alloy and 2.79, 2.59, and 2.42% at 295 MPa for the 20, 25, and 30 at.% palladium alloys, respectively. At higher stresses than these, transformation strains decreased because plastic deformation began to prohibit the transformation, inhibiting the transformation strain.

TABLE 3.6.—TRANSFORMATION STRAIN FOR TERNARY NiTiPd COMPOSITIONS WITH STRESS

Applied Stress (MPa)	Transformation Strain ε_{TF} (%)				
	$Ni_{34.5}Ti_{50.5}Pd_{15}$	$Ni_{29.5}Ti_{50.5}Pd_{20}$	$Ni_{24.5}Ti_{50.5}Pd_{25}$	$Ni_{19.5}Ti_{50.5}Pd_{30}$	$Ni_{3.5}Ti_{50.5}Pd_{46}$
0	0.00	0.00	0.00	0.00	0.00
99	2.51	1.95	1.74	1.50	——
197	2.98	2.67	2.47	2.32	——
295	2.93	2.79	2.59	2.42	——
393	——	——	2.30	2.35	——

Work output of the alloys is related to the transformation strain (eq. 2.1), and also decreased linearly with increasing palladium content for a given stress level from 8.64 J/cm^3 for $Ni_{34.5}Ti_{50.5}Pd_{15}$ to 7.15 J/cm^3 for $Ni_{19.5}Ti_{50.5}Pd_{30}$ at 295 MPa (Table 3.7, Figure 3.18). For a given alloy, an increase in stress produces a corresponding increase in work output up to some maximum value of work (Figure 3.19). Above this maximum work output, the issues preventing increased transformation strains in turn limit work output.

TABLE 3.7.—WORK OUTPUT FOR FIVE TERNARY NiTiPd COMPOSITIONS WITH STRESS

Applied Stress (MPa)	Work Output (J/cm^3)				
	$Ni_{34.5}Ti_{50.5}Pd_{15}$	$Ni_{29.5}Ti_{50.5}Pd_{20}$	$Ni_{24.5}Ti_{50.5}Pd_{25}$	$Ni_{19.5}Ti_{50.5}Pd_{30}$	$Ni_{3.5}Ti_{50.5}Pd_{46}$
0	0.00	0.00	0.00	0.00	0.00
99	2.48	1.93	1.71	1.48	——
197	5.86	5.25	4.85	4.55	——
295	8.64	8.24	7.64	7.15	——
393	——	——	9.06	9.22	——

3.4.2 Transformation Temperature

As mentioned earlier in this chapter, the application of stress produces an increase in the transformation temperatures for shape memory alloys (Figure 3.20). Above 99 MPa, this increase occurs linearly as a function of applied stress, with the A_S and M_F temperatures increasing only one-third to one-half as much as the M_S and A_F over the stress range from 99 to 295 MPa (Table 3.8). The increase in transformation temperatures is due to the application of stress making the martensite more energetically favorable than the austenite at higher temperatures. The application of stress also produces a widening of the hysteresis curve (A_F-M_S) (Figure 3.21), and an elongation (A_F-M_F) of the hysteresis over a broader temperature range (Figure 3.22). Because of this elongation, bandwidth for actuation of these materials is decreased slightly at higher stresses, as the material has to be heated and cooled over a broader temperature range to produce full transformation.

TABLE 3.8.—INCREASE IN TRANSFORMATION TEMPERATURES FROM 99 TO 295 MPa

Alloy	ΔM_F (°C)	ΔM_S (°C)	ΔA_S (°C)	ΔA_F (°C)
$Ni_{34.5}Ti_{50.5}Pd_{15}$	17	30	19	37
$Ni_{29.5}Ti_{50.5}Pd_{20}$	14	30	14	37
$Ni_{24.5}Ti_{50.5}Pd_{25}$	13	31	19	40
$Ni_{19.5}Ti_{50.5}Pd_{30}$	12	34	19	40
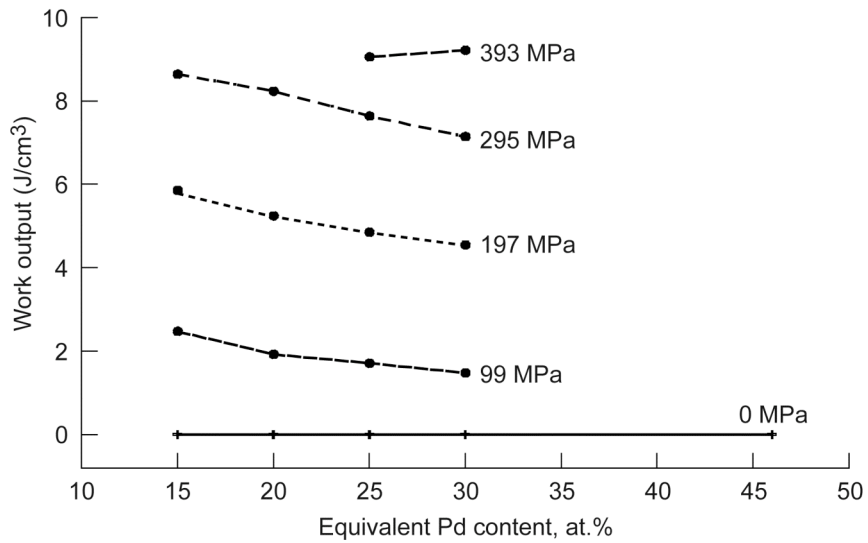
Figure 3.18.—Work output at a given stress level for NiTiPd alloys of varying palladium content.
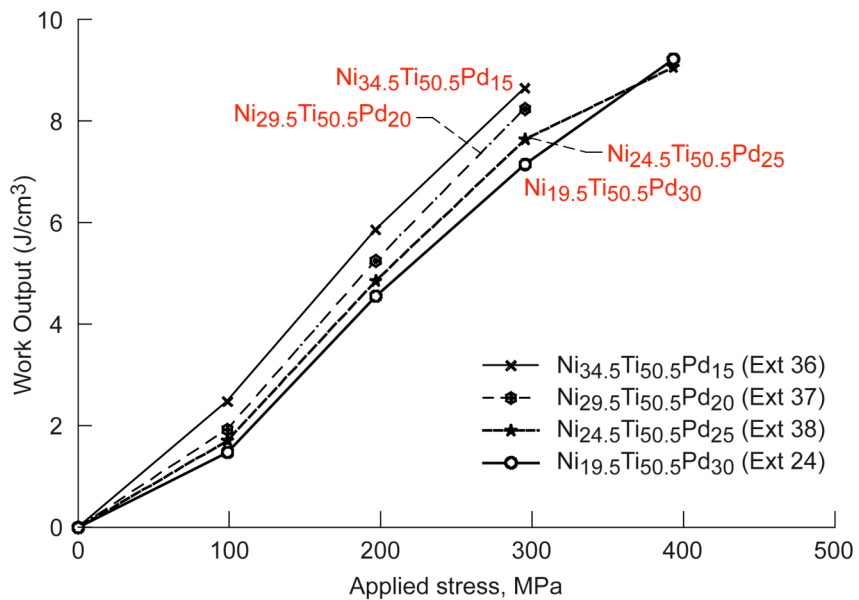
Figure 3.19.—Work output as a function of applied stress for NiTiPd alloys.
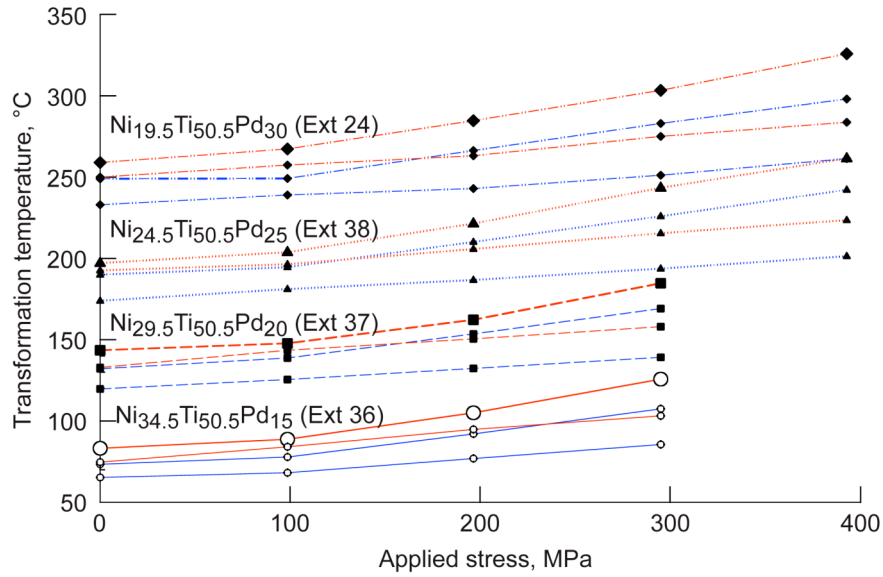
Figure 3.20.—Transformation temperatures as a function of applied stress for NiTiPd alloys. At zero stress, transformation temperatures (going from bottom to top for each alloy) are M_F, M_S, A_S, and A_F.
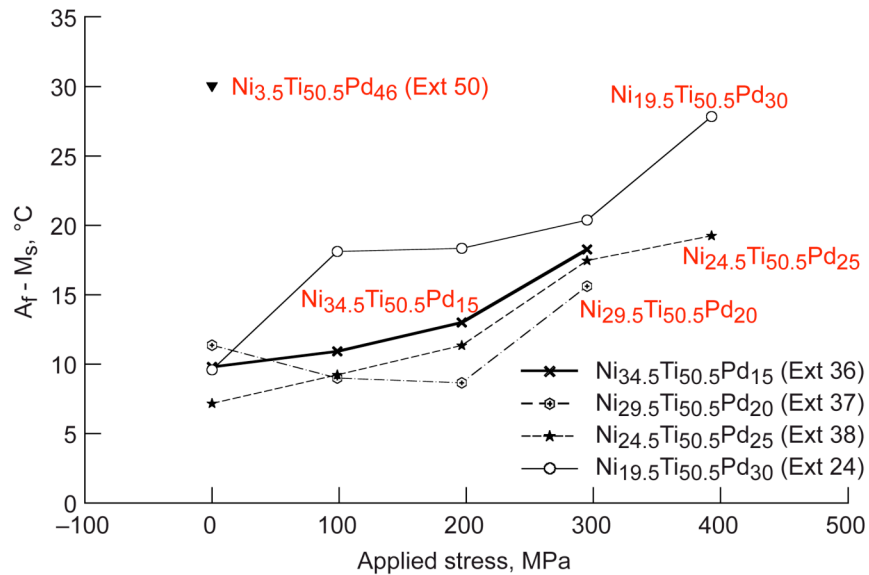
Figure 3.21.—Change in thermal hysteresis with applied stress for NiTiPd alloys.
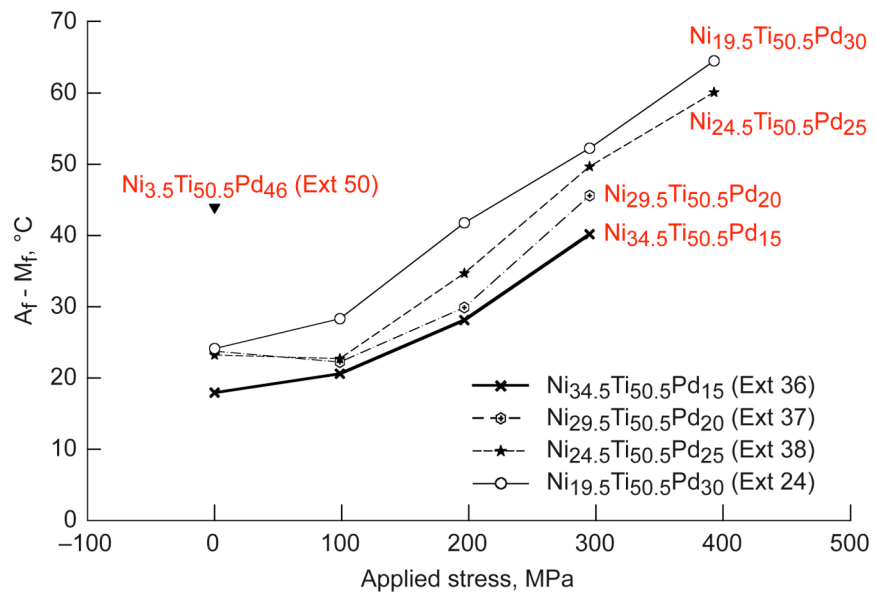
Figure 3.22.—Change in full transformation temperature range with applied stress for NiTiPd alloys.

Chapter 4—Properties Of Quaternary Ni-Ti-Pd-X (X=Pt, Au, Hf) Alloys

4.1 Material Characterization

Three different quaternary alloys were prepared to determine the effect that solid solution strengthening would have on the ternary NiTiPd shape memory alloy system. Two of these quaternary alloys were derivative compositions based on the $Ni_{19.5}Ti_{50.5}Pd_{30}$ alloy, with 5 at.% palladium replaced by 5 at.% gold ($Ni_{19.5}Ti_{50.5}Pd_{25}Au_5$) or 5 at.% platinum ($Ni_{19.5}Ti_{50.5}Pd_{25}Pt_5$). The third quaternary alloy was based on the $Ni_{3.5}Ti_{50.5}Pd_{46}$ alloy, with 3 at.% hafnium replacing an equal atomic amount of titanium. Like the ternary alloys from which the quaternary alloys were derived, the quaternary alloys were also melted with a slightly titanium-rich composition to account for the formation of second phase particles Ti(C,O) and $Ti_2(Ni,Pd,X)$ while maintaining a near stoichiometric but not nickel rich matrix. Density was measured as a basic material property. Chemical analysis of the constituent elements (Ni, Ti, Pd, Pt, Au, Hf) were made, along with measurements of impurity elements (Fe, C, N, O) and these values were compared to the target compositions. Microstructural analysis was performed to determine the type and amount of any second phase constituents present in the microstructure. This analysis was done to ensure that the quaternary alloying additions did not drive the formation of other second phases, but rather acted to strengthen the microstructure through solid solution mechanisms.

4.1.1 Composition and Density

Densities of all three quaternary alloys were greater than those of their ternary predecessors, as heavier elements were used to replace lighter ones. Substitutions of 5 at.% gold or platinum for palladium produced alloys with densities of ~8.0 g/cm³. Hafnium substitutions for 3 at.% titanium in the $Ni_{3.5}Ti_{50.5}Pd_{46}$ alloy caused a density change from 8.1 to 8.4 g/cm³ (Table 4.1).

TABLE 4.1.—COMPOSITION AND DENSITY FOR THE THREE QUATERNARY NiTiPdX ALLOYS. DATA FOR THE TERNARY BASELINE ALLOYS ARE GIVEN FOR COMPARISON

Sample ID	Density g/cm³ *Ti:Ni eq*	Ti	Ni	Pd	Au	Pt	Hf	Zr	
Ext. 24	**7.504**	35.20	16.98	47.65	0.01	<0.01	<0.005	<0.005	wt%
NiTiPd	*49.6:49.7*	*49.6*	*19.5*	*30.2*	*0.0*				*at.%*
Ext. 47	**7.983**	32.99	15.84	37.27	13.76	<0.01	<0.005	<0.005	wt%
NiTiPdAu	*49.6:49.6*	*49.6*	*19.4*	*25.2*	*5.0*				*at.%*
Ext. 48	**8.004**	32.70	15.95	37.34	0.14	13.70	<0.005	<0.005	wt%
NiTiPdPt	*49.2:50.1*	*49.2*	*19.6*	*25.3*	*0.1*	*5.1*			*at.%*
Ext. 50	**8.087**	31.51	2.76	65.53	0.01	<0.01	<0.005	<0.005	wt%
NiTiPd	*49.4:49.7*	*49.4*	*3.5*	*46.2*	*0.0*				*at.%*
Ext. 51	**8.371**	28.17	2.63	62.20	0.01	<0.01	6.61	0.18	wt%
NiTiPdHf	*49.4:49.5*	*46.3*	*3.5*	*46.0*	*0.0*		*2.9*	*0.2*	*at.%*

Nickel compositions were on target, with maximum compositional deviations of 0.1 at.% Titanium, which is less stable in the melt, and could interact with the graphite crucible or slag off as an oxide and so decrease the measured value from the target, registered at 49.2 to 49.6 at.% which, within the resolution of the measurement still encompasses the target composition of 50.5 at.% titanium. Palladium varied from the target value by 0 to 0.3 at.%, while gold, platinum, and hafnium only varied by a maximum of 0.1 at.% Carbon, oxygen, and nitrogen were all present in the alloy, with maximum carbon and oxygen

values of 0.48 and 0.51 at.% occurring in $Ni_{3.5}Ti_{47.5}Pd_{46}Hf_3$ (Table 4.2). The $Ni_{3.5}Ti_{50.5}Pd_{46}$ alloy contained the most nitrogen, at 0.023 at.%, followed by that of $Ni_{3.5}Ti_{47.5}Pd_{46}Hf_3$ at 0.022 at.% Iron was present in all alloys at 0.2 to 0.3 at.% and was probably introduced in the alloys from the extrusion process.

TABLE 4.2.—IMPURITY LEVELS IN THE NiTiPdX ALLOYS

Sample ID	Fe	C	N	O	
Ext. 24	0.02	0.078	0.004	0.061	wt%
NiTiPd	0.02	0.44	0.017	0.26	at.%
Ext. 47	0.02	0.065	0.003	0.056	wt%
NiTiPdAu	0.03	0.39	0.014	0.25	at.%
Ext. 48	0.02	0.068	0.004	0.084	wt%
NiTiPdPt	0.02	0.41	0.018	0.38	at.%
Ext. 50	0.02	0.075	0.004	0.078	wt%
NiTiPd	0.03	0.47	0.023	0.36	at.%
Ext. 51	0.02	0.073	0.004	0.104	weight%
NiTiPdHf	0.03	0.48	0.022	0.51	at.%

4.1.2 Microstructure

Room temperature microstructural analysis of the three quaternary alloys using SEM reveals a single phase martensitic microstructure with a low number density distribution of two types of particles (Figures 4.1, 4.2). These second phases appear as black and grey particles in all the micrographs (in $Ni_{19.5}Ti_{50.5}Pd_{25}Au_5$, these particles appear black and light grey to white.)

As in the ternary alloys, the black phase was determined to be Ti(O,C). In the quaternary $Ni_{19.5}Ti_{50.5}Pd_{25}Au_5$ and $Ni_{19.5}Ti_{50.5}Pd_{25}Pt_5$ alloys, the grey particles were determined to be intermetallic $Ti_2(Ni,Pd,X)$, where X is either gold or platinum depending on alloy addition. In the $Ni_{3.5}Ti_{47.5}Pd_{46}Hf_3$ alloy, this became $(Ti,Hf)_2(Ni,Pd)$, as the hafnium substituted for titanium atoms in the structure. These Ti_2Ni type particles were seen to be generally blocky in morphology due to their formation as a coarse interdendritic phase which was then broken up during extrusion. As mentioned in Chapter 3, these Ti_2Ni type particles could also have been in the oxygen stabilized form Ti_4Ni_2O. High magnification backscattered electron (BSE) images from the SEM up to 5000x showed no evidence of any other fine particles or phases, and the known binary phase diagrams show no other second phases other than $(Ti,Hf)_2(Ni,Pd,Au,Pt)$ that could be present at these compositions.

Particle sizes for the three quaternary alloys ranged from 0.5 to 3.2 µm for the Ti(O,C) and from 0.5 to 6 µm in diameter for the Ti_2Ni type particles (Table 4.3). For all three quaternary alloys, the volume fraction of Ti(O,C) decreased from the amount present in the ternary baseline alloys, going from 0.72 vol% to 0.30 and 0.60 vol% with the substitution of 5 at.% gold or platinum, respectively, and from 0.70 to 0.65 vol% with the substitution of 3 at.% hafnium for titanium. For the two alloys containing 5 at.% quaternary addition, volume fractions of Ti_2Ni type particles decreased from that present in ternary $Ni_{19.5}Ti_{50.5}Pd_{30}$. However, in the hafnium strengthened alloy, volume fraction measurements of Ti_2Ni type particles showed an increase from 2.26 to 3.63 vol% Excess hafnium in these alloys, acting in the place of excess titanium, helped to drive the formation of the Ti_2Ni type phase, leading to the increase in volume fraction. However, the majority of the hafnium, and nearly all of the gold and platinum additions in the other two alloys did not result in the generation of any other phases, but went into solution within the matrix instead. Therefore, it can be inferred that improvements in strength or properties would be due to solid solution strengthening effects, rather than strengthening by second phase particles.
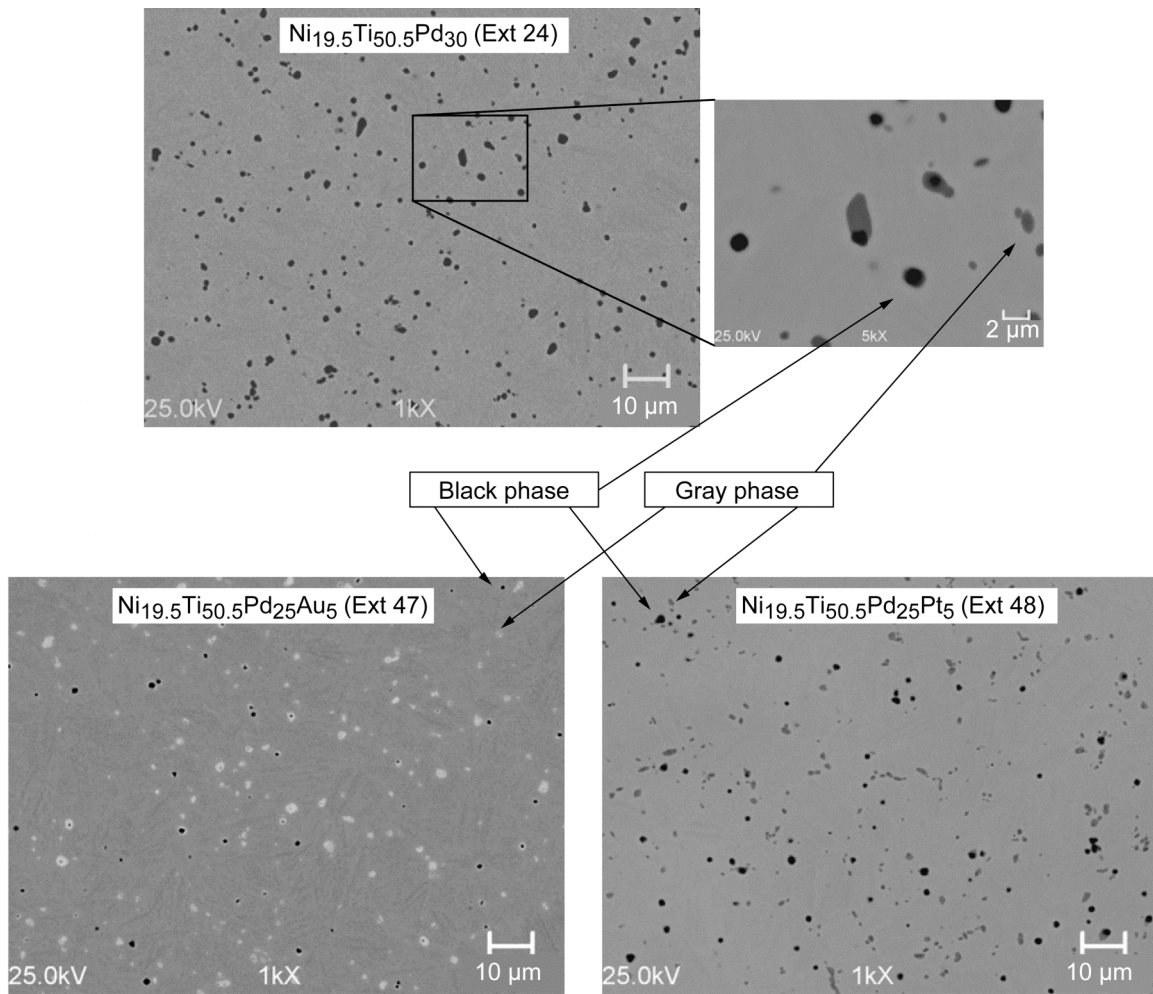
Figure 4.1.—Scanning electron micrographs of the 30 at.% palladium alloy and the two derivative quaternary alloys showing the presence of the Ti(O,C) black phase and the $Ti_2(Ni,Pd,X)$ type phase which appears dark gray in $Ni_{19.5}Ti_{50.5}Pd_{30}$ (inset shown to clarify the different phases) and $Ni_{19.5}Ti_{50.5}Pd_{25}Pt_5$ and light gray in $Ni_{19.5}Ti_{50.5}Pd_{25}Au_5$.
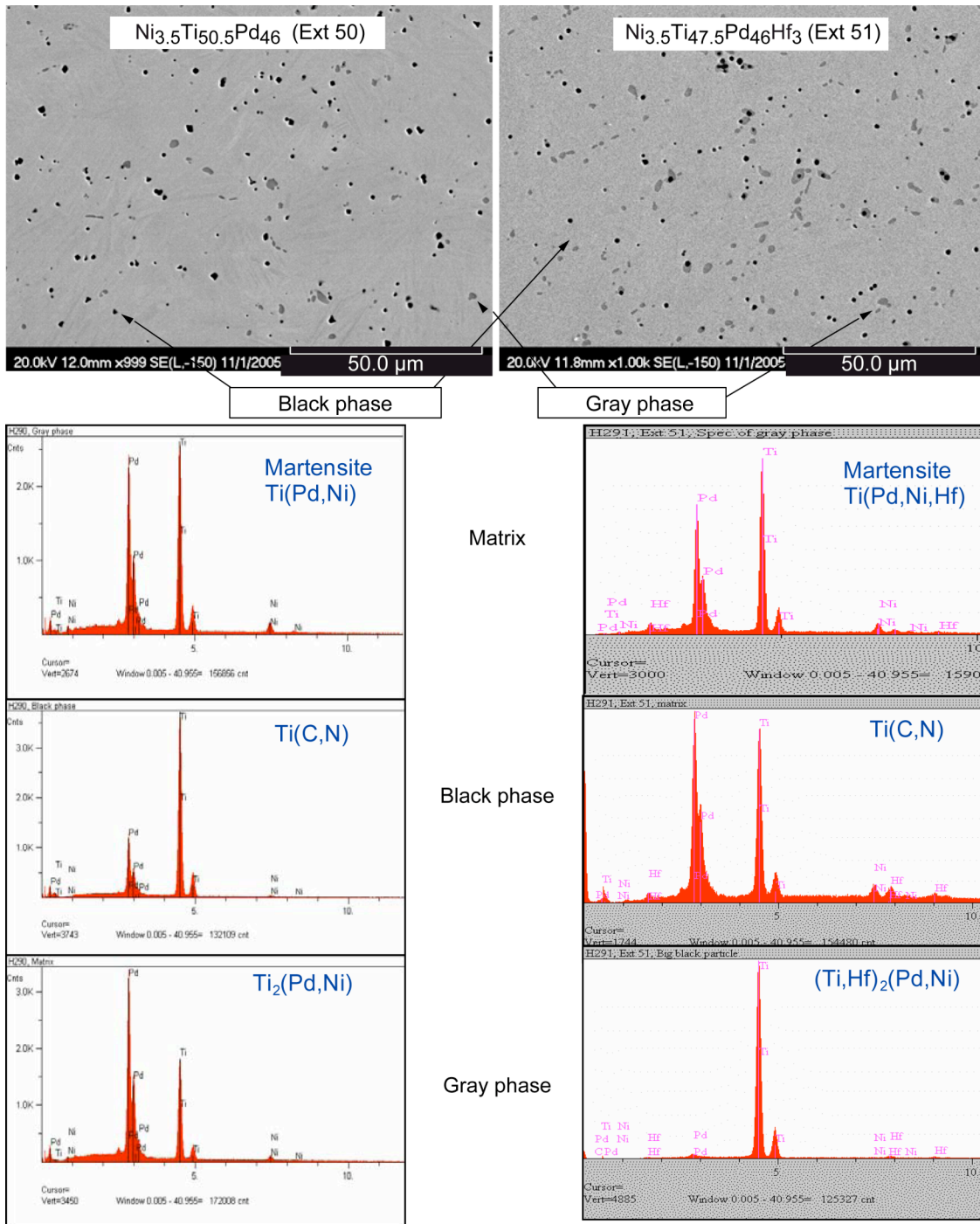
Figure 4.2.—$Ni_{3.5}Ti_{50.5}Pd_{46}$ and $Ni_{3.5}Ti_{47.5}Pd_{46}Hf_3$ alloys showing a low density distribution of $(Ti,Hf)_2(Ni,Pd)$ type particles (grey phase) and $Ti(O,C)$ particles (black phase).

TABLE 4.3.—SIZE AND VOLUME FRACTION OF SECOND PHASE PARTICLES IN
NiTiPdX QUATERNARY ALLOYS

Target Composition (at.%)						Extrusion	Particle Size (min, max, avg) (μm)						Volume Fraction (%)	
Ni	Ti	Pd	Au	Pt	Hf		Ti(C, N)			Ti$_2$(Ni,Pd)			Ti(C, N)	Ti$_2$(Ni,Pd)
19.5	50.5	30				24	0.43	1.78	0.97	0.36	3.55	1.49	0.72	3.26
19.5	50.5	25	5			47	0.49	1.54	0.96	0.49	3.48	1.53	0.30	2.13
19.5	50.5	25		5		48	0.49	3.23	1.26	0.49	5.72	1.32	0.60	2.26
3.5	50.5	46				50	0.55	2.17	1.03	0.55	4.54	1.59	0.70	2.26
3.5	47.5	46			3	51	0.49	2.28	1.04	0.49	4.23	1.45	0.65	3.63

4.2 Transformation Temperature

Transformation temperatures for each alloy were determined from zero-load load-bias curves as described in Chapter 2 (Figure 4.3). All of the quaternary alloys exhibit curves which were representative of a single step martensite to austenite transformation. Transformation temperatures are relatively unchanged for the quaternary alloys derived from Ni$_{19.5}$Ti$_{50.5}$Pd$_{30}$, being on average 227 and 258 °C for the M$_F$ and A$_F$ respectively with hysteresis averaging 13 and 31 °C for the A$_F$-M$_S$ and A$_F$-M$_F$, respectively (Table 4.4). The quaternary Ni$_{3.5}$Ti$_{47.5}$Pd$_{46}$Hf$_3$ alloy, however has transformation temperatures 60 and 70 °C below the respective M$_F$ and A$_F$ temperatures of the ternary Ni$_{3.5}$Ti$_{50.5}$Pd$_{46}$ alloy. This behavior is apparently due to suppression of the transformation temperatures by the hafnium addition, or some subtle effect on the stoichiometry of the matrix place.
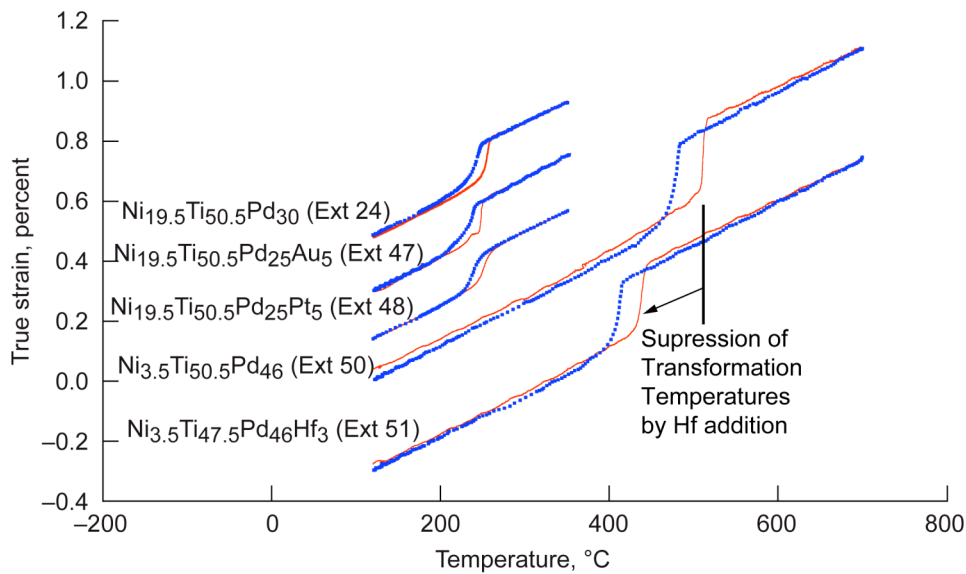
Figure 4.3.—No-load load-bias curves for the three quaternary NiTiPdX and the ternary baseline NiTiPd alloys from which they were derived. The figure shows the transformation of each alloy during heating from the low temperature martensite phase to the high temperature austenite phase, and cooling back to the initial state.

TABLE 4.4.—TRANSFORMATION TEMPERATURE, THERMAL HYSTERESIS, AND FULL
TRANSFORMATION RANGE FOR QUATERNARY NiTiPdX ALLOYS

Target Composition (at.%)						Extrusion	Transformation Temperature (°C)				Hysteresis (°C)	
Ni	Ti	Pd	Au	Pt	Hf		M_F	M_S	A_S	A_F	A_F-M_S	A_F-M_F
19.5	50.5	30.0				24	233	249	250	259	10	26
19.5	50.5	25.0	5			47	226	243	239	257	14	31
19.5	50.5	25.0		5		48	228	247	243	259	12	31
3.5	50.5	46.0				50	469	485	509	513	28	44
3.5	47.5	46.0			3	51	406	416	433	443	27	37

4.3 Isothermal Monotonic Tension Testing

Monotonic tension tests were performed on each quaternary solid-solution strengthened alloy at temperatures of M_F–50 °C and A_F+50 °C, and also at various other temperatures below and above the transformation to determine the strengths of the martensite and austenite phases (Table 4.5). Ideally, one would want a solid solution strengthening addition that would raise the yield stress in the austenite phase while either keeping the yield stress of the martensite the same, or even decreasing it. In this way, the maximum difference in yield stresses between the austenite and martensite is achieved. Also, ideally, a solid solution strengthening alloy addition will not degrade ductility, but rather improve it. Comparing the data from the ternary baseline $Ni_{19.5}Ti_{50.5}Pd_{30}$ alloy to that of its solid solution strengthened counterparts, the quaternary alloys show an increase in austenitic strength of 139 MPa for 5 at.% gold addition and 93 MPa for 5 at.% platinum addition (Figure 4.4). In the martensite state, yield strength was also increased, but only by 23 and 19 MPa, respectively (Figure 4.5). The 3 at.% hafnium substitution for palladium in $Ni_{3.5}Ti_{50.5}Pd_{46}$ produced an increase in austenite strength of 158 MPa (Figure 4.6) and a *decrease* in yield strength of the martensite of 26 MPa (Figure 4.7). This gave an overall improvement in yield strengths between the M_F–50 °C and A_F+50 °C temperatures of 116, 74, and 184 MPa, respectively for 5 at.% gold, 5 at.% platinum, and 3 at.% hafnium. While the hafnium addition did not completely bring the austenite strength up to that of the martensite, it was still improved considerably over that of the $Ni_{3.5}Ti_{50.5}Pd_{46}$. Considering that part of the hafnium came out of solution to form $(Ti,Hf)_2(Ni,Pd)$, in terms of yield stress improvement, hafnium was much more effective than gold as a solid solution strengthening addition, with both of them performing better than Pt, based on these monotonic strength results.

TABLE 4.5.—SUMMARY OF 0.2% OFFSET YIELD STRENGTHS AT VARIOUS TEST
TEMPERATURES OR NiTiPdX QUATERNARY ALLOYS AND THE BASELINE NiTiPd
ALLOYS FROM WHICH THEY WERE DERIVED

Composition	Test Temperature (°C) 0.2% Yield Stress (MPa)				
Extrusion	Below M_F–50	M_F–50	Below M_F	Above A_F	A_F+50
$Ni_{19.5}Ti_{50.5}Pd_{30}$		**183**			**309**
(Ext 24)		*196.37*			*355.02*
$Ni_{19.5}Ti_{50.5}Pd_{25}Au_5$		**176**	**200**		**307**
(Ext 47)		*219.39*	*206.30*		*494.06*
$Ni_{19.5}Ti_{50.5}Pd_{25}Pt_5$	**147**	**178**	**200**	**279**	**307**
(Ext 48)	*226.75*	*215.11*	*212.31*	*406.96*	*448.43*
$Ni_{3.5}Ti_{50.5}Pd_{46}$		**419**			**563**
(Ext 50)		*365.03*			*98.08*
$Ni_{3.5}Ti_{47.5}Pd_{46}Hf_3$	**23**	**356**	**380**	**450**	**500**
(Ext 51)	*328.84*	*338.82*	*297.87*	*262.25*	*256.33*
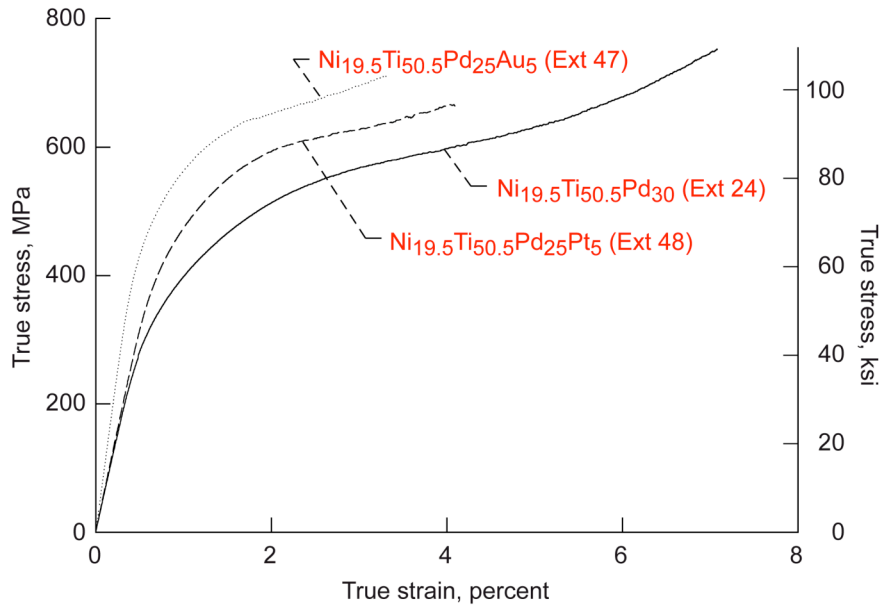
Figure 4.4.—Tensile behavior at A_F+50 °C for NiTi-30 at.% (Pd,X) alloys.
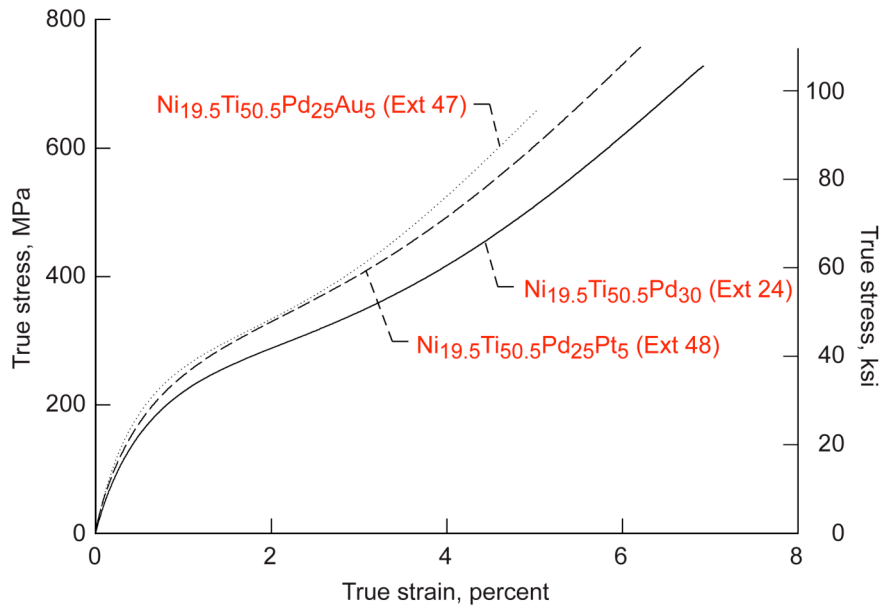
Figure 4.5.—Tensile behavior at M_F–50 °C for NiTi - 30 at.% (Pd,X) alloys.
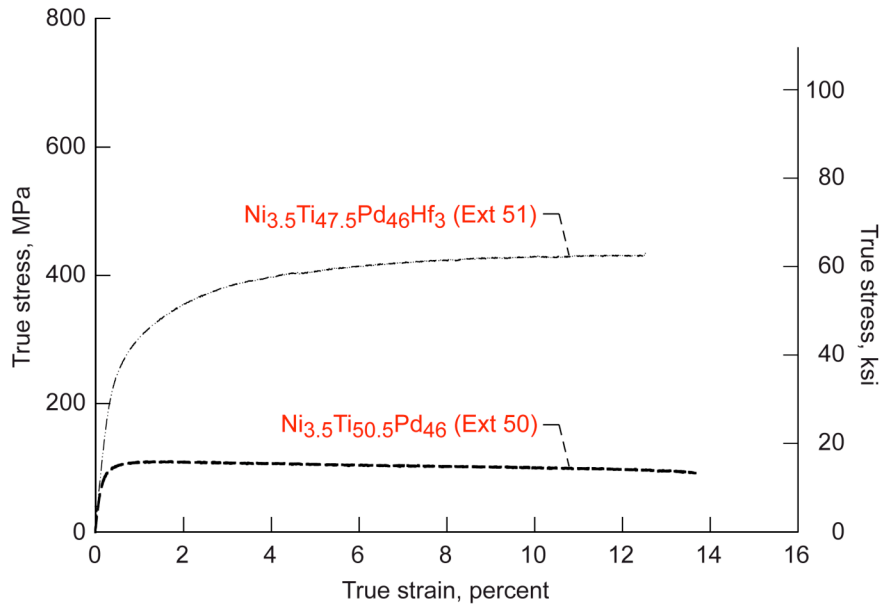
Figure 4.6.—Tensile behavior A_F+50 °C for $Ni_{3.5}Ti_{50.5}Pd_{46}$ alloys with and without hafnium substitution.
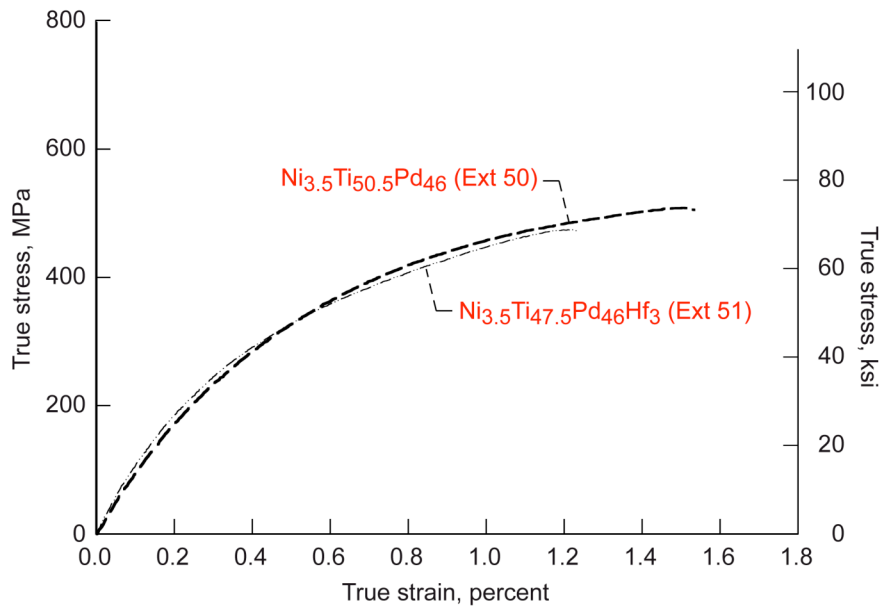
Figure 4.7.—Tensile behavior M_F–50 °C for $Ni_{3.5}Ti_{50.5}Pd_{46}$ alloys with and without hafnium substitution.

Recall that the austenite yield strength correlates to the critical stress for slip, and the martensite yield strength to the critical stress for shear. For a viable actuator, the critical stress for slip must be greater than that for shear (the greater, the better), so that when stress is applied, it produces a shape deformation via shear of the martensite twins rather than via dislocation generation and movement. The solid solution strengthened alloys derived from $Ni_{19.5}Ti_{50.5}Pd_{30}$ both improved the relative strengths of the martensite and austenite phases while effectively retaining the same high transformation temperatures. While hafnium addition to the $Ni_{3.5}Ti_{50.5}Pd_{46}$ alloy did decrease the transformation temperatures, it also brought the strengths of the martensite and austenite phases significantly closer, and nearer to desired behavior of a viable actuator material (Figures 4.8, 4.9).
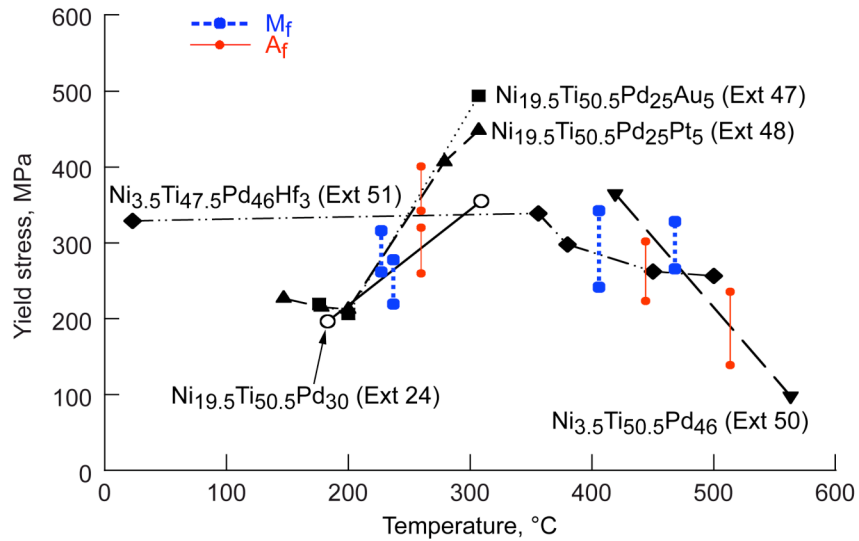
Figure 4.8.—Summary of the tensile yield behavior at various test temperatures for solid solution strengthened NiTiPdX alloys and their ternary NiTiPd baseline counterparts.
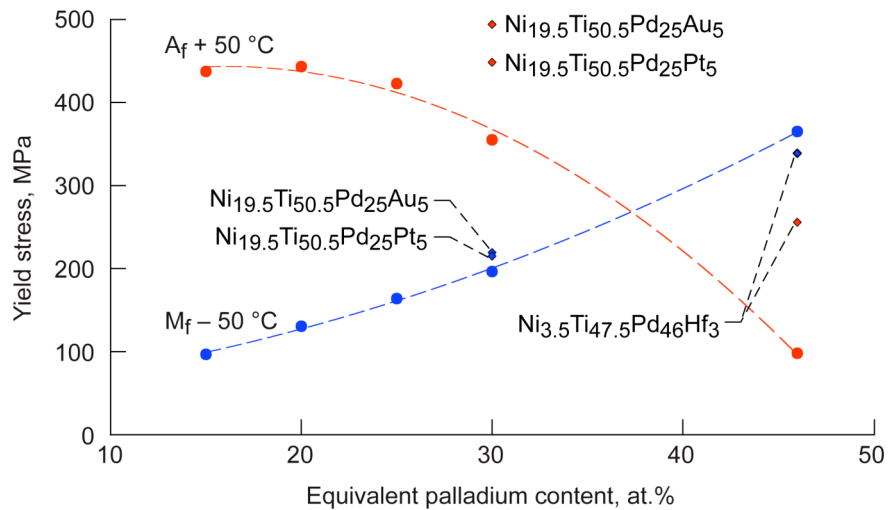
Figure 4.9.—Yield stress of the martensite and austenite phases as a function of equivalent palladium content (Pd+Au,Pt) for ternary and quaternary alloys.

4.4 Load-Bias Testing

Each of the three solid solution strengthened alloys was load-bias tested to model behavior as an actuator (Figures 4.10, 11, 12). The two solid solution strengthened alloys based on the $Ni_{19.5}Ti_{50.5}Pd_{30}$ alloy both showed good work behavior up to 393 MPa, with a maximum work output of 9.83 and 9.43 J/cm^3 for $Ni_{19.5}Ti_{50.5}Pd_{25}Au_5$ and $Ni_{19.5}Ti_{50.5}Pd_{25}Pt_5$, respectively. In accordance with the tension tests, which indicated the $Ni_{3.5}Ti_{47.5}Pd_{46}Hf_3$ alloy would show more of a trend toward shape-memory behavior, the alloy did produce work at stresses up to 197 MPa. This result shows the improvement achieved through strengthening effects since the ternary alloy had shown no work behavior and had instead elongated to failure at 99 MPa during the heating cycle (Figure 4.13).
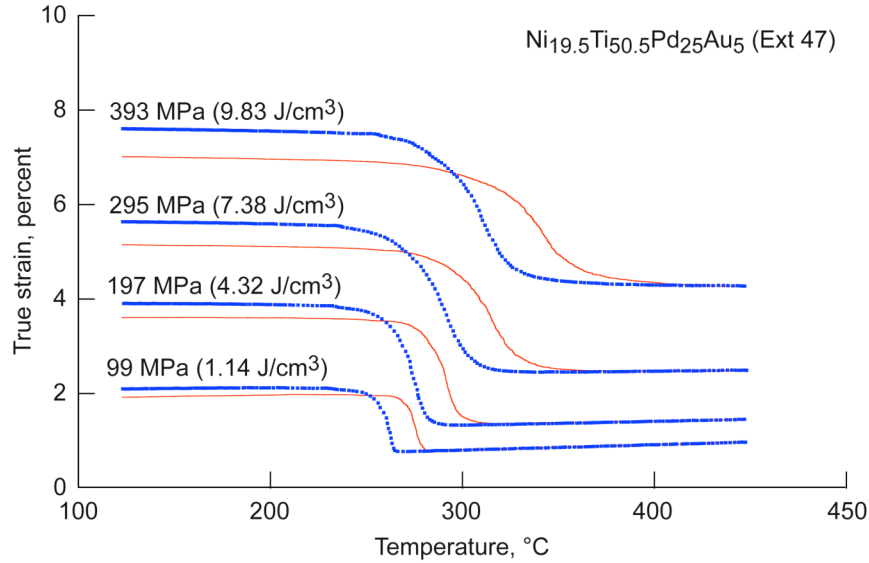
Figure 4.10.—Load-bias test for $Ni_{19.5}Ti_{50.5}Pd_{25}Au_5$ at increasing stress levels.
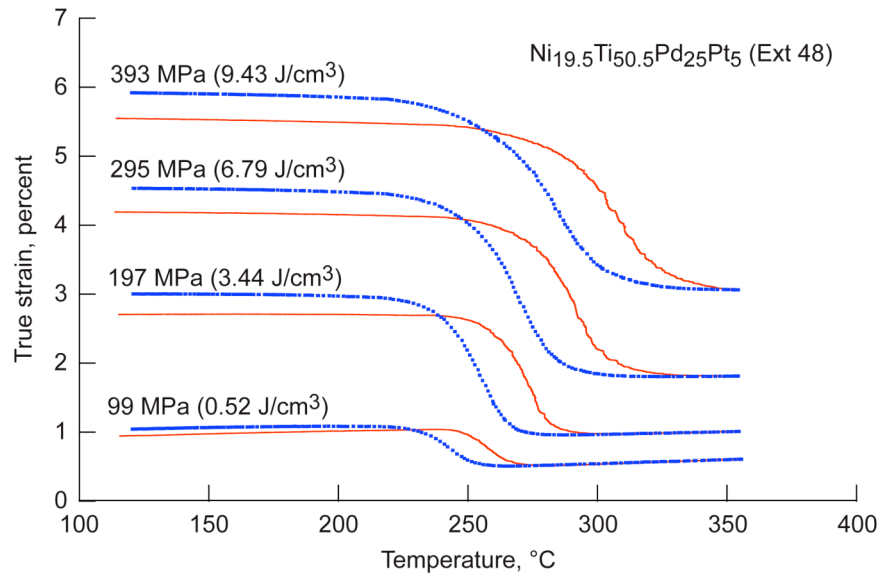
Figure 4.11.—Load-bias test for $Ni_{19.5}Ti_{50.5}Pd_{25}Pt_5$ at increasing stress levels.
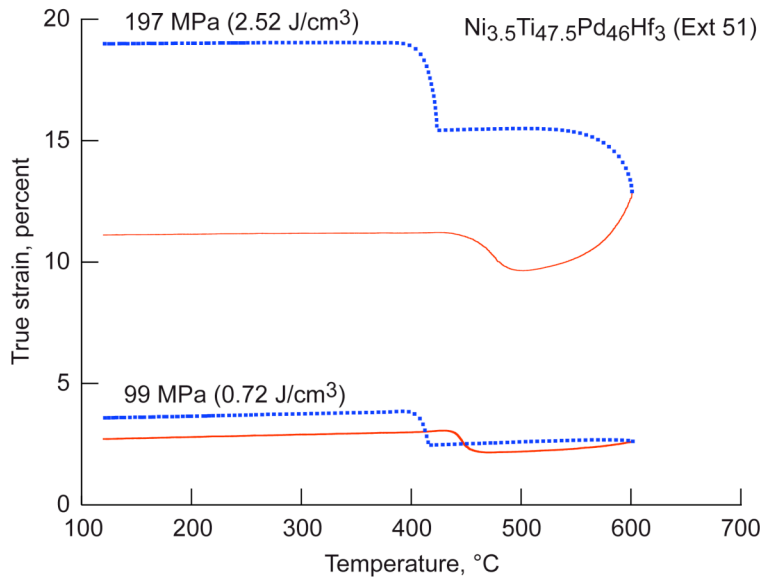
Figure 4.12.—Load-bias test for $Ni_{3.5}Ti_{47.5}Pd_{46}Hf_3$ showing work capability up to 197 MPa, but large amounts of open loop strain.
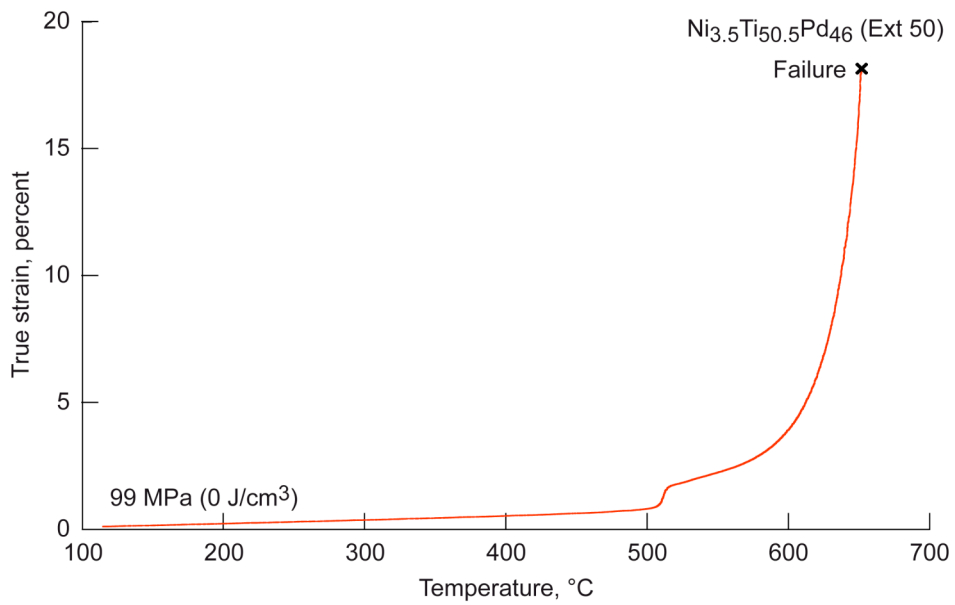
Figure 4.13.—Load-bias test for $Ni_{3.5}Ti_{50.5}Pd_{46}$ showing lack of work capability even at 99 MPa. The sample shows no positive (work producing) transformation strain and elongates to failure in the austenite phase after transforming.
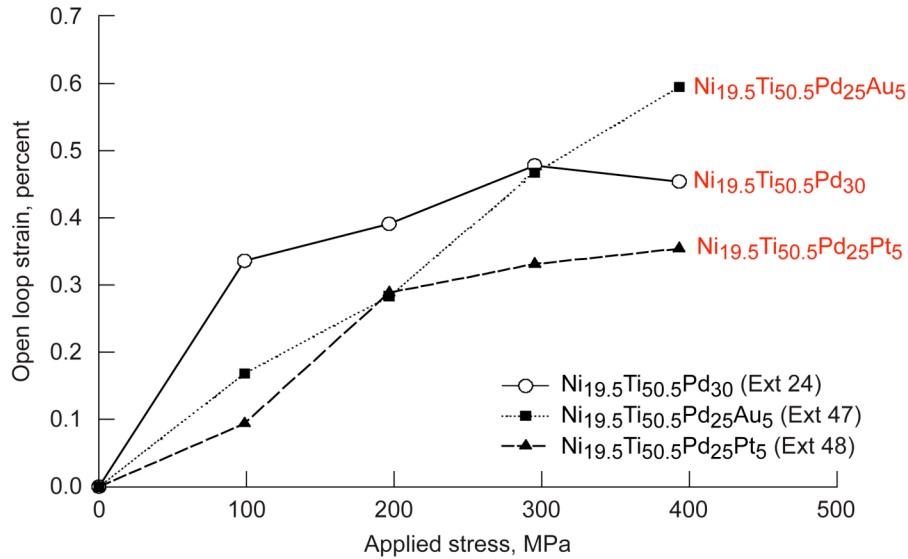
Figure 4.14.—Open loop strain as a function of applied stress for $Ni_{19.5}Ti_{50.5}Pd_{30}$, $Ni_{19.5}Ti_{50.5}Pd_{25}Au_5$, $Ni_{19.5}Ti_{50.5}Pd_{25}Pt_5$.

4.4.1 Open Loop Strain, Transformation Strain, and Work Output

Both solid solution strengthened alloys derived from the $Ni_{19.5}Ti_{50.5}Pd_{30}$ baseline alloy were capable of producing work with a smaller open loop strain compared to the ternary alloy up to a stress of 295 MPa (Figure 4.14, Table 4.6). However, the gold strengthened alloy showed poorer permanent deformation behavior at 393 MPa, having an open loop strain of 0.60% while the $Ni_{19.5}Ti_{50.5}Pd_{30}$ baseline produced 0.45% and $Ni_{19.5}Ti_{50.5}Pd_{25}Pt_5$ still showed improvement at 0.36% open loop strain. In accordance with its improvement in yield stresses over that of the $Ni_{3.5}Ti_{50.5}Pd_{46}$ alloy, hafnium additions strengthened the alloy and brought its behavior closer to that of a viable shape memory alloy. However, because the critical stress for slip was still less than that for shear, the alloy experienced large amounts of open loop strain, gaining 6.3% strain over a single cycle at 197 MPa (Figure 4.15).

TABLE 4.6.—OPEN-LOOP STRAIN FOR THREE QUATERNARY COMPOSITIONS AND TERNARY
BASELINE ALLOYS WITH STRESS

Applied Stress (MPa)	Open-Loop Strain ε_{OL} (%)				
	$Ni_{19.5}Ti_{50.5}Pd_{30}$	$Ni_{19.5}Ti_{50.5}Pd_{25}Au_5$	$Ni_{19.5}Ti_{50.5}Pd_{25}Pt_5$	$Ni_{3.5}Ti_{50.5}Pd_{46}$	$Ni_{3.5}Ti_{47.5}Pd_{46}Hf_3$
0	0.000	0.000	0.000	0	0.000
99	0.336	0.169	0.094	—	0.700
197	0.392	0.284	0.289	—	6.310
295	0.479	0.468	0.332	—	—
393	0.455	0.596	0.355	—	—

Transformation strains in the $Ni_{19.5}Ti_{50.5}Pd_{25}Au_5$ and $Ni_{19.5}Ti_{50.5}Pd_{25}Pt_5$ were slightly diminished compared to those of the ternary alloy, except at 295 and 393 MPa, where the 5 at.% platinum alloy achieved higher transformation strains (Figure 4.16, Table 4.7). The $Ni_{3.5}Ti_{47.5}Pd_{46}Hf_3$ alloy produced transformation strains equal to approximately half of those for the $Ni_{19.5}Ti_{50.5}Pd_{30}$ alloy at stresses of 99 and 197 MPa, and were higher than those strains for the $Ni_{19.5}Ti_{50.5}Pd_{25}Pt_5$ alloy at 99 MPa (no comparison with the $Ni_{3.5}Ti_{50.5}Pd_{46}$ alloy is available here). Likewise, work output for the quaternary alloys was diminished from that of $Ni_{19.5}Ti_{50.5}Pd_{30}$ at all stresses up to 197 MPa, above which, the platinum strengthened alloy showed the best results (Figure 4.17, Table 4.8).
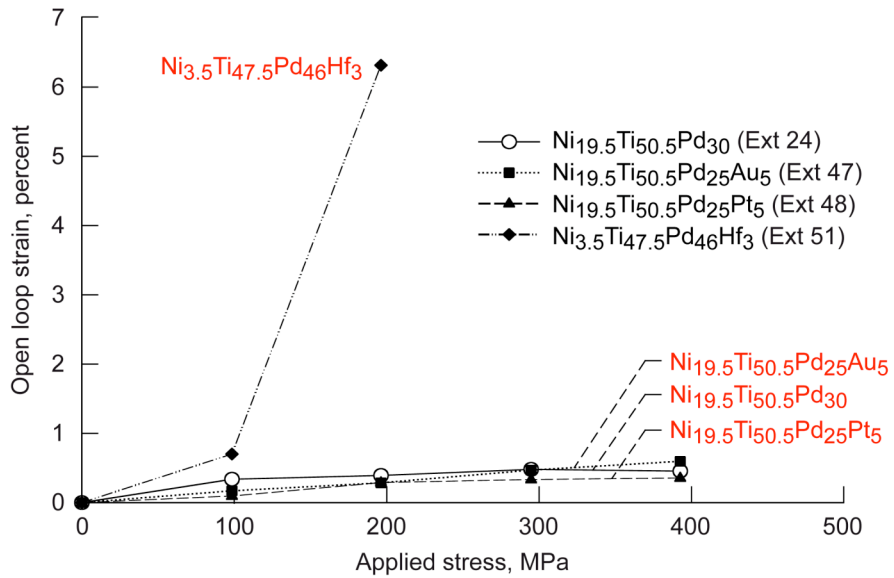
Figure 4.15.—Open loop strain as a function of applied stress for quaternary alloys and $Ni_{19.5}Ti_{50.5}Pd_{30}$, showing the large open loop strain present in the $Ni_{3.5}Ti_{47.5}Pd_{46}Hf_3$ alloy.
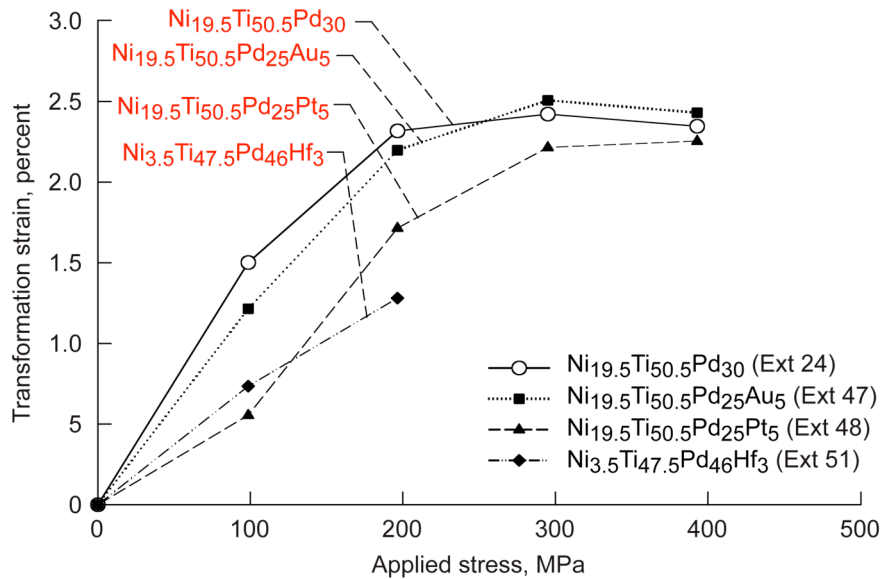
Figure 4.16.—Transformation strain capability of the ternary $Ni_{19.5}Ti_{50.5}Pd_{30}$ alloy, its quaternary descendants, and $Ni_{3.5}Ti_{47.5}Pd_{46}Hf_3$ as a function of the applied stress.

TABLE 4.7.—TRANSFORMATION STRAIN FOR THE THREE QUATERNARY ALLOYS AND THE TWO
TERNARY BASELINE ALLOYS WITH STRESS

Applied Stress (MPa)	Transformation Strain ε_{Tf} (%)				
	$Ni_{19.5}Ti_{50.5}Pd_{30}$	$Ni_{19.5}Ti_{50.5}Pd_{25}Au_5$	$Ni_{19.5}Ti_{50.5}Pd_{25}Pt_5$	$Ni_{3.5}Ti_{50.5}Pd_{46}$	$Ni_{3.5}Ti_{47.5}Pd_{46}Hf_3$
0	0.00	0.00	0.00	0	0.00
99	1.50	1.21	0.55	—	0.73
197	2.32	2.20	1.71	—	1.28
295	2.42	2.51	2.22	—	—
393	2.35	2.43	2.25	—	—

TABLE 4.8.—WORK OUTPUT FOR THE THREE QUATERNARY ALLOYS AND THE TWO TERNARY
BASELINE ALLOYS WITH STRESS

Applied Stress (MPa)	Work Output (J/cm^3)				
	$Ni_{19.5}Ti_{50.5}Pd_{30}$	$Ni_{19.5}Ti_{50.5}Pd_{25}Au_5$	$Ni_{19.5}Ti_{50.5}Pd_{25}Pt_5$	$Ni_{3.5}Ti_{50.5}Pd_{46}$	$Ni_{3.5}Ti_{47.5}Pd_{46}Hf_3$
0	0.00	0.00	0.00	0.00	0.00
99	1.48	1.20	0.55	—	0.72
197	4.55	4.32	3.37	—	2.52
295	7.15	7.40	6.54	—	—
393	9.22	9.55	8.86	—	—
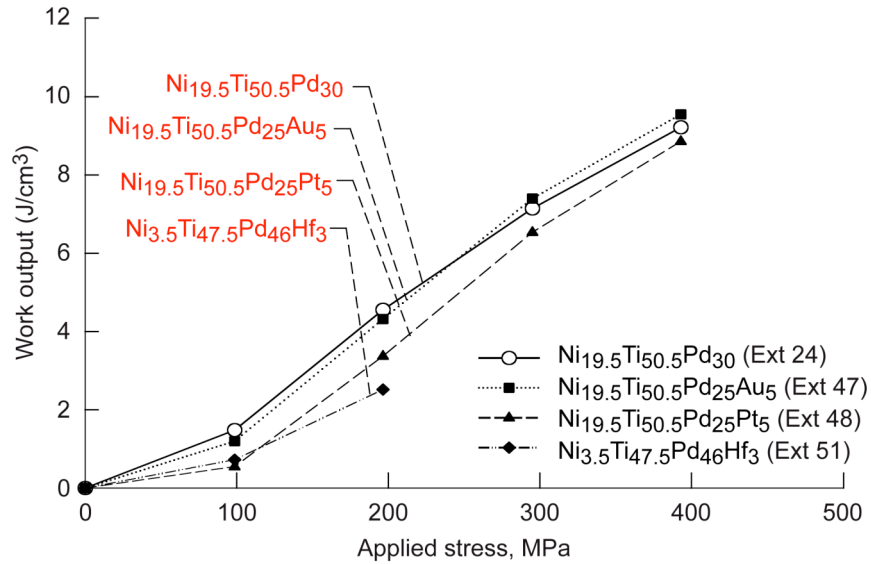
Figure 4.17.—Work output for selected alloys as a function of applied stress.

Chapter 5—Effects of Training and Thermal Excursions on The Strain-Temperature Response of Ni-Ti-Pd-X Alloys

5.1 Necessity of Training

From the results discussed in Chapters 3 and 4, it can be seen that while ternary NiTiPd alloys can be useful as high-temperature shape-memory alloys, they are also dimensionally unstable and because of the large amounts of permanent deformation per cycle, cannot be used directly as actuators in applications requiring more than a few cycles of use. For instance, in an application operating at 200 MPa where no more than 2% dimensional change can be tolerated and working temperatures dictated the use of a $Ni_{19.5}Ti_{50.5}Pd_{30}$ alloy, over the course of six to seven cycles, the material would elongate producing a sample that was permanently 2% longer than its initial length (for example, see Figure 5.1). Given the conditions just mentioned, a simple wire based actuator with physical constraints which limit the stroke would become ineffective. Deformation of the wire elements to the point where the actuator ram rests against the hard stop instead of being held by the wires would lead to an unloading of the device, thereby reducing the work capability of the actuator as a whole. This occurs because force applied to the ram is transferred directly to the hard stop. This then reduces the load on the wires, resulting in decreased transformation strain, approaching zero.

Even though solid solution strengthening of these alloys can dramatically improve the per-cycle permanent deformation (open-loop strain or ε_{OL}) at 100 MPa from 0.34% in $Ni_{19.5}Ti_{50.5}Pd_{30}$ to 0.17% in $Ni_{19.5}Ti_{50.5}Pd_{25}Au_5$ and 0.09% in $Ni_{19.5}Ti_{50.5}Pd_{25}Pt_5$, this result only extends the useable cyclic life of an actuator made from these materials by a factor of two or three. Therefore, in order for these materials to be used as long term actuators, it is absolutely necessary that methods be developed whereby they can be strengthened and stabilized against permanent deformation. Golberg et al. (ref. 78) reported that thermomechanical treatment of a $Ni_{20}Ti_{50}Pd_{30}$ alloy by cold rolling and subsequent heat treatment successfully improved the no-load shape-memory behavior of the alloy to 100% recovery of 5% total strain from 100% recovery of 0.5% total strain for the baseline alloy, and 2% for a precipitation strengthened composition reported by Shimizu et al. (ref. 71). Recent research (ref. 88) at the NASA Glenn Research Center on NiTiPt wires thermally cycled under load revealed a significant reduction in the amount of per-cycle permanent deformation. This ability to stabilize the material through thermal cycling under load is the basis for the training research performed on these alloys, in an effort to better quantify and understand this process.

One sample from each of the three quaternary alloys and from the ternary $Ni_{19.5}Ti_{50.5}Pd_{30}$ alloy was tested under complex thermomechanical cycles consisting of two no-load stain-temperature cycles to "recover" the material to a consistent baseline, training consisting of ten thermal cycles under a constant stress of 345 MPa, finally followed by an evaluation phase. (Training was carried out at this load because it is a higher stress than that usually accommodated by an actuator, and therefore, the training and stabilization should occur more rapidly, but it is not such a high stress that the sample will fail prematurely in tension, preventing the training from occurring.) The evaluation phase consisted of either repeated cycling at 172 MPa, or unloading of the sample followed by a standardized incremental load-bias test in order to determine the effects of training on the dimensional stability of the alloys. The $Ni_{3.5}Ti_{50.5}Pd_{46}$ alloy, though the baseline alloy for the solid solution strengthened $Ni_{3.5}Ti_{47.5}Pd_{46}Hf_3$ alloy, exhibited such poor strain recovery behavior that it was not included in this set of tests. The $Ni_{3.5}Ti_{47.5}Pd_{46}Hf_3$ alloy, although stronger than the $Ni_{3.5}Ti_{50.5}Pd_{46}$ alloy, exhibited a great amount of open loop strain at low stresses and in both tests failed while cooling from the austenite state during the first training cycle after 6.6 and 7.7% strain. As a result, only the data for the ternary $Ni_{19.5}Ti_{50.5}Pd_{30}$ alloy and the two derivative quaternaries, $Ni_{19.5}Ti_{50.5}Pd_{25}Au_5$ and $Ni_{19.5}Ti_{50.5}Pd_{25}Pt_5$, are presented here.
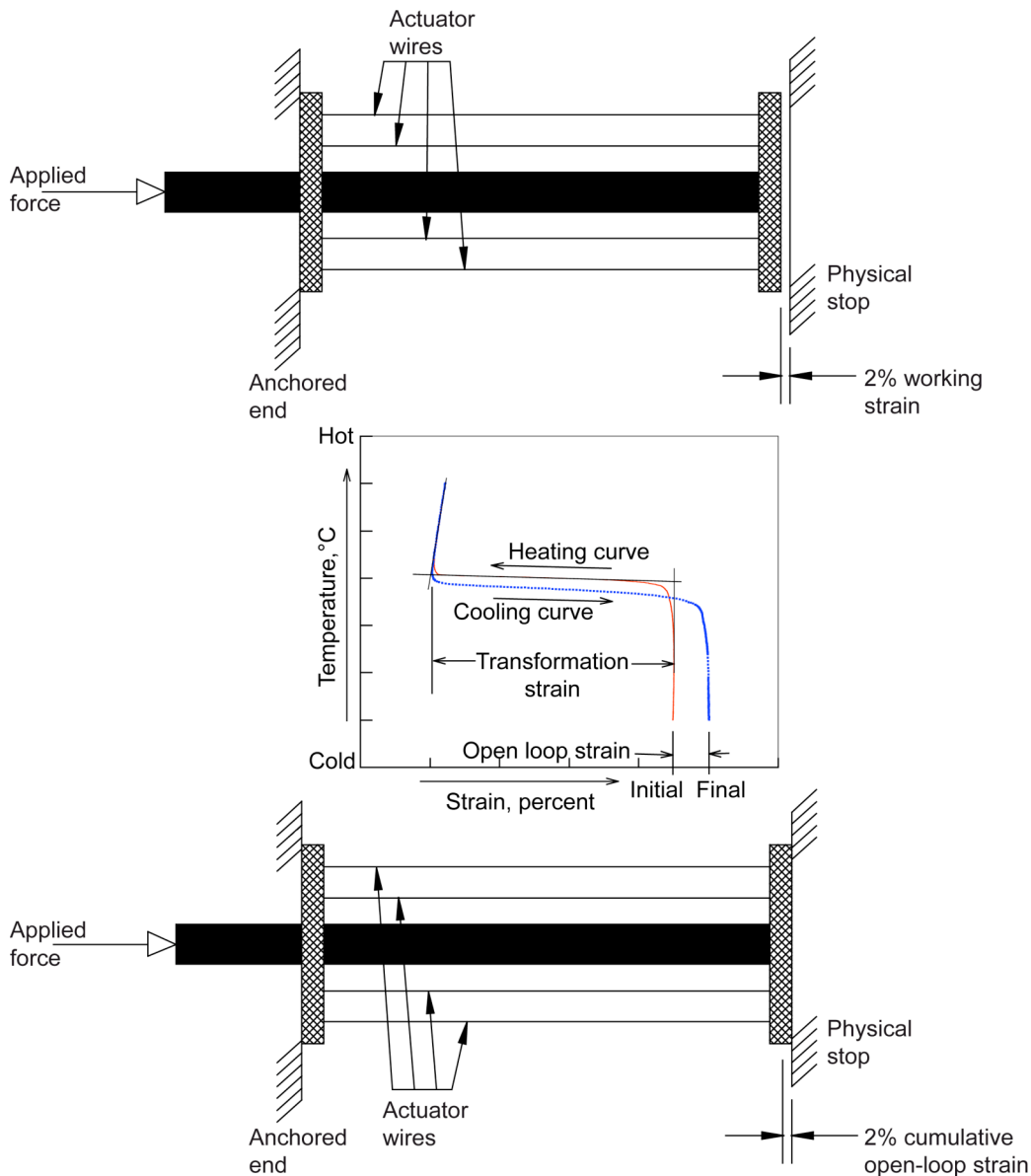
Figure 5.1.—Actuator with hard physical stop being rendered inoperable by cumulative open-loop strain. Over several thermal cycles, actuator wires elongate to the point where the actuator ram reaches the physical stop, the applied force is then transferred to the physical stop instead of the wires, and stress on the wires becomes zero, so that the wires can no longer be reset to actuate on additional cycles.

5.2 Open-Loop Strain in Post Trained Cycles

In samples that were thermally cycled at 172 MPa after training, an intermediate step of two cycles at 172 MPa was performed between the no-load stress relief cycles and the training cycles. The amount of permanent deformation in the sample resulting from this intermediate step (the baseline ε_{OL}) was used to determine the effectiveness of the training upon the structural stability of the sample. During training, one immediate benefit of solid solution strengthening was seen, in that the ε_{OL} saturates more quickly in the solid solution strengthened alloys (Figure 5.2). As the training progressed, the single-cycle open loop strain decreased more quickly in the solid solution strengthened samples compared to the ternary baseline $Ni_{19.5}Ti_{50.5}Pd_{30}$ (Figure 5.3). This higher rate of stabilization means that training was more efficient in the
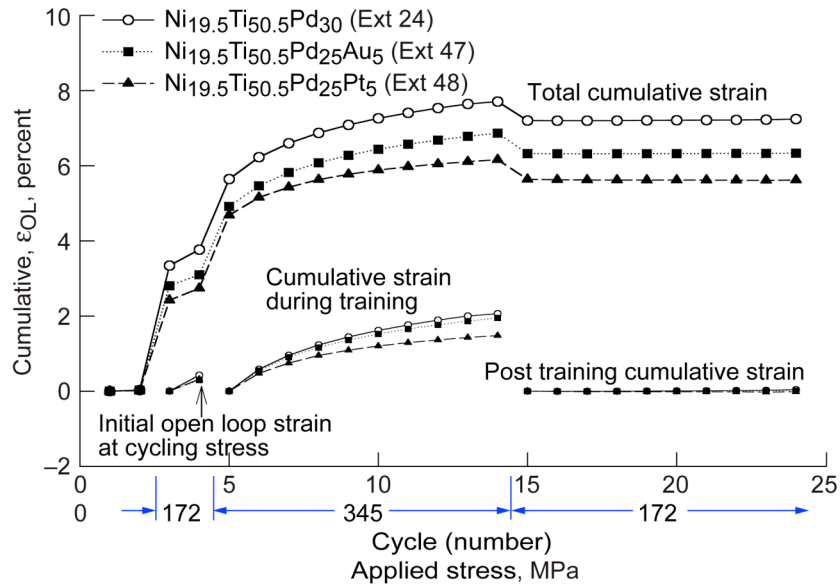
Figure 5.2.—Illustration of training and cycling tests on the ternary and quaternary alloys with individual test portions separated.
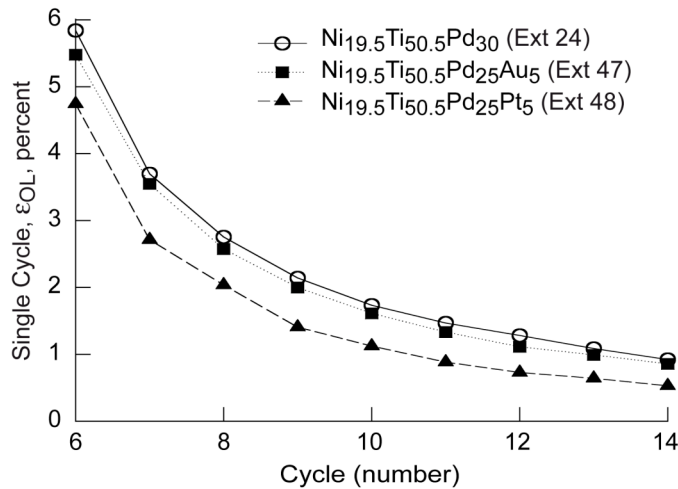
Figure 5.3.—Plot showing the individual cycle ε_{OL} for the training cycles. The platinum containing quaternary alloy was more efficient at decreasing permanent deformation in the sample, as can be seen by the lower ε_{OL} and lower slope for the quaternary alloys during the same cycle.

quaternary alloys than it was in the ternary alloys, and fewer cycles were needed to reach the same ε_{OL}. Another indication that training is more effective in the solid solution strengthened alloys is that after the same number of training cycles (same training regimen), the average open loop strain was smaller in the quaternary alloys (1.24E-3 and -1.87E-3% for the $Ni_{19.5}Ti_{50.5}Pd_{25}Au_5$ and $Ni_{19.5}Ti_{50.5}Pd_{25}Pt_5$) than it was for the ternary alloy (3.89E-3% in $Ni_{19.5}Ti_{50.5}Pd_{30}$) (Figure 5.4, Table 5.1). Training seems to be equally effective in all the alloys, producing essentially the same percent reduction in ε_{OL}, but results in a greater overall effect in the solid solution strengthened alloys because of the smaller baseline and thus a smaller post-training single-cycle ε_{OL} (Table 5.1, Chapter 4).
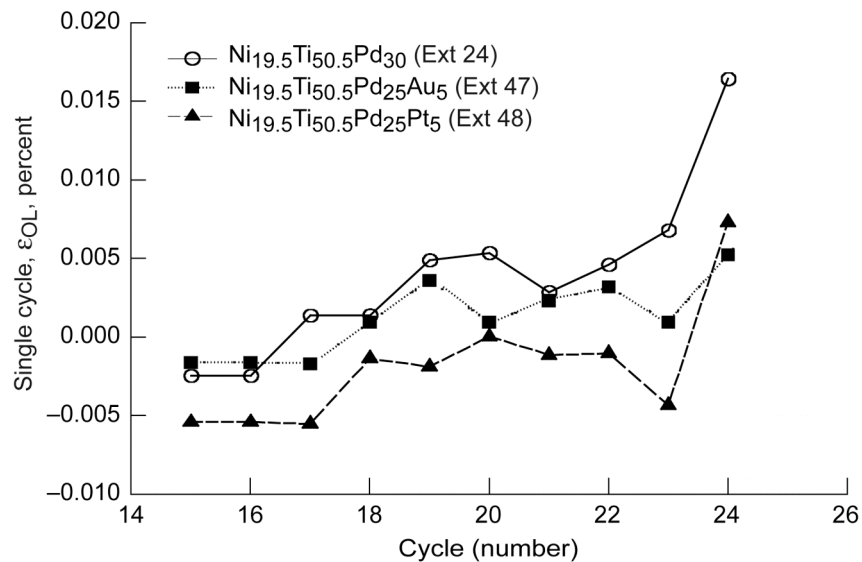
Figure 5.4.—Post training single-cycle open loop strain in the 30 at.% palladium and related quaternary alloys. A lower average ε_{OL} per cycle is realized in the quaternary alloys.

TABLE 5.1.—COMPARISON OF BASELINE AND POST-TRAINING ε_{OL} FOR SAMPLES TRAINED FOR 10 CYCLES AT 345 MPa

Alloy	Baseline ε_{OL} (%)	Average Post-Training Single-Cycle ε_{OL} (%)	Reduction in ε_{OL} (%)
$Ni_{19.5}Ti_{50.5}Pd_{30}$	0.423	0.00389	99.08
$Ni_{19.5}Ti_{50.5}Pd_{25}Au_5$	0.294	0.00124	99.58
$Ni_{19.5}Ti_{50.5}Pd_{25}Pt_5$	0.317	−0.00187	100.59

As training progresses, the ε_{OL} per cycle decreased (Figures 5.2, 5.3). This was due to the operation of various dislocation processes. Dislocations were generated within the matrix and moved under the applied stress until they began to pile up against obstacles such as grain boundaries and particles. The back-stress from the dislocation pile-ups inhibited the generation and movement of additional dislocations, thus decreasing the cyclic ε_{OL}. In the $Ni_{19.5}Ti_{50.5}Pd_{25}Au_5$ and $Ni_{19.5}Ti_{50.5}Pd_{25}Pt_5$ alloys, solid solution strengthening of the matrix raised the critical stress for slip as seen in Chapter 4 thus making dislocation generation and movement more difficult. Thus, when a stress was applied and the sample thermally cycled, fewer dislocations were generated, and those that were, along with the critical stress for slip, more quickly reached a stress level equivalent to the resolved stress on each plane. This is supported by the data just described, in that for a single stress level, the cumulative permanent strain (a measure of the dislocations generated or moved) is less in solid solution strengthened alloys than it is for the ternary alloy, and by the fact that the permanent strain saturates more quickly in the quaternary alloys than in the ternary alloy.

5.3 Load-Bias Testing on Trained Samples

Cumulative open loop strains for the samples which were trained, unloaded, and then tested using a standardized incremental load bias test are shown in Figure 5.5, with training cycles and load-bias cycles separated to isolate the behavior in each section. Cycles during training show good repeatability with data
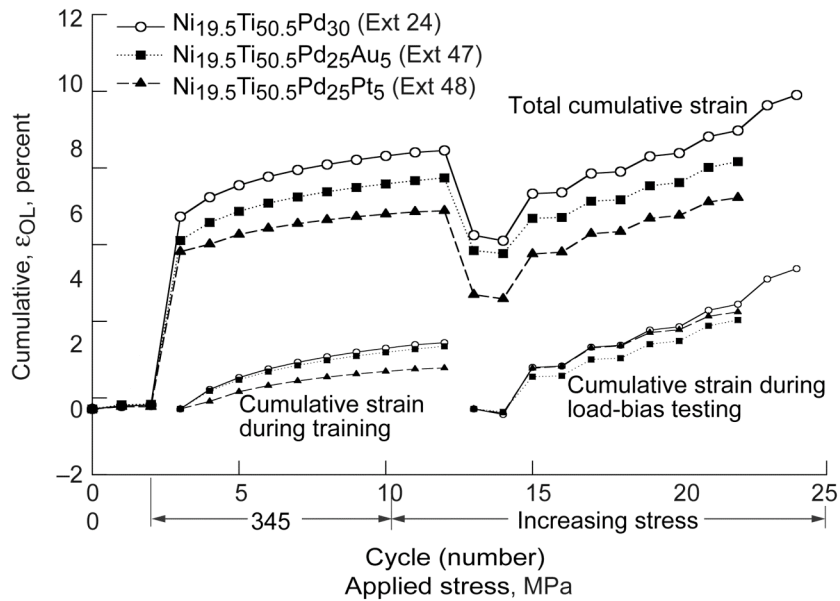
Figure 5.5.—Cumulative open loop strain as a function of cycle for a test where samples were trained, unloaded, and a standard load-bias test run to determine the effect of training on permanent strain and work output.

from the training and cycling tests (Figures 5.2 and 5.4) in which the solid solution strengthened samples show better response to training, with training being most effective in the $Ni_{19.5}Ti_{50.5}Pd_{25}Pt_5$. Open loop strains during load-bias testing of the trained materials are negative at 0 MPa and become positive at applied stresses of 99 MPa and above (Figure 5.6). Both of the quaternary alloys show a plateau effect in which single-cycle open-loop strains are approximately equal at stresses of 99 and 197 MPa, and in the $Ni_{19.5}Ti_{50.5}Pd_{25}Pt_5$ alloy, at 295 MPa as well. Although open loop strains in the trained $Ni_{19.5}Ti_{50.5}Pd_{25}Pt_5$ alloy are only less than those open loop strains for the trained $Ni_{19.5}Ti_{50.5}Pd_{30}$ alloy at stresses above 197 MPa, the $Ni_{19.5}Ti_{50.5}Pd_{25}Au_5$ alloy exhibits the lowest cyclic ε_{OL} at all stresses except for 0 MPa. Compared to the untrained samples, training greatly improves the open loop strains, and therefore the stability of the material, at all stress levels (Figure 5.7), with a maximum improvement of 88.5% being realized in the $Ni_{19.5}Ti_{50.5}Pd_{30}$ alloy at 99 MPa (Table 5.2). However, at all stresses above 99 MPa, the reduction in ε_{OL} is greatest in the $Ni_{19.5}Ti_{50.5}Pd_{25}Au_5$ alloy.

While training significantly improves the dimensional stability or permanent deformation behavior of all three alloy systems, with the solid solution strengthened alloys showing the greatest improvement with training, the transformation strains of the trained samples are not significantly greater than those for the untrained samples, showing improvement only at 0 and 99 MPa (Figure 5.8). However, training does produce an interesting plateau effect regarding transformation strains. This plateau effect is the direct result of the effect the applied training stress has on the distribution of martensite variants. When the samples are trained, self accommodating martensite twin variants are reoriented such that the strain produced during transformation to and from austenite acts along the tensile axis. The plateau effect is representative of equivalent amounts of variants being oriented in the preferred direction, or a saturation of the effect, producing equivalent transformation strains at a variety of stress levels. While all of this means that work output is only improved at 99 MPa over that for untrained samples (Figure 5.9), it also results in all three alloys producing equivalent amounts of work at all stress levels up to 393 MPa.
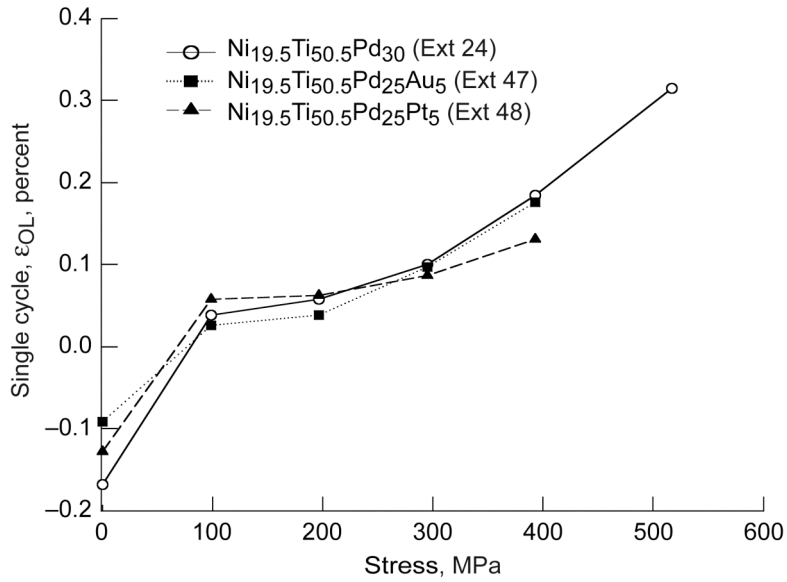
Figure 5.6.—Single cycle open loop strain for post trained samples.
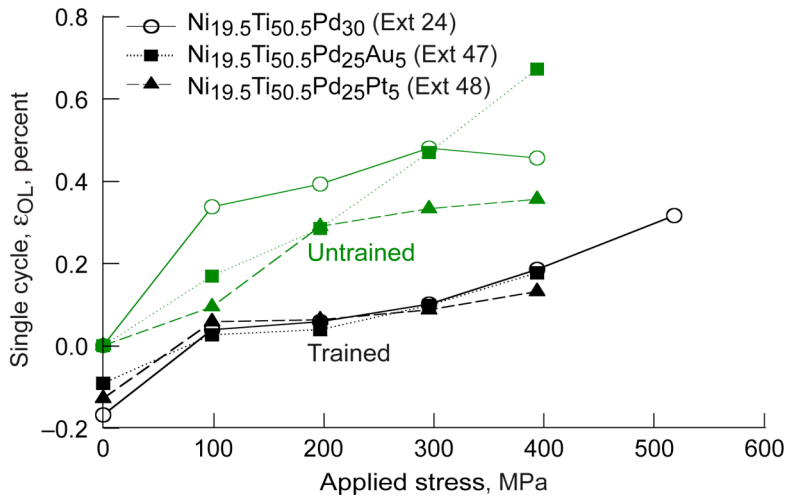
Figure 5.7.—Permanent deformation (ε_{OL}) as a function of applied stress for trained and untrained samples. It can be seen that training equalizes the permanent deformation of all three compositions.
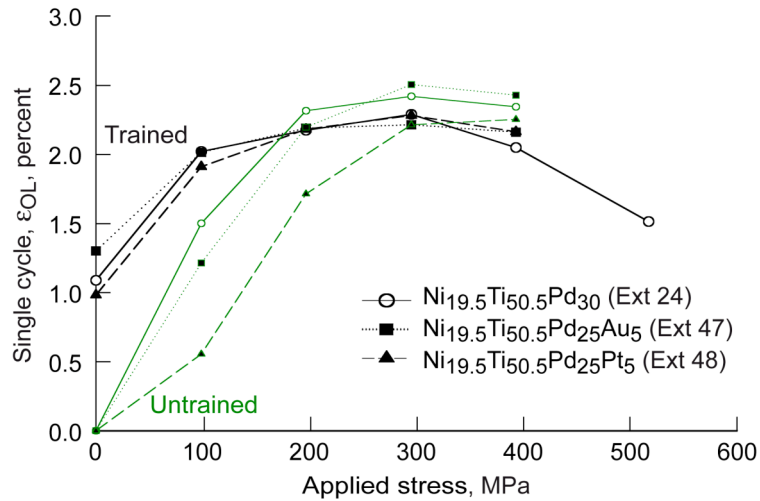
Figure 5.8.—Single cycle transformation strain as a function of applied stress for untrained and trained samples. A plateau effect can be seen in the trained samples in which the transformation strain is approximately equal at stresses of 99 to 395 MPa.

TABLE 5.2.—COMPARISON OF ε_{OL} FOR UNTRAINED AND TRAINED SAMPLES DURING LOAD-BIAS TESTING

Alloy	Applied Stress (MPa)	Untrained ε_{OL} (%)	Post-Training ε_{OL} (%)	Reduction in ε_{OL} (%)
$Ni_{19.5}Ti_{50.5}Pd_{30}$	0	0.000	-0.168	—
	99	0.336	0.039	88.5
	197	0.392	0.058	85.2
	295	0.479	0.101	79.0
	393	0.455	0.185	59.3
	517	—	0.315	—
$Ni_{19.5}Ti_{50.5}Pd_{25}Au_5$	0	0.000	-0.091	—
	99	0.169	0.026	84.4
	197	0.284	0.039	86.3
	295	0.468	0.097	79.2
	393	0.670	0.176	73.7
$Ni_{19.5}Ti_{50.5}Pd_{25}Pt_5$	0	0.000	-0.128	—
	99	0.094	0.058	38.6
	197	0.289	0.063	78.3
	295	0.332	0.087	73.8
	393	0.355	0.131	63.0
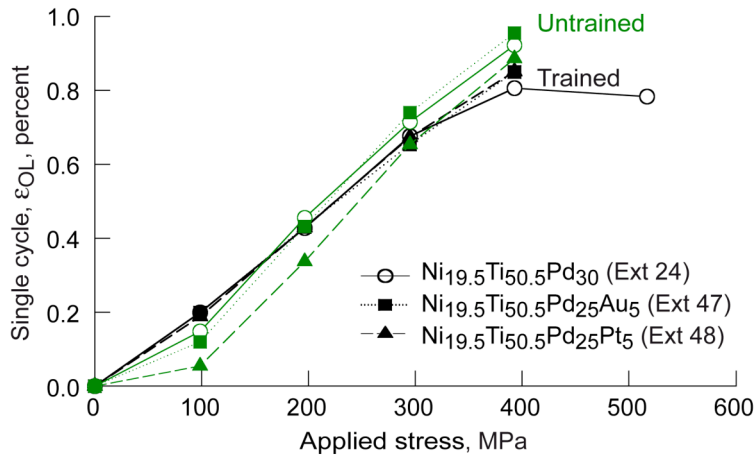
Figure 5.9.—Work output as a function of applied stress showing that all alloys have effectively the same work output after training.
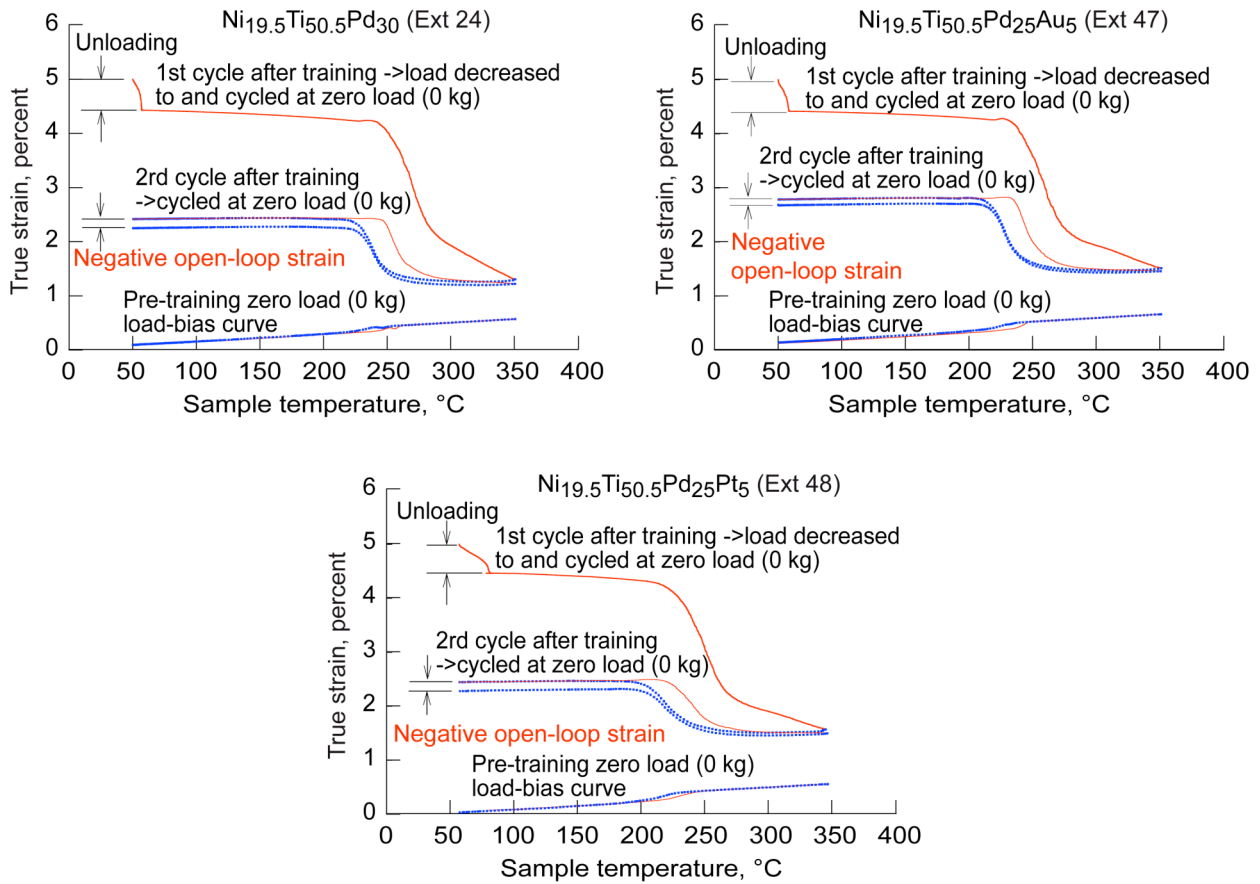
Figure 5.10.—Plots of pre and post training no-load hysteresis curves. In the pre-trained curves, the permanent deformation is zero and the loop completely closes. After training at 345 MPa, the no-load hysteresis cycle shows negative open loop strain, due to continuing recovery of residual training stresses.

As can be seen in Figures 5.4, 5.6, 5.7, and Table 5.1, the open loop strain in the first couple of cycles after training can have negative open loop strains. This negative strain means that the material is actually shorter at the end of a cycle than it was at the beginning. This phenomenon occurs in many samples after training (Figure 5.10) for two reasons: (1) residual internal stresses in the material produced by cycling under high load are greater than those internal stresses that would be imposed by the lesser load applied after training, and (2) the number of variants preferentially oriented by the training stress is greater than the number that would otherwise be preferentially oriented in that direction by the lower stress. While all of the initial variants are acting to produce strain during the heating cycle, some of those preferentially oriented variants revert to a self accommodating mode upon cooling, and so the transformation strain upon cooling is less than that during heating. Thus, as the sample is heated, and then cooled, these two processes work against the applied load and produce a decrease in strain over the cycle, which translates into negative open loop strain.

5.4 Thermal Stability

One problem that occurs when using shape-memory actuators is that their properties are degraded if cycled to too high a temperature. To illustrate this, two samples were each trained and load-bias tested using the same stresses and progression of steps. However, one sample was only cycled to a high temperature of 350 °C (Figure 5.11), while the other was cycled to a high temperature of 450 °C (Figure 5.12); both samples were cooled to below 100 °C. In a comparison plot of the 295 MPa cycle for both tests (Figure 5.13) shows the dramatic difference in deformation behavior between these two tests, with the sample cycled to a high temperature of 450 °C exhibiting over 1.5% open loop strain compared to 0.1% for the sample cycled to 350 °C. Also, the sample cycled to a high temperature of 450 °C shows evidence of creep, as indicated by the strain-temperature curve sloping upward at high temperatures (strain is increasing, meaning the sample is softening and elongating under load), rather than the data exhibiting a linear region of austenite coefficient of linear expansion (CTE) as seen in the samples discussed previously.
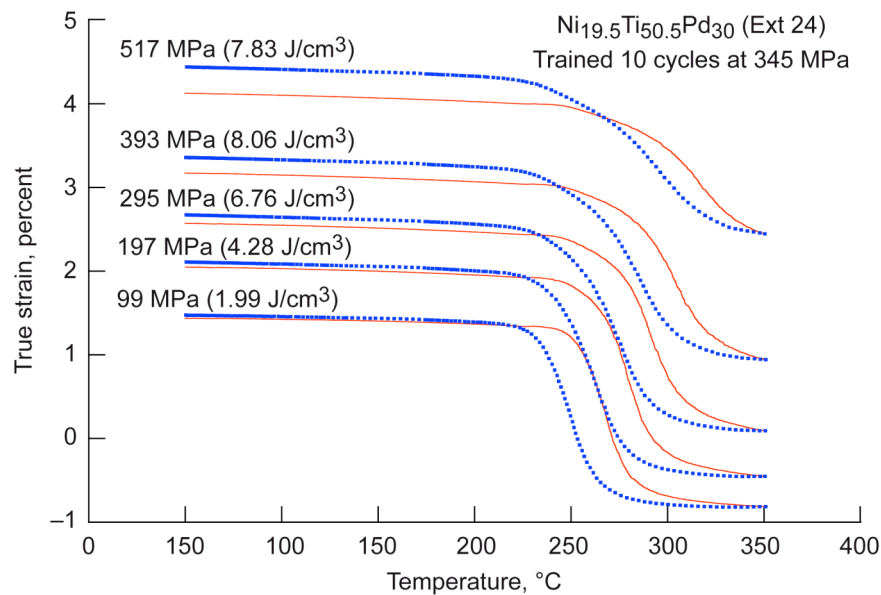
Figure 5.11.—Load-bias test for a ternary 30 at.% palladium sample trained ten
cycles at 345 MPa to dimensionally stabilize it.
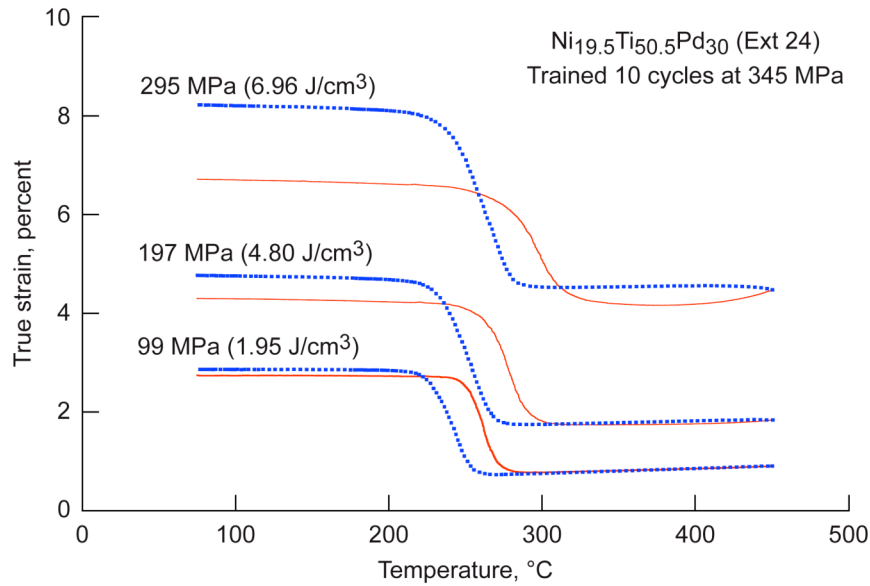
Figure 5.12.—Load-bias test for a $Ni_{19.5}Ti_{50.5}Pd_{30}$ sample which had been trained ten cycles at 345 MPa to dimensionally stabilize it. However, the sample was overheated by cycling to 450 °C. High temperature softening negated the normal training benefit.
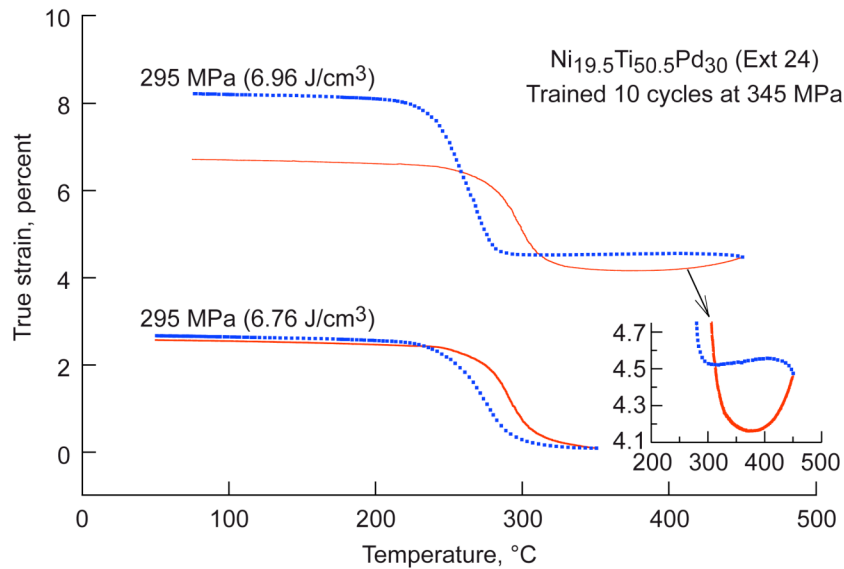
Figure 5.13.—Comparison of equally trained samples of $Ni_{19.5}Ti_{50.5}Pd_{30}$ where one sample was conservatively cycled to 350 °C, and the other to 450 °C. The sample cycled to the higher temperature softened and elongated in creep-like fashion in the austenite phase.

While overheating a trained sample does produce a large increase in open loop strain compared to trained and even untrained samples cycled to a high temperature of 350 °C (Figure 5.14), the transformation strain, and therefore work output of the material is not significantly affected (Figures 5.15 and 5.16). The large increase in open loop strain in the overheated sample is due to deformation of both the austenite and martensite phases; high temperature creep in the austenite phase, and softening of the martensite phase (relaxation of training effects). Training stabilizes the material against plastic
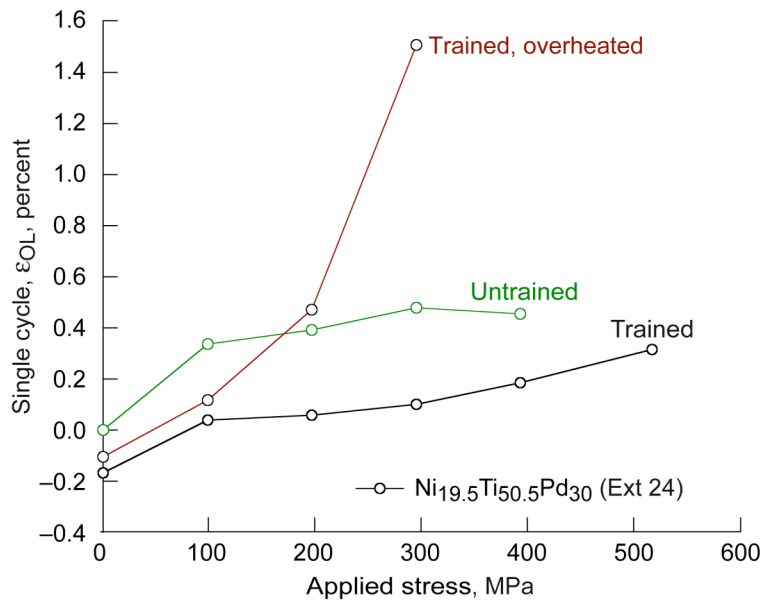
Figure 5.14.—Effect of training and overheating on open loop strain.
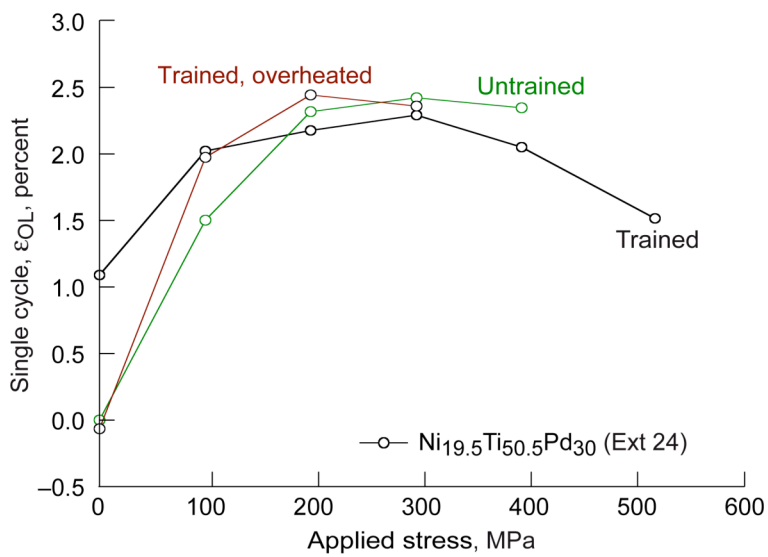
Figure 5.15.—Effect of training and overheating on transformation strain.
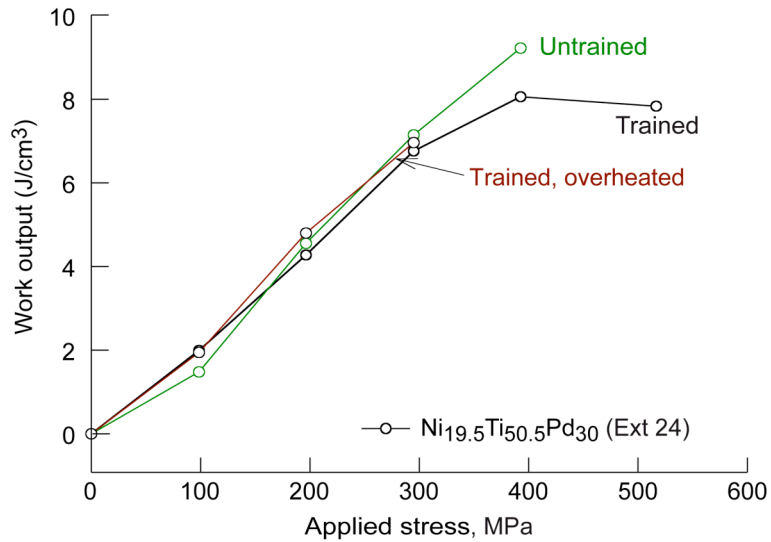
Figure 5.16.—Effect of training and overheating on work output showing
relatively no effect on work output, but a decrease in strength (in that
it failed above ~300 MPa).

deformation in the martensite, but if the material is subsequently overheated during cycling, the benefits of the training are reversed, and performance degrades to a state worse than that for the untrained material. In addition to post training effects, overheating a sample during training can cause dynamic recovery of any dislocation structure, effectively negating the beneficial effect of training on ε_{OL}. During training cycles on the $Ni_{19.5}Ti_{50.5}Pd_{30}$ alloy where the sample was cycled between 75 and 450 °C, the open loop strain initially decreased as the sample was conditioned to that stress. Then, as the training progressed, recovery in the microstructure caused the open loop strain to increase, rather than decrease as it should have (Figure 5.17).

There are two main methods for use of these materials in actuators—differential strain control or on/off actuation. In differential strain control, temperature and/or current in the material are closely controlled, allowing the user to partially transform the material. However, this method is complicated, and extensive control algorithms are necessary along with extensive characterization of the strain-temperature behavior with relation to previous thermomechanical treatment and applied stress, as well as current-temperature characterization if current is to be the controlling factor. Because of this complexity, many applications rely on on/off type actuation where the material is either fully strained in the martensitic state or fully recovered and in the austenite state. As such, hard stops can be used to limit strain if needed. Temperature is often not of great concern to the user, the only requirement being that it is either above the A_F or below the M_F. This lack of close monitoring and control can lead to overheating of the sample, which as discussed, can lead to softening, and eventual disablement of the actuator. Therefore, the material must not only be characterized for mechanical tensile or compressive behavior, permanent deformation, and work output but must also be evaluated for thermal stability with respect to the highest operating temperature that can be reached without leading to a degradation of other properties. This way, an upper use temperature can be determined for the material, which can be used as a guiding parameter for actuator design and use.

By training samples and mechanically stabilizing them, the influence of upper cycle temperature on the sample behavior can be determined. To do this, the samples can be trained to dimensionally stabilize them and reduce or eliminate permanent deformation. Then, as the samples are thermally cycled, the decrease in dimensional stabilization with temperature can be determined by measuring the increase in plastic deformation of each cycle.
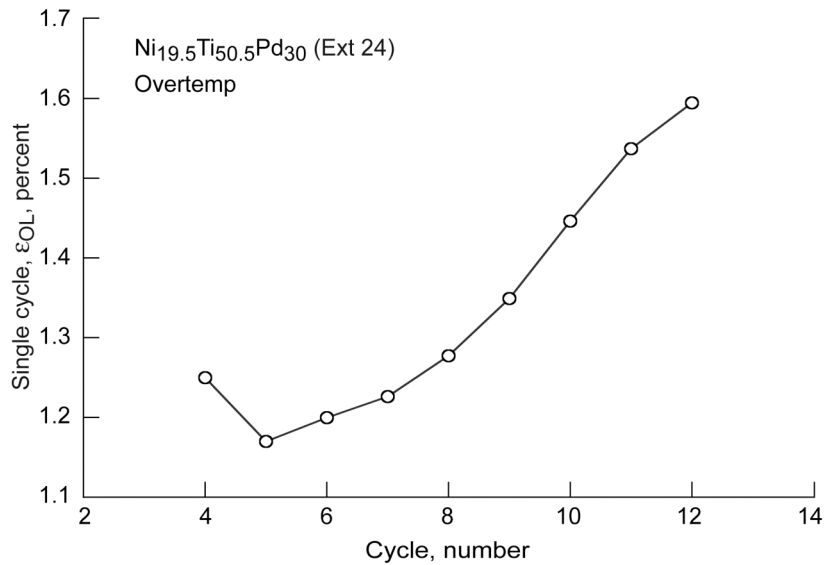
Figure 5.17.—Effect of overheating during the training regime. Instead of the training producing a reduction in the plastic deformation behavior of the material, the material experiences recovery while training, and so the material actually softens instead of stabilizing.
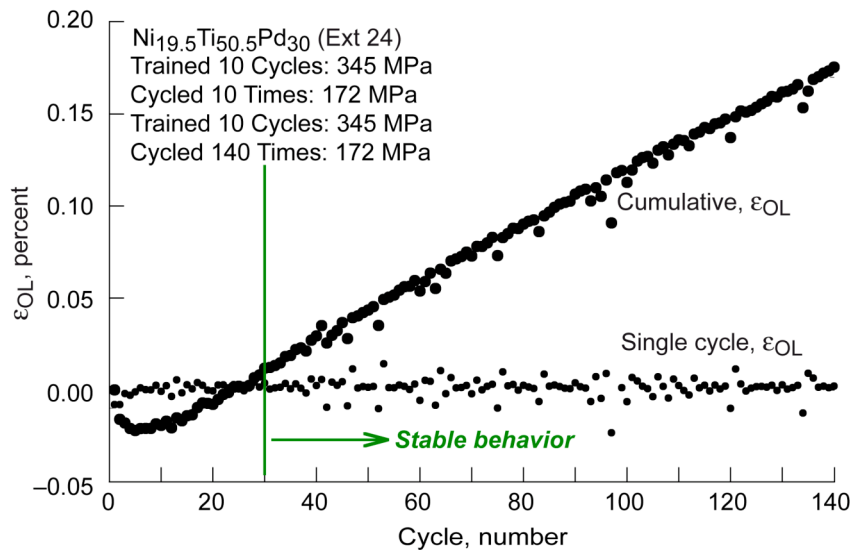
Figure 5.18.—Open loop strain in a 30 at.% palladium sample after training for twenty cycles. The sample is seen to be recovering part of the residual stress from the training during the first couple of cycles. Stable behavior exists for the final 110 cycles.

A $Ni_{19.5}Ti_{50.5}Pd_{30}$ sample which was trained, as discussed previously, by cycling a total of 20 times at 345 MPa and cycled thereafter at 172 MPa had an average ε_{OL} of 1.25E-3%t per cycle in the 140 cycles after training (Figure 5.18). As can be seen, the first couple of cycles after training produced negative open loop strain due to the sample being cycled at a lower stress level than it was trained, and therefore was still recovering some of the residual stress put into it at 345 MPa. After these initial cycles, the

sample stabilized, and the open loop stress per cycle leveled out to a more constant level. The sample averaged 1.48E-3% strain per cycle over the last 110 cycles, during which time it exhibited stable behavior. This 110 cycle average open loop strain is higher than the average over the total 140 cycles only because the 140 cycle average included those cycles whose open loop strain was negative due to stress recovery.

This same sample, with a known stable average ε_{OL} was then tested to determine the effect of increasing temperature above the A_F on stability, i.e. its thermal stability. As described in Section 2.2.5: Thermal Stability, this involved cycling the sample under load to a high temperature limit beginning at 350 °C and then increasing the upper temperature limit by 10 °C after each ten cycles, adding up to a total of 110 cycles between 350 and 450 °C. Also, another sample of the same composition which had only ten cycles of training was tested for thermal stability in the same manner (Figure 5.19).
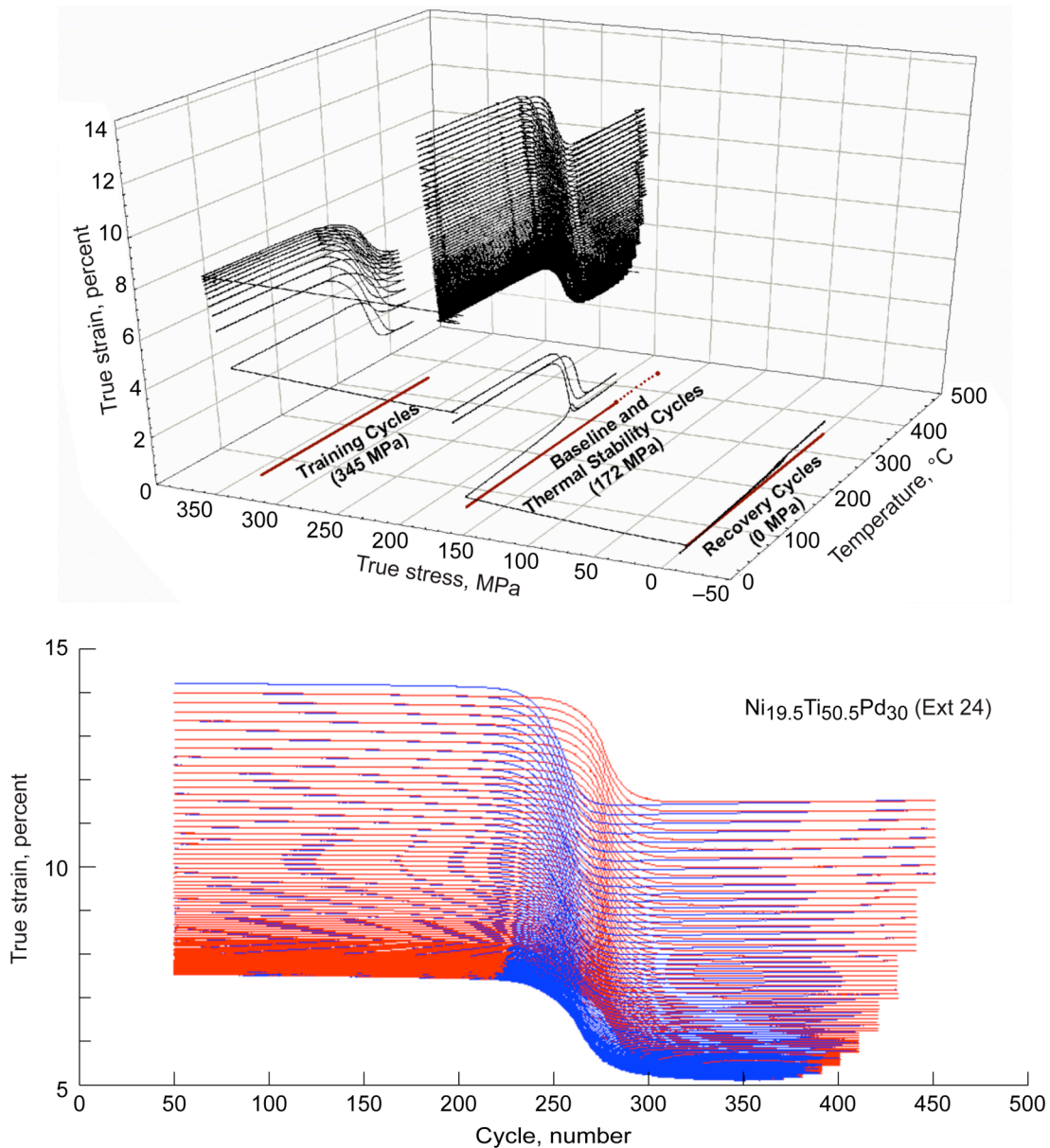
Figure 5.19.—Strain-stress-temperature plot of the thermomechanical training test for $Ni_{19.5}Ti_{50.5}Pd_{30}$, illustrating the individual test segments and extents of heating/cooling (shadow line.) During the thermal stability portion of the test (enlarged in the bottom figure for clarity), the high temperatures reached for

each of the ten-cycle segments are illustrated by dots on the shadow line corresponding to the thermal stability cycles.

When the first sample was only cycled to a maximum of 350 °C, over those 110 cycles mentioned previously, it remained stable over all 110 cycles, with a cumulative ε_{OL} of 0.163%. However, when this sample (trained for 20 cycles) was cycled at 172 MPa to incrementing high temperatures it developed high levels of permanent deformation which were affected more strongly by the higher temperatures and resulted in 5.55% cumulative ε_{OL} over 110 cycles. The other sample, which was trained for ten cycles and then cycled at 172 MPa thereafter, also developed high levels of permanent deformation which increased more rapidly as temperature increased and resulted in 6.47% cumulative ε_{OL} over the 110 total cycles (Figure 5.20).

Because the single cycle ε_{OL} was comparable between the two trained and thermally tested samples (Figure 5.21), and because of the low ductility of the compositions being tested, it was decided to use a ten cycle training regimen to prepare the remaining two alloys for the thermal stability tests. (Therefore, during the entirety of this work, the only sample trained for 20 cycles instead of the standard 10 cycles was this one—used to prove that the $Ni_{19.5}Ti_{50.5}Pd_{30}$ was thermally and dimensionally stable up to a high temperature of 350 °C, and then subsequently used to show that dimensional stability degraded with increasing high temperature between 350 and 450 °C.) With the improved training response of the quaternary alloys derived from the ternary alloy, ten training cycles would still provide enough training to stabilize the materials while minimizing the possibility of overstraining and fracturing the sample. Despite this precaution, the $Ni_{19.5}Ti_{50.5}Pd_{25}Pt_5$ alloy of extrusion 48 still failed on the 97th cycle of the thermal stability part of the test (the sample had accumulated 1.5% strain over the 97 thermal stability cycles and a maximum total strain of 6.5% including that for the recovery, training, and thermal stability cycles) and another sample had to be tested, which successfully completed 110 thermal stability cycles. Although premature failure occurred, useful results were still obtained since the data for the two tests on that composition match until six cycles prior to failure. This observation shows both the reproducibility of the test and that the influence of crack growth on the open loop strain can be isolated to an extent.
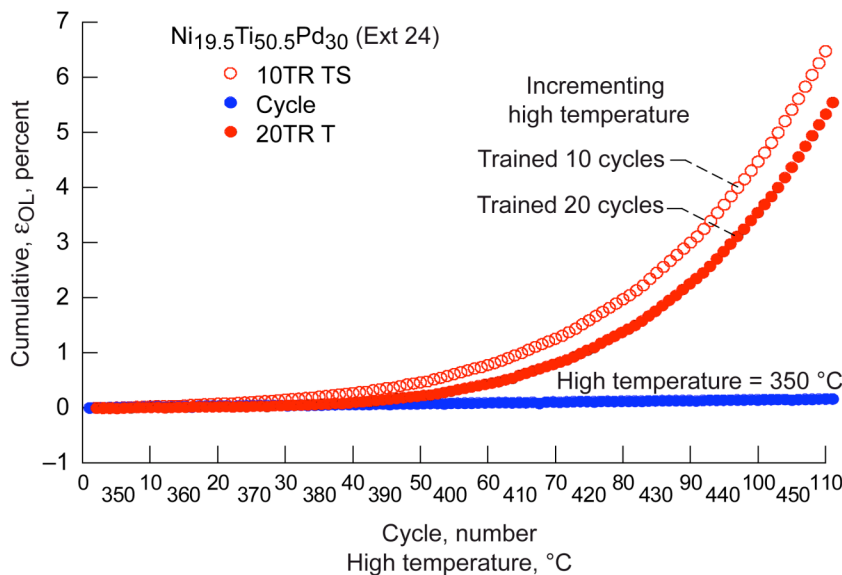
Figure 5.20.—Comparison of a sample trained twenty cycles and then cycled to a constant temperature of 350 °C (showing stable behavior) and for samples trained ten and twenty cycles and then cycled to incrementing higher temperatures (unstable behavior).
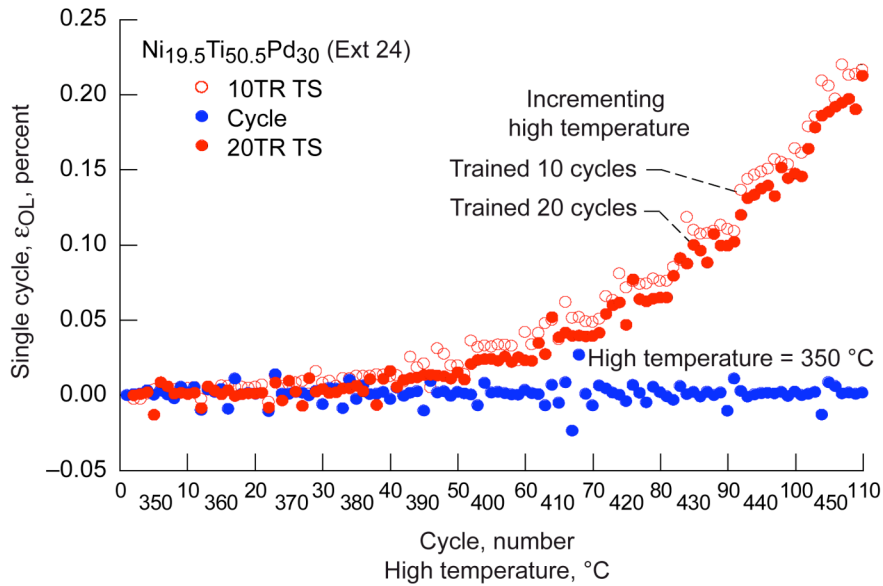
Figure 5.21.—Though some long term benefit can be gained from training twenty cycles, such as slightly decreased cumulative open loop strain (Figure 5.20), on an individual cycle basis, the ε_{OL} behavior is the same for samples trained 10 and 20 cycles.
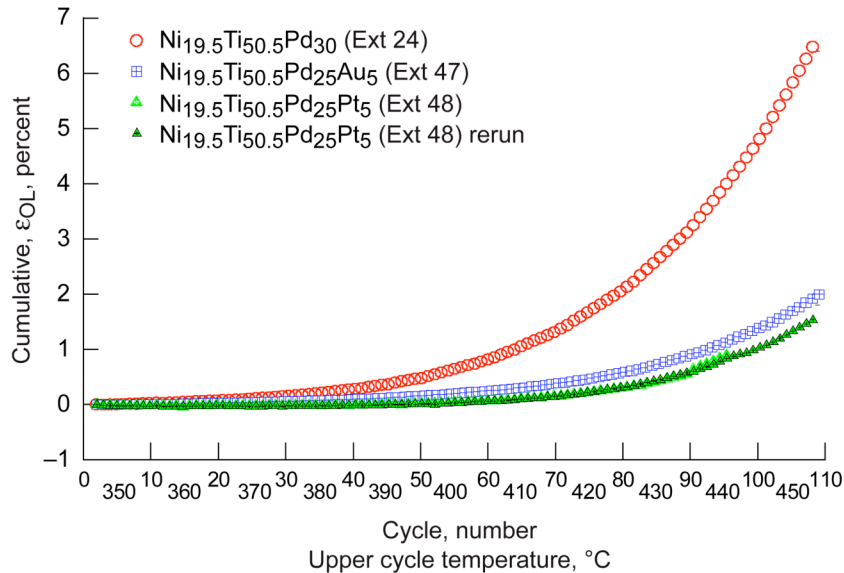
Figure 5.22.—Cumulative open loop strain in samples cycled to incrementing high temperatures from 350 to 450 °C in ten-cycle increments. The data shows evidence of secondary and tertiary creep for all samples, but for the ternary alloy tertiary creep occurs at a much lower temperature and there is greater softening than in the quaternary alloys.

Over the course of the 110 thermal stability cycles, the two quaternary $Ni_{19.5}Ti_{50.5}Pd_{25}Au_5$ and $Ni_{19.5}Ti_{50.5}Pd_{25}Pt_5$ alloys accumulated only 1.99 and 1.54% permanent strain respectively, less than one-third of that accumulated by the baseline $Ni_{19.5}Ti_{50.5}Pd_{30}$ alloy over the same number of cycles (Figure 5.22). In order to isolate individual temperatures and quantify the effect on permanent deformation, the data from the 110 cycles was split up into separate 10-cycle bins. Each bin contained

data wherein the strain was rezeroed at the start of the ten-cycle block and was referred to the highest temperature reached during those 10 cycles (Figure 5.23). In this way, only the strain accumulated in each block was reported. From this data, it can be seen that softening of the $Ni_{19.5}Ti_{50.5}Pd_{30}$ alloy really begins to take affect around 390 to 400 °C, which correlates well with the data from Xu et al. (ref. 79) in which a large decrease in hardness is seen centered around 400 °C. In comparison, the quaternary alloys show an improvement in high temperature thermal stability due to solid solution strengthening, and begin to be largely affected by softening at 420 to 430 °C, an increase of 30 °C over the ternary alloy.
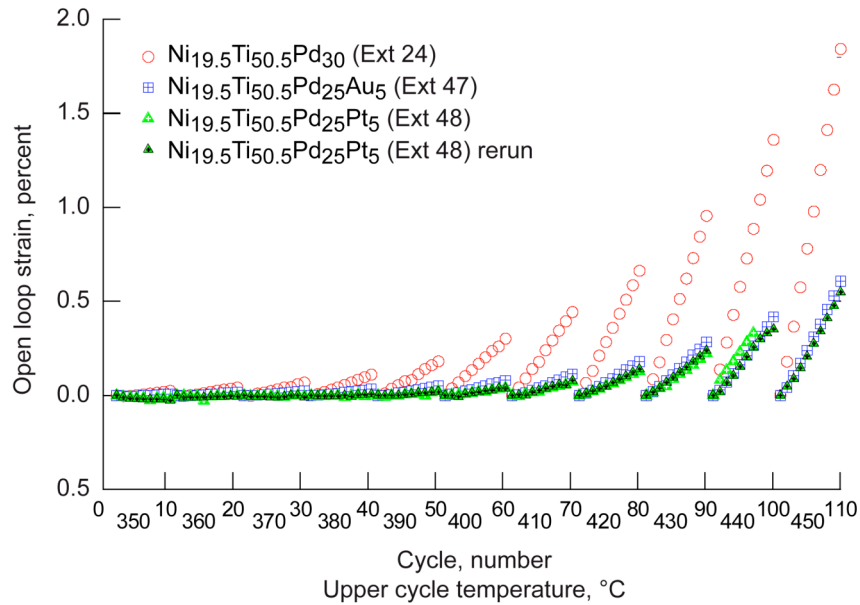
Figure 5.23.—Cumulative open loop strain broken up into temperature bins to reflect the effect of each temperature on the dimensional stability of the materials.

Chapter 6—Summary and Conclusions

6.1 Ternary NiTiPd Alloys

Five ternary alloys with compositions of $Ni_{49.5-x}Ti_{50.5}Pd_x$ were melted, cast, and extruded at 900 °C with an area reduction ratio of 7:1. Density measurements of the five compositions revealed that density increased linearly with increasing palladium content from 6.97 g-cm^{-3} for the 15 at.% palladium to 8.09 g-cm^{-3} for 46 at.% palladium. Room temperature microstructural analysis of the alloys showed that they were predominantly a single phase martensite, with small amounts of second phase particles Ti(O,C) and Ti_2(Ni,Pd), with no more than 4 vol% total of second phase particles in any one alloy.

Transformation temperatures were determined through thermal cycling under zero load. Martensite start temperatures, like the M_F, A_S, and A_F, increased linearly with palladium content, ranging from M_S = 65 °C in the $Ni_{34.5}Ti_{50.5}Pd_{15}$ alloy to 469 °C in $Ni_{3.5}Ti_{50.5}Pd_{46}$. Thermal hysteresis for all alloys was approximately 10 °C, except for $Ni_{3.5}Ti_{50.5}Pd_{46}$, which was 28 °C. The full range transformation ranged between 18 and 26 °C for the 15 through 30 at.% alloys, and was 44 °C for the 46 at.% alloy.

Monotonic tension tests revealed that as palladium content in the ternary alloys increased, the yield strength in the martensite phase increased from 97 to 365 MPa, while the yield strength in the austenite phase decreased from 437 to 98 MPa. This produced a relative difference in yield strength between the austenite and martensite phases which decreased from +341 MPa at 15 at.% palladium to –267 MPa at 46 at.% palladium. Therefore, while increasing palladium content raises transformation temperatures, it also decreases the relative yield stress between the austenite and martensite phases to a point where alloys above approximately 37 at.% palladium would not be expected to behave well as actuators.

Load bias tests performed on the samples at increasing stresses from 99 to 393 MPa showed that transformation strain and work output increased with an increase in applied stress. In contrast, transformation strains and therefore work output decreased with increasing palladium content. Open loop strains increased both with increases in stress and palladium content, reaching a maximum of 0.479% in a single cycle at 295 MPa in the $Ni_{19.5}Ti_{50.5}Pd_{30}$ alloy. In agreement with the monotonic tensile data which qualitatively indicated $Ni_{3.5}Ti_{50.5}Pd_{46}$ did not have the properties needed for a viable actuator material, in load-bias testing at 99 MPa, the $Ni_{3.5}Ti_{50.5}Pd_{46}$ alloy was not able to produce a positive transformation strain and elongated to failure after transforming to the weak austenite phase.

6.2 Quaternary NiTiPdX Alloys

Three quaternary alloys of compositions $Ni_{19.5}Ti_{50.5}Pd_{25}Au_5$, $Ni_{19.5}Ti_{50.5}Pd_{25}Pt_5$, $Ni_{3.5}Ti_{47.5}Pd_{46}Hf_3$ were produced in the same melt → cast → heat treat → extrude process as the ternary NiTiPd alloys. Density increased from 7.5 g-cm^{-3} in the $Ni_{19.5}Ti_{50.5}Pd_{30}$ alloy to ~8.0 g-cm^{-3} in the $Ni_{19.5}Ti_{50.5}Pd_{25}Au_5$ and $Ni_{19.5}Ti_{50.5}Pd_{25}Pt_5$ alloys. Hafnium substitution for titanium in the $Ni_{3.5}Ti_{47.5}Pd_{46}Hf_3$ alloy caused a density change from 8.1 to 8.4 g-cm^{-3}. Chemical analysis indicated on-target compositions for all elements except for titanium, which was lower than the target composition for all of the alloys. Room temperature microstructural analysis of the alloys revealed a martensitic matrix with a low density distribution of second phase particles Ti(O,C), and $(Ti,Y)_2$(Ni,Pd,X) (where Y=Hf, and X=either Au or Pt). The volume fraction of second phase particles decreased to 2.13 and 2.26% in the $Ni_{19.5}Ti_{50.5}Pd_{25}Au_5$ and $Ni_{19.5}Ti_{50.5}Pd_{25}Pt_5$ alloys from that of 3.26% in $Ni_{19.5}Ti_{50.5}Pd_{30}$. In the $Ni_{3.5}Ti_{47.5}Pd_{46}Hf_3$ alloy, volume percent of $(Ti,Hf)_2$(Ni,Pd) particles increased to 3.63% from 2.26% in ternary $Ni_{3.5}Ti_{50.5}Pd_{46}$. However, as the majority of the gold, platinum or hafnium alloying addition ended up in solution in the matrix, it was inferred that whatever improvement in strength or properties was gained due to solid solution strengthening, rather than particulate strengthening.

Transformation temperatures were again determined from no-load load-bias tests. Additions of gold or platinum to $Ni_{19.5}Ti_{50.5}Pd_{30}$ left the transformation temperatures relatively unchanged. However, the

addition of hafnium to the $Ni_{3.5}Ti_{50.5}Pd_{46}$ alloy suppressed the transformation temperature by 63 °C in the M_F, and by 70 °C in the A_F. Thermal hysteresis was increased from 10 °C in the $Ni_{19.5}Ti_{50.5}Pd_{30}$ alloy to 14 °C in $Ni_{19.5}Ti_{50.5}Pd_{25}Au_5$ and 12 °C in the $Ni_{19.5}Ti_{50.5}Pd_{25}Pt_5$ alloy. The full range transformation also increased, from 26 °C in $Ni_{19.5}Ti_{50.5}Pd_{30}$ to 31 °C in both $Ni_{19.5}Ti_{50.5}Pd_{25}Au_5$ and $Ni_{19.5}Ti_{50.5}Pd_{25}Pt_5$. Thermal hysteresis remained relatively unchanged with the addition of 3 at.% hafnium to $Ni_{3.5}Ti_{50.5}Pd_{46}$, but the full range transformation decreased from 44 to 37 °C.

Monotonic tension tests reveal that all three quaternary alloying additions improved the relative strengths of the martensite and austenite phases. Gold additions of 5 at.% increased martensitic yield stress by 23 MPa and austenite yield strength by 139 MPa. Platinum additions of 5 at.% increased martensitic yield stress by 19 MPa and that of austenite by 93 MPa. Hafnium, however, decreased the martensite yield stress by 26 MPa and improved the yield stress of austenite by 158 MPa. All of the quaternary alloying additions studied improved monotonic tensile behavior. In total, the gold additions of 5 at.% increased the relative yield strengths of the martensite and austenite phases by 116 MPa, the 5 at.% platinum produced an increase of 74 MPa, and 3 at.% hafnium an increase of 184 MPa. Considering the fact that not all of the hafnium actually made it into solution to act as a solid solution strengthening agent, on a per quantity addition basis, hafnium was much more effective than gold and platinum at solid solution strengthening, with gold the second most effective, and platinum the least but still effective agent, based on the monotonic tensile data.

In accordance with the monotonic tension data, load-bias testing of the hafnium strengthened alloy showed the ability to produce work at stresses up to 197 MPa, where the ternary $Ni_{3.5}Ti_{50.5}Pd_{46}$ alloy produced no work even at 99 MPa. However, also in accordance with the monotonic tension data, which still showed a deficiency in austenite yield strength relative to martensite yield strength of 183 MPa, the alloy experienced large amounts of plastic deformation while cycling under load, and gained 6.3% strain over a single cycle at 197 MPa. Permanent deformation, measured as open loop strain was decreased at all stresses in the $Ni_{19.5}Ti_{50.5}Pd_{25}Pt_5$ alloy over that for $Ni_{19.5}Ti_{50.5}Pd_{30}$, but in the $Ni_{19.5}Ti_{50.5}Pd_{25}Au_5$ alloy, only ε_{OL} at 99 and 197 MPa were improved, while ε_{OL} at 295 MPa was the same as that for $Ni_{19.5}Ti_{50.5}Pd_{30}$ at 0.47%, and at 393 MPa was greater, at 0.60% compared to 0.455%.

6.3 Training and Thermal Stability

Because of the large amounts of open loop strain that occur during thermal cycling of these materials, it is necessary to stabilize them dimensionally through a thermomechanical process known as training. Training was performed on the $Ni_{19.5}Ti_{50.5}Pd_{30}$ and its derivative quaternary alloys $Ni_{19.5}Ti_{50.5}Pd_{25}Au_5$ and $Ni_{19.5}Ti_{50.5}Pd_{25}Pt_5$ by cycling samples at 345 MPa for ten cycles between 50 and 350 °C. This process makes use of the "work hardening" effect, whereby dislocations are generated and pile up against obstacles such as grain boundaries and particles, thereby strengthening the material against further plastic deformation. During this process, it was seen that training was more efficient in the quaternary alloys than the ternary alloy, as the single cycle ε_{OL} decreased more rapidly with training in the quaternary alloys than in the ternary. This increase in training efficiency in the quaternary alloys means that for a given starting ε_{OL}, the same number of training cycles would reduce the ε_{OL} more in the quaternary alloys than it would in the ternary alloy. This result correlates well with the data from the monotonic tension tests which showed that the critical stress for slip in the quaternary alloys was more than that for the ternary alloy, meaning that fewer dislocations needed to be generated and moved to strengthen the material to a point where it would be able to resist further dislocation movement.

After training, samples unloaded to 172 MPa and cycled at this stress showed a decrease in open loop stress, over that for a virgin untrained sample, of 99.0, 99.6, and 100.59% in the $Ni_{19.5}Ti_{50.5}Pd_{30}$, $Ni_{19.5}Ti_{50.5}Pd_{25}Au_5$, and $Ni_{19.5}Ti_{50.5}Pd_{25}Pt_5$ alloys respectively. Samples tested using the standard load-bias procedure show an improvement in open loop strains for all compositions, with the ternary alloy showing the greatest percentage improvement in ε_{OL}, at 88.5% reduction in ε_{OL} at 99 MPa. However, the gold strengthened alloy has a smaller post-training ε_{OL} than the ternary alloy at all stresses except 0 MPa, and

the platinum strengthened alloy has a smaller ε_{OL} than the ternary at stresses above 197 MPa. Transformation strain and work output for the trained samples were all approximately equal, and were neither benefited, nor degraded by the training except for at 99 MPa, where transformation strain and work output were greater for the trained samples than for the untrained.

Another purpose of training is to dimensionally stabilize samples such that the effect of cycling to high temperatures on the stability of the alloy can be evaluated apart from any other factor. For example, a trained sample of the $Ni_{19.5}Ti_{50.5}Pd_{30}$ alloy which was cycled to a high temperature of 350 °C had a cumulative permanent strain increase of 0.163% over 110 cycles, which averages to be 1.48E-3% per cycle. In comparison, trained samples of the $Ni_{19.5}Ti_{50.5}Pd_{30}$, $Ni_{19.5}Ti_{50.5}Pd_{25}Au_5$, and $Ni_{19.5}Ti_{50.5}Pd_{25}Pt_5$ alloys were thermally cycled to increasing high temperatures from 350 to 450 °C where the high temperature was increased 10 °C after every ten cycles. These samples accumulated 6.47, 1.99, and 1.53% strain respectively over the 110 cycles. Data from this test is representative of second and third stage creep, with stable elongation leading to unstable elongation. From this test, it can be seen that the $Ni_{19.5}Ti_{50.5}Pd_{30}$ alloy is only dimensionally stable while cycled to temperatures below 390 to 400 °C, while the $Ni_{19.5}Ti_{50.5}Pd_{25}Au_5$ and $Ni_{19.5}Ti_{50.5}Pd_{25}Pt_5$ alloys are stable up to 420 to 430 °C, an improvement of 30 °C in stability.

6.4 Conclusions and Relevance to Actuator Applications

By alloying NiTi with increasing amounts of palladium, the transformation temperatures of the material can be increased. However, this increase in transformation temperatures comes with a corresponding decrease in work output and dimensional stability of the alloy. Therefore, actuators made from these materials would be able to operate at higher temperatures, but would have shorter life spans due to the accumulation of permanent deformation.

Quaternary alloying with gold, hafnium, and platinum can improve the dimensional stability of virgin extruded NiTiPd based shape memory alloys by a factor of two to three. In the case of the gold and platinum additions, this improved stability comes at no cost to the transformation temperatures, while hafnium additions come at minimal cost to the transformation temperature. With all three quaternary alloying additions, the relative yield strengths were improved over those for the baseline ternary alloys. This means that in addition to improving the dimensional stability of ternary NiTiPd alloys, these quaternary additions could possibly also be used to strengthen NiTiPd alloys with compositions around 37 at.% palladium, where the inversion in yield strengths occurs. In strengthening these alloys, it might be possible to retain the type of behavior desired for a viable actuator, and therefore develop actuators with increased transformation temperatures. Nonetheless, it has been shown that quaternary alloying improves dimensional stability of the studied alloys, and therefore alone, could be used to make a better actuator that would have two to three times the lifetime of a ternary NiTiPd actuator.

Training has a stronger effect than quaternary alloying, and alone can increase the dimensional stability of NiTiPd alloys. In fact, training can effectively produce equal work output and permanent deformation behavior in ternary NiTiPd alloys and quaternary solid solution strengthened alloys. In all three alloys that were trained ($Ni_{19.5}Ti_{50.5}Pd_{30}$, $Ni_{19.5}Ti_{50.5}Pd_{25}Au_5$, $Ni_{19.5}Ti_{50.5}Pd_{25}Pt_5$), training was successfully used to decrease the permanent deformation per cycle by over 99%. Thus, while quaternary alloying can improve the properties of a virgin extruded NiTiPd alloy, training alone can be used to produce a good, stable actuator from the quaternary $Ni_{19.5}Ti_{50.5}Pd_{25}Au_5$, $Ni_{19.5}Ti_{50.5}Pd_{25}Au_5$, or even the ternary $Ni_{19.5}Ti_{50.5}Pd_{30}$. This actuator material would be able to operate for more than 250 times the lifetime of an untrained ternary actuator, as long as it was not overheated during use.

If the material were to be overheated during use, quaternary alloying with gold or platinum would provide the additional benefit of increased thermal stability. It can be used to boost thermal stability by 30 °C over ternary $Ni_{19.5}Ti_{50.5}Pd_{30}$. This means that an actuator material has a greater safety factor against overheating if made of the quaternary alloy. This would allow the end user more design flexibility, as the material would not have to be monitored as closely for temperature to guard against overheating.

So, in conclusion, a good actuator (high work output with low plastic deformation) could be made from ternary NiTiPd by training the material to strengthen it against permanent deformation. This actuator would be able to operate for several thousand cycles as long as temperature was closely controlled or monitored. Quaternary alloying could be used to further improve the high temperature performance of the material, and allow a greater thermal safety factor for operation, while also providing increased training response, and therefore, greater life than a ternary alloy trained and cycled under the same conditions.

Appendix A—Normalized Test Temperatures for Monotonic Tensile Testing

TABLE A1.—SUMMARY OF MARTENSITIC TEST TEMPERATURES FOR MONOTONIC TENSION
TESTS SHOWING NORMALIZED TEST TEMPERATURES RANGING FROM 0.88 TO 0.93. ALSO
SHOWN IS THE MARTENSITE TEST TEMPERATURE THAT WOULD RESULT IF ALL TEST
TEMPERATURES WERE NORMALIZED TO M_F(K)*0.9

Pd (at.%)	Ext (#)	M_F (°C)	M_F-50 (°C)	Martensite Test Temperature Normalized To Mf (K)*0.9 (°C)	M_F (K)	M_F-50 (K)	M_F-50/M_F (K)/(K)
15	36	65	23	31	338	296	0.876
20	37	123	73	83	396	346	0.874
25	38	178	128	133	451	401	0.889
30	24	233	183	182	506	456	0.901
25	47	226	176	176	499	449	0.900
25	48	197	147	150	470	420	0.894
46	50	469	419	395	742	692	0.933
46	51	406	356	338	679	629	0.926

TABLE A2.—SUMMARY OF TEST TEMPERATURES FOR MONOTONIC TENSION TESTS IN
THE AUSTENITE STATE SHOWING NORMALIZED TEST TEMPERATURES RANGING
FROM 1.06 TO 1.14. ALSO SHOWN IS THE AUSTENITE TEST TEMPERATURE THAT
WOULD RESULT IF ALL TEST TEMPERATURES WERE NORMALIZED TO A_F(K)*1.1

Pd (at.%)	Ext (#)	A_F (°C)	A_F+50 (°C)	Austenite Test Temperature Normalized To Af (K)*1.1 (°C)	A_F (K)	A_F+50 (K)	A_F+50/A_F (K)/(K)
15	36	83	133	119	356	406	1.14
20	37	143	193	185	416	466	1.12
25	38	197	247	244	470	520	1.11
30	24	259	309	312	532	582	1.09
25	47	257	307	310	530	580	1.09
25	48	229	279	279	502	552	1.10
46	50	513	563	592	786	863	1.06
46	51	443	493	515	716	766	1.07

Appendix B—Chemical Analysis and Polishing Procedures

Summary of Chemical Analysis and Density Measurement Procedures

Sample Preparation

Surface contamination (discoloration/oxidation) is physically removed using abrasive paper or a dremmel tool. The samples were then cut into small pieces with a cut-off wheel and/or shear. The pieces were rinsed with petroleum ether to remove any surface oils. The samples were ready for interstitial gas analysis or ICP preparation.

For analysis by ICP, approximately 100 mg sample is weighed into a teflon digestion vessel. 3 mL HCl, 1 mL HNO3, and 1 mL HF (all concentrated, tracemetal grade) were added to the sample and the vessel is placed in a block digester. The sample is heated at 100 to 130 °C until dissolution is complete (generally 1 to 2 hr). The sample is then transferred quantitatively to a 100 mL volumetric flask and is ready for ICP analysis.

ICP Analysis

The prepared solutions were analyzed for alloying elements and impurities using the Varian Vista-Pro Inductively Coupled Plasma (ICP) Emission Spectrometer. The solution is aspirated by capillary action into an argon plasma which is generated by an RF coil surrounding a stream of argon gas. At the extremely high temperatures of the plasma, the sample is ionized and excited, each element emitting its characteristic wavelengths. The emitted light is introduced to the optical system though the entrance slit, is diffracted by the Echelle polychrometer, and finally detected using a CCD (charge coupled device) detector. The detector is capable of simultaneously detecting up to 73 different elements in the range of 167 to 785 nm.

Several emission lines were selected for each analyte. The ICP is calibrated using NIST-traceable solution standards which bracket the concentration range of the alloys. The emission intensity at each wavelength is proportional to the concentration of analyte present in the sample and can be extrapolated from the calibration curves. The reported value for each element is an average of the selected emission lines.

N/O Analysis

Small sample pieces (~100 mg) were analyzed for oxygen and nitrogen using the Leco TC-436 Nitrogen/Oxygen Determinator. An empty graphite crucible is placed between two electrodes of a furnace. A high current is passed through the crucible, creating high heat which drives off the gas which is trapped within the crucible. A sample is then loaded into the crucible and sealed from the atmosphere. A high current is again passed through the crucible and the sample, which drives off the gases trapped inside of the sample. The oxygen that is released combines with the carbon from the crucible to form CO. The CO is passed through rare earth copper oxide which converts it to CO_2. The CO_2 is passed through an IR cell where it is detected and measured. The CO_2 is then trapped by the ascarite forming H_2O vapor, which is then removed by the anhydrone. The remaining gases were passed through a thermal conductivity cell which detects the amount of N_2 which is present.

C/S Analysis

Small sample pieces (100 to 200 mg) were analyzed for carbon and sulfur using the Leco CS-444LS Carbon/Sulfur Determinator. In analysis by the combustion-instrumental measurement method, the

carbon is converted into carbon dioxide and the sulfur is converted into sulfur dioxide in the presence of oxygen. This reaction takes place during the combustion of the sample in a closed loop system. The carbon dioxide and sulfur dioxide gases that were formed absorb energy at specific infrared wavelengths. The amount of energy that is absorbed at each infrared detector is proportional to the amount of carbon or sulfur which is present in the sample.

Density Determination

The density is performed by Archimedes' Principle using a Mettler XS205 Analytical Balance with attached density apparatus. The sample is weighed in air, and then weighed again while immersed in an auxiliary liquid of known density. The density can then be determined by the following equation

Density, ρ (rho) = $[A/(A-B)]$ $(\rho_0 - \rho_L) + \rho_L$
where   A = wt of sample in air
           B = wt of sample in liquid
           p_0 = density of auxiliary liquid
           p_L = Air density (0.0012g/cc3)

Material	Shape Memory Alloy Ni Ti Pd				

	Surface	MD Piano	Predose	3 sec	Direction	>>
Step 1	Grit/Grain	220 grit		Main Phase		Final Phase
	Lubricant	Water	Time/Removal	2 min 0 sec		30 sec
	Mode	Time	Force	25 N		25 N
	Disc Speed	150 rpm	Abrasive Dosing	Off		Off
	Cleaning	Program 2	Lubricant Dosing	Open		Open

	Surface	MD Plan	Predose	6 sec.	Direction	>>
Step 2	Grit/Grain	6 micron		Main Phase		Final Phase
	Lubricant	DP-Red	Time/Removal	13 min 30 sec		1 min 30 sec
	Mode	Time	Force	25 N		25 N
	Disc Speed	150 rpm	Abrasive Dosing	9		9
	Cleaning	Program 6	Lubricant Dosing	10		10

	Surface	MD Dac	Predose	3 sec.	Direction	>>
Step 3	Grit/Grain	3 µm		Main Phase		Final Phase
	Lubricant	DP-Red	Time/Removal	4 min 30 sec		30 sec
	Mode	Time	Force	25 N		25 N
	Disc Speed	150 rpm	Abrasive Dosing	9		9
	Cleaning	Program 4	Lubricant Dosing	10		10

	Surface	MD DAC	Predose	6	Direction	>>
Step 4	Grit/Grain	1 µm		Main Phase		Final Phase
	Lubricant	DP-Red	Time/Removal	2 min 10 sec		50 sec
	Mode	Time	Force	25 N		25 N
	Disc Speed	150 rpm	Abrasive Dosing	8		8
	Cleaning	Program 4	Lubricant Dosing	9		9

	Surface	Attack Polish*	Predose	Off	Direction	><
Step 5	Grit/Grain	Chem Cloth		Main Phase		Final Phase
	Lubricant	none	Time/Removal	3 min 30 sec		30 sec
	Mode	Time	Force	25 N		25 N
	Disc Speed	150 rpm	Abrasive Dosing	18		18
	Cleaning	Program 6	Lubricant Dosing	Off		Off

*Attack Polish:(200 mL Colloidal Silica + 100 mL H_2O)+ 30 mL Hydrogen Peroxide,30% + 30 mL Ammonium Hydroxide.

Appendix C—Glossary of Terms

A_F: Austenite finish temperature—temperature at which the martensite to austenite transformation is completed on heating.

A_S: Austenite start temperature—temperature at which martensite begins transforming to austenite on heating.

BFR: Bend free recovery—test whereby a rectangular prism of material is bent and then allowed to freely recover while being heated through transformation; the degree of angular recovery is measured with respect to temperature.

CLD: Constant load dilatometry—test whereby a sample of material is cycled under load; the change in length or strain is measured with respect to temperature.

CTE: Coefficient of thermal expansion—the amount of length change effected in a material by a 1 °C (K) change in temperature.

DSC: Differential scanning calorimetry—test whereby a sample is heated at a constant rate; the change in thermal energy of the sample is measured as a function of temperature.

ε_{OL}: Open loop strain—difference between the starting and final strain in the martensite state when undergoing a thermal cycle under load (heat from martensite to austenite, then cool back to martensite.) Also referred to as permanent deformation or plastic deformation.

ε_{TF}: Transformation strain—the amount of strain recovered upon heating from martensite to austenite. Measured as the strain at the A_S minus the strain at the A_F.

H: Thermal hysteresis—temperature difference between the M_S and A_F.

LB: Load-bias (See CLD).

M_d: Martensite deformation temperature—highest temperature at which it is still possible to stress induce martensite.

M_F: Martensite finish temperature—temperature at which the material is fully martensitic on cooling.

M_S: Martensite start temperature—temperature at which martensite begins to form on cooling.

Nitinol: Trade name for binary Ni~50 at.% Ti: after its composition and location of discovery **Ni Ti N**aval **O**rdnance **L**ab.

SMA: Shape-memory alloy—alloy that exhibits the ability to return to a preset shape after low temperature deformation, by heating through a transformation temperature.

SME: Shape-memory effect—ability of a material to be deformed while in a low-temperature martensite state and recover that deformation through thermal cycling through the transformation.

References Cited

1. Chang LC and Read TA 1951. *Trans. AIME.* **189**:47–52
2. Buehler WJ, Gilfrich JW, and Wiley RC 1963. *J. Applied Physics.* **34**:1475–1477
3. Buehler WJ and Wiley RC 1962. *Trans. ASM.* **55**:269–276
4. Chen CW 1957. *J. Metals*, **10**:1202
5. Au YK and Wayman CM 1972. *Scr. Metall.* **6**:1209–1214
6. Fonda RW, Jones HN, and Vandermeer RA 1998. *Scr. Mater.* **39**:1031–1037
7. Hornbogen E and Wassermann G 1956. *Z. Metallkd.* **47**:427
8. Burkart MW and Read TA 1953. *Trans. AIME.* **197**:1516–1523
9. Basinski ZS and Christian JW 1954. *Acta Metall.* **2**:101–116
10. Webster PJ, Ziebeck KRA, Town SL, and Peak MS 1984. *Phil. Mag. B.* **49**:295–310
11. Wayman CM 1971. *Scr Metall.* **5**:489
12. Koval YN, Kokorin VV, and Khandros LG 1981. *Phys. Met. Metall. No. 6.* **48**:162
13. Sato A, Chishima E, Soma K, and Mori T 1982. *Acta Metall.* **30**:1177
14. Duwez P and Taylor JL 1950. *Trans. AIME.* **188**:1173
15. Poole DM and Hume-Rothery W 1954–1955. *J. Inst. Met.* **83**:473
16. Purdy GR and Parr JG 1961. *Trans. Metall. Soc. AIME.* **221**:636
17. Hwang CM and Wayman CM 1983. *Scripta Metall.* **17**:381
18. Miyazaki S and Otsuka K 1986. *Metall. Trans.* **17A**:53
19. Fukuda T, Saburi T, Doi K, and Nenno S 1992. *Mater. Trans. JIM.* **33**:271
20. Saburi T, Wayman CM, Takata K, and Nenno S 1980. *Acta Metall.* **28**:15–32
21. Otsuka K and Ren XB 1999. *Intermetallics* **7**:511
22. 2005. ASTM F2005-05: Standard terminology for nickel-titanium shape memory alloys. ASTM International.
23. 2005. ASTM F2004–05: Standard test method for transformation temperature of nickel-titanium alloys by thermal analysis. ASTM International
24. 2003. ASTM F2082–03: Standard test method for transformation temperature of nickel-titanium shape memory alloys by bend and free recovery. ASTM International
25. Mavroidis C 2002. *Res. Nondestr. Eval.* **14**:1
26. Otsuka K and, Ren X 2005. *Prog Matls Sci* **50**:511–678
27. Ling HC and Kaplow R 1980. *Metall. Trans.* **11A**:77
28. Ling HC and Kaplow R 1981. *Metall. Trans.* **12A**:2101
29. Ling HC and Kaplow R 1981. *Mater. Sci. Eng.* **51**:53
30. Wasilewski RJ, Butler SR, Hanlon JE, and Worden D 1971. *Metall. Trans.* **2**:229
31. Otsuka K and Ren X 2002. *Maters. Sci. Forum.* **177**:394–395
32. Melton KN 1990 in <u>Engineering Aspects of Shape Memory Alloys</u>, Eds. Duerig TW, Melton KN, Stockel D, and Wayman CM. London:Butter.-Hein. pp. 21–35
33. Nishida M, Wayman CM, and Honma T 1986. *Metall. Trans.* **17A**:1505–1515
34. Nishida M, Wayman CM, and Honma T 1984. *Scripta Met.* **18**:1923
35. Suzuki Y and Horikawa H 1992. in <u>Shape-Memory Materials and Phenomenon- Fundamental Aspects and Applications</u>, Eds. Liu CT, Kunsmann H, Otsuka K, and Wuttig M. Warrendale, PA: Mat. Res. Soc. Symp. Proc. Vol. 246 p. 389
36. Miyazaki S, Otsuka K, and Suzuki Y 1981. *Scr. Metall.* **15**:287.
37. Miyazaki S, Imai T, Otsuka K, and Suzuki Y 1981. *Scr. Metall.* **15**:853.
38. Miyazaki S, Ohmi Y, Otsuka K, and Suzuki Y 1982. *J. de Phys. 43, Suppl.* **12**:C4–255.
39. Saburi T, Nenno S, Nishimoto Y, and Zeniya M 1986. *J. Iron and Steel Inst. Japan (Tetsu-to-Hagane)* **72**:571
40. Duerig TW, Stockel D, and Keeley A 1990. in <u>Engineering Aspects of Shape Memory Alloys.</u> Eds. Duerig TW, Melton KN, Stockel D, and Wayman CM. London:Butter.-Hein. pp. 181–194

41. Rondelli G, Vincentini B, and Cigada A 1988. in <u>Corrosion properties of NiTi shape-memory alloys.</u> Tokyo, Japan: Mat. Res. Soc. p. 345
42. Skrobanek KD, Kohl M, and Miyazaki S 1996 *Proc. of SPIE* **2779**:499–504
43. Krulevitch P, Lee AP, Ramsey PB, Trevino JC, Hamilton J, and Northrup MA 1996. *J Microelectromech S*ys **5:**270–282
44. Rÿha¨nen J 2000. *Min. Invas. Ther. Allied Technol.* **9:**99–106
45. Wever DJ, Veldhuizen AG, De Vries J, Busscher HJ, Uges DRA, and Van Horn JR 1998. *Biomaterials.* **19:**761–769
46. Suzuki T and Shigeaki U 1980. in <u>Titanium 80, Science & Technology, Proceedings of the 4th</u> <u>International Conference on Titanium</u>, Eds.Kimura H and Izumi O. Warrendale, PA: The Metallurgical Society of AIME. pp. 1255–1263
47. 2004. NASA Glenn Research Center, High-Temperature Shape Memory Alloy Group, unpublished research
48. Chu CL, Wu SK, and Chen YC 1996. *Maters. Sci. Eng.* **A216**:193
49. Firstov GS, Vichev RG, Kumar H, Blanpain B, and Van Humbeeck J 2002. *Biomaterials* **23**:4863
50. 1990. <u>Binary alloy phase diagrams, 2nd edition, vol. 3.</u> Eds. Massalski TB, Okamoto H, Subramanian PR, and Kacprzak L, Materials Park, OH: ASM Intnl. p. 2874
51. Van Humbeeck J 1999. *J. Eng. Mater. Technol.* **121:**98
52. Lindquist PG and Wayman CM 1990. in <u>Engineering Aspects of Shape-Memory Alloys.</u> Eds. Duerig TW, Melton KN, Stockel D, and Wayman CM. London:Butter.-Hein. pg. 58
53. Wu SK and Wayman CM 1987. *Metallography.* **20**:359
54. Angst DR, Thoma PE, and Kao MY 1995. *J. Phys IV* **5:**C8–747 to C8-752
55. Pu Z, Tseng H, and Wu K 1995. *Smart Structures and Materials 1995: Smart Materials, SPIE Proc.* **2441**:171
56. Noebe RD, Biles T, and Padula II SA 2006. in <u>Advanced Structural Materials: Properties, Design,</u> <u>Optimization, and Applications.</u> Ed. Soboyejo WO. Boca Raton, FL: Taylor & Francis.
57. Donkersloot HC and Van Vucht JHN 1970. *J. Less-Common Mets.*, **20**:83–91
58. Biggs T, Cortie MB, Witcomb MJ, and Cornish LA 2001. *Metall. Maters. Trans. A*, **32A**:1881
59. Rios O, Noebe R, Biles T, Garg A, Palczer A, Scheiman D, Seifert HJ, and Kaufman M 2005. *Proc. of SPIE* **5761**:376–387.
60. Noebe R, Gaydosh D, Padula II S, Garg A, Biles T, and Nathal M 2005. *Proc of SPIE* **5761**:364.
61. Zhu YR, Pu ZJ, Li C, and Wu KH 1994 in <u>Proceedings of the International Symposium on Shape</u> <u>Memory Materials</u>. Eds. Youyi C and Hailings TU. Beijing, China: International Academic Publishers pp. 253–257
62. Hsieh SF and Wu SK 2000. *Maters. Charac.* **45**:143
63. Hsieh SF and Wu SK 2000. *J. Alloys Compds.* **312**:288
64. Boriskina NG and Kenina EM 1980. in <u>Titanium 80, Science & Technology, Proceedings of the 4th</u> <u>International Conference on Titanium</u>. Eds. Kimura H and Izumi O. Warrendale, PA: The Metallurgical Society of AIME. pp. 2917–2927
65. Bozzolo G, Noebe RD, and Mosca HO 2005. *J. of Alloys and Compounds* **386**:125
66. Massalski TB, Okamoto H, Subramanian PR, and Kacprzak L 1990. in <u>Binary Alloy Phase Diagrams</u> <u>(2nd Edition)</u>. Materials Park, OH:ASM International
67. Predel B and Madelung O 1998. <u>Group IV Physical Chemistry - Phase Equilibria, Crystallographic</u> <u>and Thermodynamic Data of Binary Alloys, Volume 5—Light Metal Structural Alloys</u>, Springer-Verlag.
68. Goldberg D, Xu Y, Murakami Y, Otsuka K, Ueki T, and Horikawa H 1995. *J. Mater. Lett.* **22**:241–248
69. Khachin VN, Matveeva NA, Sivokha VP, and Chernov DV 1981. *Acad Nauk SSSR.* **257**:167
70. Enami K, Hoshiya T. *Proc. Mat. Tech.* **90**:1
71. Shimizu S, Xu Y, Okunishi E, Tanaka S, Otsuka K, and Mitose K 1998. *Maters. Lett.* **34**:23
72. Cai W, Tanaka S, and Otsuka K 2000. *Maters. Sci. Forum* **279**: 327–328

73. Stachowiak GB and McCormick PG 1988. *Acta Metall.* **36**:291
74. Matveeva NM, Khachin VN, and Shivokha VP 1985.in Stable and Metastable Phase Equilibrium in Metallic Systems. Ed. Drits ME. Moscow: Nauka p. 25 (in Russian)
75. Tian Q and Wu J 2002. *Intermetallics* **10**:675–682
76. Kachin VN, Matveeva NM, Sivokha VP, Chernov DB, and Yu K 1981. Koveristyi. *Doklady Akad. Nauk SSR* **257**:167
77. Otsuka K, Oda K, Ueno Y, Piao M, Ueki T, and Horikawa H 1993. *Scripta Metall. Mater.* **29**:1355
78. Goldberg D, Xu Y, Murakami Y, Morito S, Otsuka K, Ueki T, and Horikawa H 1994. *Scr. Metall. et Mater.* **30**:1349
79. Xu Y, Shimizu S, Suzuki Y, Otsuka K, Ueki T, and Mitose K 1997. *Acta Mater.* **45:**1503–1511
80. Xu Y, Otsuka K, Furubayashi E, Ueki T, and Mitose K 1997. *Mater. Lett.* **30**:189
81. Xu Y, Otsuka K, Furubayashi E, and Mitose K 1998. *Mater. Lett.* **34**:14
82. Yang WS and Mikkola DE 1993. *Scripta Metall. Mater.* **28**:161–165.
83. Suzuki Y, Xu Y, Morito S, Otsuka K, and Mitose K 1998. *Maters Lett.* **36:**85
84. Cai W, Tanaka S, and Otsuka K 2000. *Maters. Sci. Forum* **279:**327–328
85. Winzek B and Quandt E 1999. *Zeitschr. Metallkd.* **90:**796–802
86. 2001. ASTM E1876–01: Standard test method for dynamic young's modulus, shear modulus, and poisson's ratio by impulse excitation of vibration. ASTM International.
87. Noebe R, Padula II S, Bigelow G, Rios O, Garg A, and Lerch B 2006. *Proc. of SPIE.* **6170**:617010–1-617010–13
88. Noebe R, Draper S, Gaydosh D, Garg A, Lerch B, Penney N, Bigelow G, Padula II S, and Brown J 2006. *Proc of SMST.* (in Press)

REPORT DOCUMENTATION PAGE

1. REPORT DATE (DD-MM-YYYY) 01-07-2008	2. REPORT TYPE Technical Memorandum	3. DATES COVERED (From - To)

4. TITLE AND SUBTITLE
Effects of Palladium Content, Quaternary Alloying, and Thermomechanical Processing on the Behavior of Ni-Ti-Pd Shape Memory Alloys for Actuator Applications

5a. CONTRACT NUMBER

5b. GRANT NUMBER

5c. PROGRAM ELEMENT NUMBER

6. AUTHOR(S)
Bigelow, Glen

5d. PROJECT NUMBER

5e. TASK NUMBER

5f. WORK UNIT NUMBER
WBS 953033.01.03.17

7. PERFORMING ORGANIZATION NAME(S) AND ADDRESS(ES)
National Aeronautics and Space Administration
John H. Glenn Research Center at Lewis Field
Cleveland, Ohio 44135-3191

8. PERFORMING ORGANIZATION REPORT NUMBER
E-15903

9. SPONSORING/MONITORING AGENCY NAME(S) AND ADDRESS(ES)
National Aeronautics and Space Administration
Washington, DC 20546-0001

10. SPONSORING/MONITORS ACRONYM(S)
NASA

11. SPONSORING/MONITORING REPORT NUMBER
NASA/TM-2008-214702

12. DISTRIBUTION/AVAILABILITY STATEMENT
Unclassified-Unlimited
Subject Category: 26
Available electronically at http://gltrs.grc.nasa.gov
This publication is available from the NASA Center for AeroSpace Information, 301-621-0390

13. SUPPLEMENTARY NOTES
Submitted in partial fulfillment of the degree (Master of Science) at the Colorado School of Mines. Successfully defended on April 14, 2006.

14. ABSTRACT

The need for compact, solid-state actuation systems for use in the aerospace, automotive, and other transportation industries is currently driving research in high-temperature shape memory alloys (HTSMA) having transformation temperatures above 100 °C. One of the basic high temperature systems under investigation to fill this need is NiTiPd. Prior work on this alloy system has focused on phase transformations and respective temperatures, no-load shape memory behavior (strain recovery), and tensile behavior for selected alloys. In addition, a few tests have been done to determine the effect of boron additions and thermomechanical treatment on the aforementioned properties. The main properties that affect the performance of a solid state actuator, namely work output, transformation strain, and permanent deformation during thermal cycling under load have mainly been neglected. There is also no consistent data representing the mechanical behavior of this alloy system over a broad range of compositions. For this thesis, ternary NiTiPd alloys containing 15 to 46 at.% palladium were processed and the transformation temperatures, basic tensile properties, and work characteristics determined. However, testing reveals that at higher levels of alloying addition, the benefit of increased transformation temperature begins to be offset by lowered work output and permanent deformation or "walking" of the alloy during thermal cycling under load. In response to this dilemma, NiTiPd alloys have been further alloyed with gold, platinum, and hafnium additions to solid solution strengthen the martensite and parent austenite phases in order to improve the thermomechanical behavior of these materials. The tensile properties, work behavior, and dimensional stability during repeated thermal cycling under load for the ternary and quaternary alloys were compared and discussed. In addition, the benefits of more advanced thermomechanical processing or training on the dimensional stability of these alloys during repeated actuation were investigated. Finally, the effect of quaternary alloying on the thermal stability of NiTiPdX alloys is determined via thermal cycling of the materials to increasing temperatures under load. It was found that solid solution additions of platinum and gold resulted in about a 30 °C increase in upper use temperature compared to the baseline NiTiPd alloy, providing an added measure of over-temperature protection.

15. SUBJECT TERMS
Shape memory alloys; Nitinol alloys; Martensite; Austenite; Thermomechanical treatment; Solid solutions; Alloying; Dimensional stability; Tensile properties; Mechanical properties; Smart materials; Actuators

16. SECURITY CLASSIFICATION OF:			17. LIMITATION OF ABSTRACT	18. NUMBER OF PAGES	19a. NAME OF RESPONSIBLE PERSON Glen Bigelow
a. REPORT U	b. ABSTRACT U	c. THIS PAGE U	UU	94	19b. TELEPHONE NUMBER (include area code) 216-433-6603

Standard Form 298 (Rev. 8-98)
Prescribed by ANSI Std. Z39-18